Temperature Responsive Nano-Phase Separated Waterborne Polymer Dispersions

Gordana Siljanovska Petreska

Supervised by: Dr. Clemens Auschra and Dr. Maria Paulis

University of the Basque Country UPV/EHU

Donostia-San Sebastián

2019

The research carried out in this thesis is funded by the European Union's Horizon 2020 research and innovation programme under the Marie Sklodowska-Curie grant agreement No. *642514* – TRACKWAY - H2020-MSCA-ITN-2014.

Contents

Chapter I. Introduction and objectives

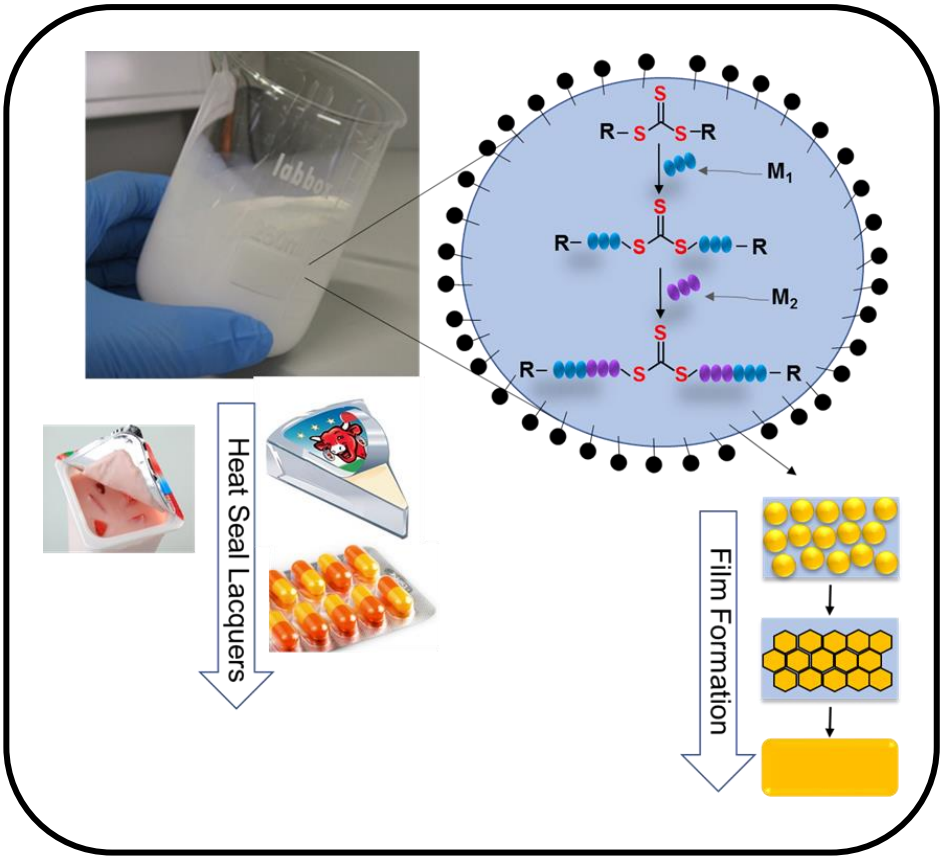

I.1. Controlled Radical Polymerization

Free radical polymerization (FRP) is one of the most widely used industrial process for the commercial production of high molecular weight polymers, as approximately 50% of all commercial polymers are produced by radical polymerization[1]. This type of polymerization can be performed either in homogeneous media, such as bulk or solution or in heterogeneous media such as emulsion polymerization[2]. The process is very versatile, can be used with extensive range of olefinic monomers and has high tolerance to impurities such as water, traces of oxygen and stabilizers, thus its implementation in an industrial plant is very easy. In FRP each chain is initiated, propagates and terminates in a pretty short period of time relative to the length of the reaction. Initiation process is slow and free radical initiator is often left unconsumed at the end of the reaction. Propagating radical life time, which is the time that passes between initiation and ending of a given chain, is typically of the order of one second and chains are continuously initiated throughout the polymerization. Chain termination occurs when the propagating radicals react by combination, disproportionation or chain transfer reaction. The molecular weight of the chains formed in the early stage of polymerization is high and will reduce with conversion because of monomer depletion (Figure I.1). These characteristic features including also chain transfer or other side reactions limit the possibility of FRP to control the molar mass, the molar mass distribution (MWD), the chain/end

functionalities and the macromolecular architecture of polymers. The breadth of the molecular weight distribution or polydispersity is governed by statistical factors and the polydispersity obtained by FRP is rather broad (Mw/Mn>1.5).

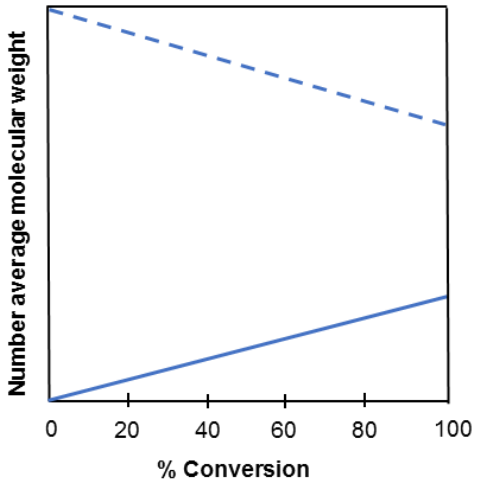

Figure I.1. Evolution of molecular weight with monomer conversion for a conventional radical polymerization with constant rate of initiation (– – –) and a living radical polymerization (-)[16]

Therefore, to control these features, there was a huge demand of a new type of polymerization where the chain transfer and termination reactions will be suppressed. This kind of polymerization, named as living polymerization was first described in 1956 by Szwarz[3]. In an ideal living polymerization all chains are initiated at the beginning of the reaction, grow at the same rate and their active sites are not lost and will continue to propagate if more monomer is added to the system.

Therefore, block copolymers will be formed if the second monomer differs from the first one. The prediction of the molecular weight can be done by controlling the ratio of monomer to initiator and the MWD obtained is narrow (Mw/Mn<1.1), indicating that the polymerization proceeded in a well-controlled manner. Moreover, the number average molar mass is linearly dependent on conversion (Figure I.1) and the number of polymer chains is constant during polymerization. Living anionic polymerization was the first living polymerization developed[4]. Although living anionic polymerization provides excellent living character, this type of polymerization is restricted to relatively few types of monomers like e.g. certain olefinic monomers and requires special reaction conditions, e.g. complete exclusion of moisture and oxygen, which prevents widespread commercial applications. Thus, invention of a living like radical polymerization by stopping chain radicals from being killed, compatible with a large variety of monomers and tolerant to impurities was highly desirable. For many decades these issues exercised the minds of the polymer chemists who during the late 1980 and nineties developed several strategies for massively reducing termination though not entirely eliminating it. Three main types of living radical polymerizations were developed and received great attention; (i) nitroxide mediated polymerization (NMP)[5], (ii) atom transfer radical polymerization (ATRP)[6] and (iii) reversible addition fragmentation transfer polymerization (RAFT)[7,8]. These types of polymerization initially named as living polymerization by IUPAC in 2009, were given a generic term as reversible-deactivation radical polymerization (RDRP). In RDRP[9–11],

initiation is fast and all chains are initiated at the beginning of the reaction and grow throughout the course of the reaction which eventually enables control over chain architecture. The lifetime of growing chain is extended from one second in FRP to more than one hour in RDRP. This is achieved through participation of dormant species and intermittent reversible activation, where the propagating radicals are being reversibly deactivated i.e. alternating between active and dormant states. Rapid equilibrium between an active and dormant form ensures that all chains will grow, albeit intermittently. Almost all the chains are dead in FRP, whereas in CRP the amount of dead chains is usually below 10%. In principle, there are two main mechanisms that explain RDRP, (i) reversible deactivation mechanism (Figure I.2a) which includes NMP and ATRP and (ii) reversible chain transfer mechanism which includes RAFT (Figure I.2b).

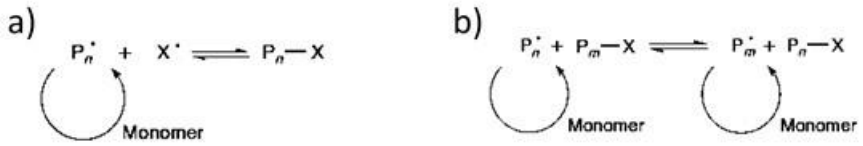

Figure I.2. General Dormant- Active equilibrium in a) reversible deactivation mechanism and b) reversible chain mechanism

In reversible deactivation, the polymer chain is end-capped with a moiety that can reversibly undergo homolytical cleavage. In NMP, this moiety is a nitroxide, while in ATRP a halide is reversibly transferred to a transition-metal complex. In processes

based on reversible chain transfer, there is a fast exchange of growing radicals via a transfer agent. In the RAFT process, small molecules typically thiocarbonylthio compounds are responsible for this exchange, which proceeds via an intermediate radical. The synthesis of polymers with well-defined architecture is of ongoing high interest for many application areas and has experienced tremendous expansion with the development of reverse deactivation radical polymerizations (RDRP).

Among all the RDRP, RAFT has shown to be the most versatile and robust technique, allowing the polymerization of a broader range of functional monomers (both polar and nonpolar)[12] with a higher tolerance to diverse functional groups than do competing techniques (NMP and ATRP), in a wide range of reactions conditions, including bulk, solution and aqueous dispersions[13,14] through the use of different classes of chain transfer agents (CTAs). RAFT provides good control over the polymerization of vinyl esters (vinyl acetate) and vinylamides (i.e. N-vinylpyrrolidone), where NMP and ATRP typically provide minimal control.

I.2. RAFT Polymerization

Since the first publication of RAFT polymerization by the pioneering work of Rizzardo, Moad, and Thang in 1998[15] at the Commonwealth Scientific and Industrial Research Organization (CSIRO), RAFT has become a powerful polymerization technology for the synthesis of tailor-made polymers with predetermined molecular

weights, with narrow polydispersities, high end group fidelity, and with highly complex architectures[16]. The key feature of the RAFT mechanism outlined in Figure I.3 is a sequence of addition-fragmentation equilibria[15]. In the initial stages of polymerization, a propagating radical ($P_n^{\bullet}$) adds to the thiocarbonylthio compound (RSC(Z)=S,**1**) followed by fragmentation of the intermediate radical, which delivers a polymeric thiocarbonylthio compound (PnS(Z)C=S,**3**) and a new radical ($R^{\bullet}$). The new radical ($R^{\bullet}$) reacts with monomer which leads to formation of a new propagating radical ($P_m^{\bullet}$). The rapid equilibrium between the active formed propagating radicals ($P_n^{\bullet}$ and $P_m^{\bullet}$) and the dormant polymeric thiocarbonylthio compound (PnS(Z)C=S,**3** and PmS(Z)C=S,**5**) offers equal probability for all the chains to grow and permits the production of narrow polydispersity polymers ($k_{addP} \gg k_p$ and $k_{\beta} \gg k_p$). In an effective RAFT process, where the rate of chain equilibrium is rapid with respect to propagation, there should be less than one monomer unit added per activation cycle, therefore the degree of polymerization (n and m) of the species on the two sides of the equilibria should be similar. When the polymerization is complete (or stopped) most of the chains retain the thiocarbonylthio end group upon completion of the polymerization and can be isolated as stable materials. There is still ongoing discussions on the detailed kinetics of the RAFT process, the rapidity at which various equilibria are established and the side reactions which may occur complicating the process[17–19].

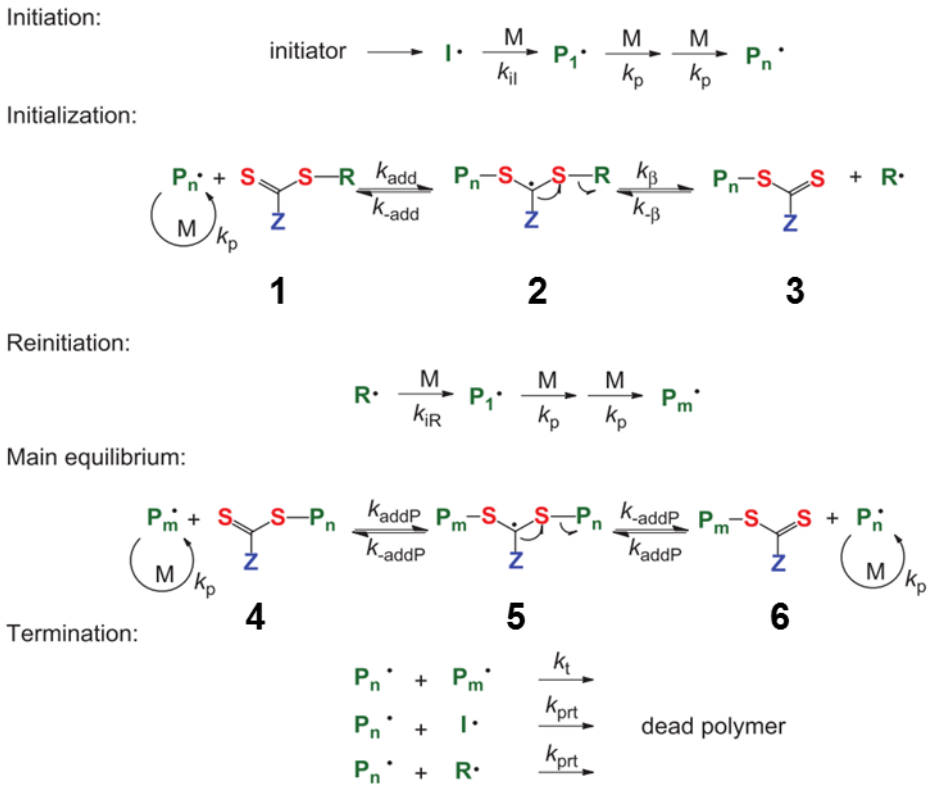

Figure I.3. Mechanism of RAFT polymerization

Upon slow fragmentation, the intermediate species (**2** or **4**) are consumed in side reactions, and upon slow or inefficient re-initiation retardation or inhibition can occur[20]. Initiation, propagation and radical-radical termination occurs as in conventional free radical polymerization. The radicals are neither formed nor destroyed by the RAFT steps, thus RAFT polymerization will not take place without

an external supply of radicals from an initiator. However, all radical species (initiating radicals, propagating radicals, even intermediates), can in principle, be involved in termination by radical-radical reactions. Thus, it is important to choose reaction conditions such that termination events are minimized. Under Living polymerization conditions, the molecular weight of the polymer which is formed is significantly lower than the one formed in the absence of a RAFT agent and the number of polymer molecules containing RAFT agent derived ends is greater than the ones formed because of termination.

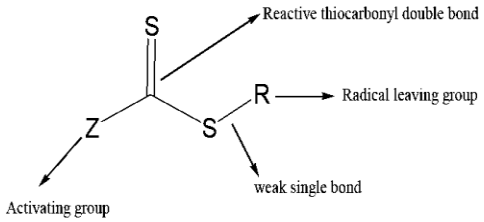

R	Z	Class of RAFT agent
$(CH_3)_2C(COOEt)$	C_nH_{2n+1}, Ph, Bz	Dithioester
$(CH_3)_2CCN$	NR'R"	Dithiocarbamate
$(CH_3)CHPh$	OR'	Xanthate (MADIX agent)
$PhCH_2$	SR, SR'	Trithiocarbonate

Figure I.4. The structure of a RAFT agent

The key of the degenerative chain transfer in RAFT polymerization is the chemical structure of the RAFT agent[21] (Figure I.4). The substituents around the C=S group are labelled as Z and R and the effectiveness of the RAFT agent depends on the monomer being polymerized and the transfer constant (C_{tr}) which is the determined by the nature of the Z and the R groups, respectively.

Careful choice of RAFT agent, reaction conditions and monomer being polymerized is critical for achieving good control over the polymerization and therefore well-defined polymeric products. Depending on the substituent group next to the C=S functionality, thiocarbonylthio RAFT agents can be divided into four groups; namely dithioesters, dithiocarbamates, trithiocarbonates and xanthates (Figure I.5). The Z group is responsible for the activation of the C=S double bound and stabilization of the intermediate radical formed, while the R group should be a good free radical and be capable of reinitiating free radical polymerization.[15]

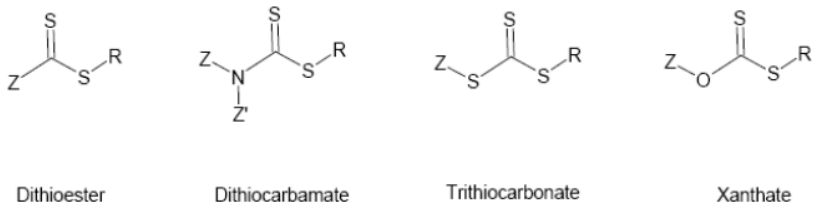

Figure I.5. Structures of different classes of RAFT agents.

The most effective RAFT agents are dithioesters and trithiocarbonates which have carbon or sulfur adjacent to the thiocarbonylthio group. RAFT agents with a lone pair on nitrogen or oxygen adjacent to the thiocarbonyl group, such as the O-alkyl xanthates, N,N-dialkyldithiocarbamates, and N-alkyl-N-aryldithiocarbamates, have much more reactivity towards radical addition[21]. Two transfer coefficients characterize RAFT agents. A rate coefficient for chain transfer (k_{tr}) defined in terms of the rate

constant for addition (k_{add}) and a partition coefficient (φ), which defines how the adduct is partitioned between products and starting materials (equation I.1). The chain transfer coefficient is then defined in terms of k_{tr} and propagation rate constant k_p (equation I.2). The RAFT agents that have higher C_{tr} are more active and produce more chain transfer events per propagation cycle. As a result, when using this type of RAFT agents, linear increase of Mn with conversion and narrower molar mass distribution (PDI < 1.2) are obtained.

$$k_{tr} = k_{add} \frac{k_\beta}{k_{-add} + k_\beta} = \varphi k_{add} \quad \textbf{(I.1)}$$

$$C_{tr} = \frac{k_{tr}}{k_p} \quad \textbf{(I.2)}$$

The most active RAFT agents have C_{tr}>100[22]. Partition coefficient (φ) relates the relative rates of fragmentation of the intermediate **3** to the starting materials, $P_n^{\bullet}$ and **1** (k_{-add}), or the products $R^{\bullet}$ and **2** (k_β), through equation I.3; the rate constant for which are defined in Figure I.3.

$$\varphi = \frac{k_\beta}{k_{-add} + k_\beta} \quad \textbf{(I. 3)}$$

For a controlled polymerization and for preparation of polymers with low polydispersity, the R group of the RAFT agent (**2**, ZC(=S)SR) requires to be a good homolytic leaving group with respect to Pn• (i.e. φ≥0.5), such that the intermediate **3**, formed by addition of $P_n^{\bullet}$ to **2**, both fragments rapidly and partitions in favour of **4** and $R^{\bullet}$. The expelled radical ($R^{\bullet}$) must also be able to reinitiate polymerization efficiently (i.e., $ki_{,R} > kp$); otherwise, retardation is likely[23].

Radically polymerizable monomers can nominally be divided into two broad classes, (i) the “more activated monomers” (MAMs) and (ii) the “less activated monomers” (LAMs). MAMs are those monomers which have the vinylic group conjugated to a neighboring functionality such as an aromatic ring (e.g., styrene (St), vinylpyridine), to a carbonyl group (e.g., (methyl)acrylate, (methyl)acrylamide), or to a nitrile (e.g., acrylonitrile). In contrast LAMs are the monomers where the vinylic group is adjacent to an electron rich atom, such an oxygen, nitrogen, halogen or sulfur lone pairs (e.g., vinyl acetate, vinyl esters, vinylamides; N-vinylpyrrolidone, N-vinylcarbazole etc.). The classification of monomers as a MAM or LAM refers to its ability to react in a free radical process; MAMs react more readily with radicals than do LAMs. In this context the relative reactivity of the propagating radicals derived from these monomers are at odds with these classifications. Propagating radicals with a terminal more active monomer (MAM) unit are more stable and less reactive in radical addition (lower k_p, lower k_{add}) than LAMs, therefore they require a Z- group

that will help with the stabilization of the intermediate radical to favour radical addition on the C=S. The poly(MAM) propagating radicals are relatively good homolytic leaving groups (higher k_{β}, k_{-add}), thus retardation because of slow fragmentation is very unlikely. Preparation of low polydispersity polymers from MAMs can be achieved using the more active RAFT agents (high Ctr) such as the dithioesters (typically dithiobenzoathes, PhC(=S) S-R, or S-alkyl trithiocarbonates (R'= alkyl)), and aromatic dithiocarbamates, as these provide a high rate of reversible chain transfer via addition-fragmentation with respect to propagation. This allows for rapid equilibrium of growing polymer chains. On the other hand, due to lower transfer constants (low Ctr) N-alkyl-N-aryldithiocarbamates and the O-alkyl xanthates RAFT agents generally provide poor control. Propagating radicals having terminal less activated monomer (**LAM**) unit are highly reactive in radical addition (higher k_p, higher k_{add}). For this reason, in RAFT polymerization of LAMs typically less active (low Ctr) RAFT agents are used. In this context, N-alkyl-N-aryldithiocarbamates (R'= alkyl, (R''= aryl) and the O-alkyl xanthates (R'= alkyl)) can be employed for the polymerization of LAMs. The lone pair electrons poly(LAM) propagating radicals are relatively poor homolytic leaving groups (higher k_{β}, k_{-add}). Therefore, when more active RAFT agents are used in LAM polymerization, fragmentation is slow thus inhibition or retardation is likely. General guidelines for the selection of Z and R groups are shown in Figure I.6. The RAFT agent transfer constant is generally enhanced when electron-withdrawing groups are present on Z and also by the ability of Z group to stabilize an adjacent

radical center[24]. Moreover, Z group also stabilizes the intermediate radicals **3** and **5**. The rate of intermediate radical fragmentation is slower, and the intermediate radical is stabilized when Z is aryl.

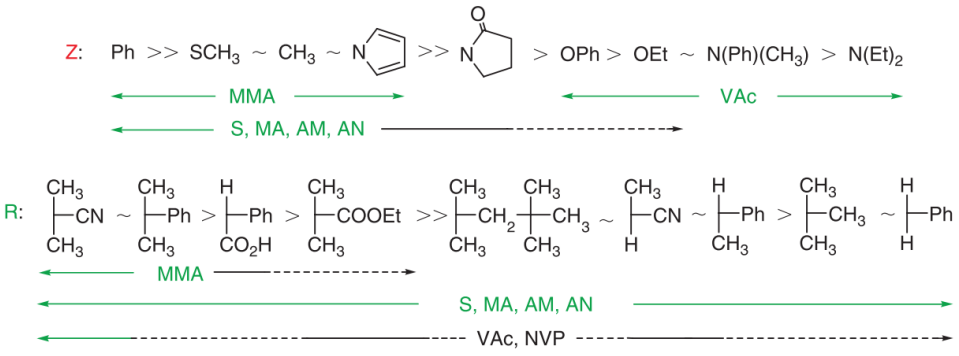

Figure I.6. Guidelines for selection of a proper RAFT agent for various monomers polymerization[16]. For Z, addition rate decreases, and fragmentation rates increase from left to right. For R, fragmentation rates decrease from left to right. Dashed line indicates partial control (i.e. control of molecular weight but broader polydispersity or substantial retardation in the case of VAc or NVP).

This is not the case when the atom of Z group is connecting sp^3 carbon, oxygen, or nitrogen or sulphur. As shown in Figure I.6, the benzylic radicals and tertiary alkyl radicals add to most LAMs very slowly and an inhibition period is often observed with these R groups[25].

RAFT polymerization has been widely used for the preparation of block copolymers[13,26–28]. The simplest and most common method for the preparation of block copolymers is through incorporation of two (or more) monomers through

sequential polymerization processes, with purification undertaken before each additional polymerization (Figure I.7).

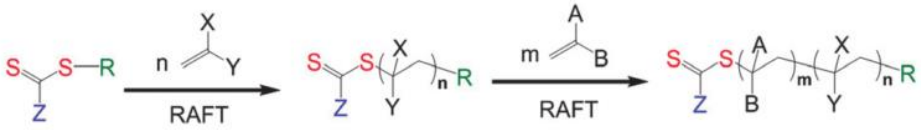

Figure I. 7 Block copolymers by sequential RAFT polymerizations.

In the preparation of well-defined block copolymers using RAFT polymerization, the order in which the monomers are incorporated into a block copolymer is pivotal, as the first block serves as a macro-R during polymerization of the second monomer. The macro-R group must be good homolytic leaving group with respect to the propagating radical of the second monomer and must reinitiate polymerization of the second monomer efficiently. Due to the presence of greater steric stabilization, and hence better leaving group ability, monomers that produce stabilized tertiary propagating radicals (i.e. methacrylates, methacrylamides) should be polymerized prior to those that produce stabilized secondary propagating radicals (i.e. styrenes, acrylates, acrylamides)[12,29]. Moreover, these should be introduced before monomers which have more reactive secondary propagating radicals (vinyl esters, vinylamides).

I.3. Block Copolymers

Block copolymers stand for an interesting group of polymeric materials belonging to the family identified as “soft materials”. They are made of blocks of different and often thermodynamically incompatible monomer units covalently bonded to each other. Block copolymers self-assemble into organized microdomain structures when the thermodynamic repulsion between the covalently bonded chains is high enough and this structural organization is called “microphase separation”.

The prefix “micro” used for this type of structures simply means “small”. However, their periodicity can range from few nanometers to several hundred nanometers, depending on the molecular weight of the component polymers. Generally, in bulk, block copolymers phase separate into a variety of morphology such as spheres (S), cylinders (C), bicontinous gyroids (G), lamellae (L), etc., as shown in Figure I.8[30]. Block copolymers phase behaviour has been investigated both theoretically and experimentally[30–32] and a number of theories have been developed dealing with the phase behaviour of diblock copolymers in bulk[33–35] . The degree of microphase separation of diblock copolymers is determined by χN, where χ represents the Flory-Huggins interaction parameter and N represents the total degree of polymerization. Two segregation limits in terms of χN exists: (i) weak segregation limit (WSL) ($\chi N<10$)

and (ii) strong segregation limit (SSL) (χN »10). In Figure I.8. the phase diagram of diblock copolymers predicted by the self-consistent mean-field (SCMF) is shown [30,35].

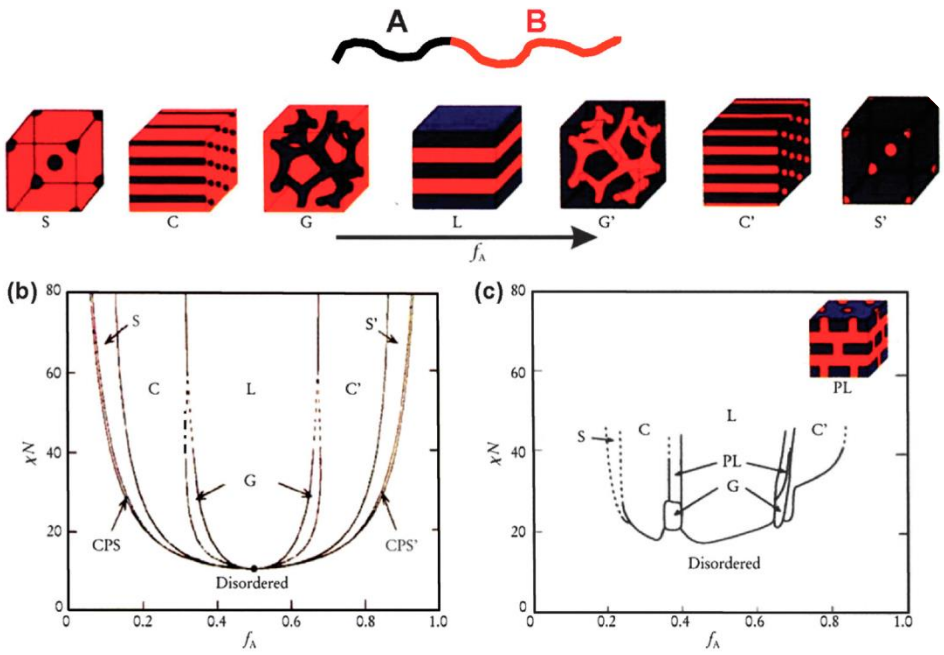

Figure I.8. Equilibrium morphologies of AB diblock copolymers in bulk: S and S' = body-centered-cubic spheres, C and C' = hexagonally packed cylinders, G and G' = bicontinuous gyroids, and L = lamellae. (b) Theoretical phase diagram of AB diblocks predicted by the self-consistent mean-field theory, depending on volume fraction (*f*) of the blocks and the segregation parameter, χN; CPS and CPS' = closely packed spheres. (c) Experimental phase diagram of polystyrene-*b*-polyisoprene copolymers, in which f_A represents the volume fraction of polyisoprene, PL = perforated lamellae[32]

As seen from Figure I.8, when the volume fraction of A-block (f_A) is increased at a fixed χN above the order-to-disorder transition (ODT) (χN > ~10.5), the order-to-order

transition (OOT) starts from closely packed spheres (CPS, which separates the disordered state and S phase), passing through body-centered cubic spheres (S), hexagonally packed cylinders (C) and bicontinuous gyroids (G), to lamellae (L). When the composition is inverted, morphological inversion takes place (L → G' → C' → S' → CPS' → disordered). Three parameters play a crucial role in the microphase separation:

1. The volume fraction of the A and B blocks (f_A and f_B, with $f_A+f_B=1$),
2. The total degree of polymerization ($N=N_A+N_B$)
3. The Flory-Huggins parameter, χ_{AB}, which specifies the degree of incompatibility between the A and B blocks, which drives the phase separation.

The relationship between χ_{AB} and the temperature is given by the equation[30,36],

$$\boldsymbol{\chi AB} = \left(\frac{z}{k_B T}\right)\left[\varepsilon_{AB} - \frac{1}{2}(\varepsilon_{AA} + \varepsilon_{BB})\right] \qquad \textbf{(I. 4)}$$

where z is the number of nearest neighbours per repeat unit in the polymer, k_B is the Boltzmann constant, k_BT is the thermal energy, and ε_{AB}, ε_{AA}, and ε_{BB} are the interaction energies of A–B, A–A, and B–B pairs, respectively. In diblock copolymers where there are no strong specific interactions like hydrogen bonding or ionic charges, the χN is positive and small, e.g. for polyisoprene-block-polystyrene. The segregation

product χN governs the degree of microphase separation. With increasing temperature or decreasing χN the incompatibility between the constituent blocks decreases, while the combinatorial entropy increases, the copolymers show order-to-disorder transition (ODT) and become disordered. T_{ODT} is the temperature at which ODT occurs.

Incorporation of crystallizable block in the block copolymers introduces additional complexity in the microphase separation behaviour [37–39]. The structural development in crystalline block copolymers is controlled by two competing self-organizing mechanisms, namely microphase separation and crystallization. Thus, these type of block copolymers exhibit richer phase behaviour which is more difficult to predict. Block copolymers where one of the blocks is crystalline and the other is amorphous are the most widely studied crystalline diblock copolymers. Diverse morphologies can be generated in these types of block copolymers based on segregation strength and on the relative values of the glass transition temperature of the amorphous block (Tg), the crystallization temperature (Tc), and the T_{ODT}, which are very well explained in several review articles [39–41]. Figure 1.9 schematically shows the possible structure formation in crystalline-amorphous diblock copolymers. At temperatures above the melting point of crystalline blocks (Tm), crystalline-amorphous diblock copolymers form microdomain structures as in the case of amorphous-amorphous diblock copolymers. When quenched to lower temperatures

the crystalline block in these microphase separated structures starts to crystallize and various morphologies are formed based on the molecular characteristics of the block copolymers (Figure 1.9)[42].

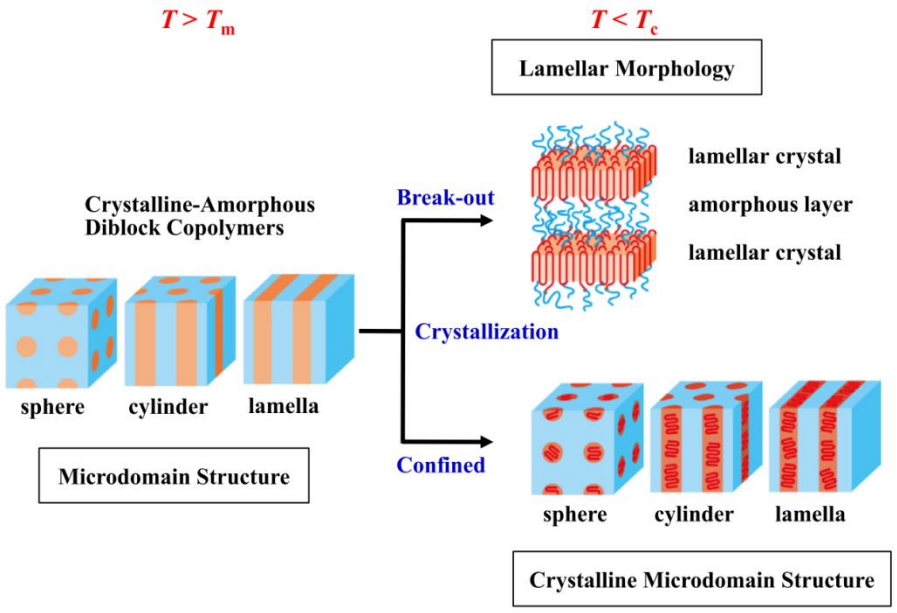

Figure I.9. Possible crystallization behaviors of microphase separated crystalline-amorphous diblock copolymers[39].

When the initial microdomain structure is not sufficiently stable against the crystallization (this is case when the segregation strength between different blocks is not large enough), it is completely replaced with a crystalline lamellar morphology, an alternating structure consisting of lamellar crystals and amorphous layers known as

break-out crystallization. On the contrary, when the microdomain structure is stable against crystallization or it is practically frozen due to the vitrification of amorphous blocks, the crystallization occurs within the nanodomain or microdomain structures to yield crystalline microdomain structures, known as confined crystallization. When the glass transition temperature of amorphous blocks is sufficiently higher than the crystallization temperature of crystalline blocks, the microdomain structure is practically frozen during crystallization and hence it is not transformed into the crystalline lamellar morphology. Consequently, the crystalline block crystallizes within hard (or glassy) nanodomains to form crystalline structures within the corresponding block copolymer microphase.

It is generally observed for the crystallization in hard nanodomains that the melting temperature is considerably low, and the final crystallinity is extremely small as compared with the case in which the crystalline lamellar morphology is formed by break-out crystallization. This is mainly attributed to the formation of immature crystals because the hard nanodomain cannot deform satisfactorily to increase the total crystallinity of confined crystalline blocks. For weakly segregated crystalline amorphous block copolymers where the T_{ODT}>Tc>Tg, the crystallization destroys the melt structure generated by microphase separation and crystalline lamellae are formed[39,40,43].

Block copolymers have been widely synthesized via RAFT non-aqueous dispersions[44] and their self-assembly has been studied. However, aqueous dispersed systems are favored because of low environmental impact, good heat transfer and low viscosity.

I.4. RAFT in dispersed media

RAFT polymerization has been quite successfully employed in bulk and solution polymerization and complex structures like stars[45], block copolymers[28] and brush amphiphilic copolymers[46] have been produced in these homogeneous media.

In this sense, employing RAFT in disperse media has not enjoyed the same success, mainly due to the difficulties found when transporting the RAFT agent to the locus of polymerization, namely from monomer droplets to polymer particles. The following problems were reported: (i) poor colloidal stability[47,48], (ii) poor control of the number- average molecular weight[47,48] or (iii) poor control of the polydispersity[48].

In order to better understand the problems that may arise from the RAFT in dispersed media, details about emulsion polymerization and miniemulsion polymerization are discussed in the following sections.

I.4.1. Emulsion Polymerization

Wide range of specialty polymers including adhesives, binders for nonwoven fabrics, additives for paper, textiles and construction materials are produced using emulsion polymerization. Emulsion polymerization[2,49] is a free radical polymerization in a heterogeneous reaction mixture, where monomers are dispersed in an aqueous solution of surfactant which exceeds the critical micellar concentration[2]. Surfactants are adsorbed on the surface of the monomer droplets, stabilizing them. Generally, the amount of surfactant exceeds the amount needed to cover the droplets thus, the rest of the surfactants form aggregates known as micelles which are swollen with monomer. In most of the cases thermal water-soluble initiators are used to initiate the polymerization. The radicals are formed in the aqueous phase and they are too hydrophilic to directly enter the organic phases (monomer droplets). They react with the monomer dissolved in the aqueous phase and form oligoradicals which slowly grow due to the low concentration of monomer in the aqueous phase. Once enough monomer units are added, the oligoradicals become hydrophobic enough and can enter the organic phases of the system. The monomer droplets are much larger (1-10 μm) than the monomer swollen micelles (10-20 nm) and thus their surface area is much lower (the surface area of the micelles is about three orders of magnitude higher than the one of the monomer droplets).

Thus, the probability of oligoradicals to enter the micelles is much higher than the monomer droplets. When the oligoradicals enter the micelles, they find the monomer rich area there and grow fast enough and form polymer particles. This is called ***heterogeneous*** nucleation. When the oligoradicals grow in the aqueous phase beyond the length at which they are still soluble in the water, they precipitate and are stabilized by the emulsifier present in the aqueous phase. This process of formation of particles is called ***homogenous*** nucleation (Figure I.10).

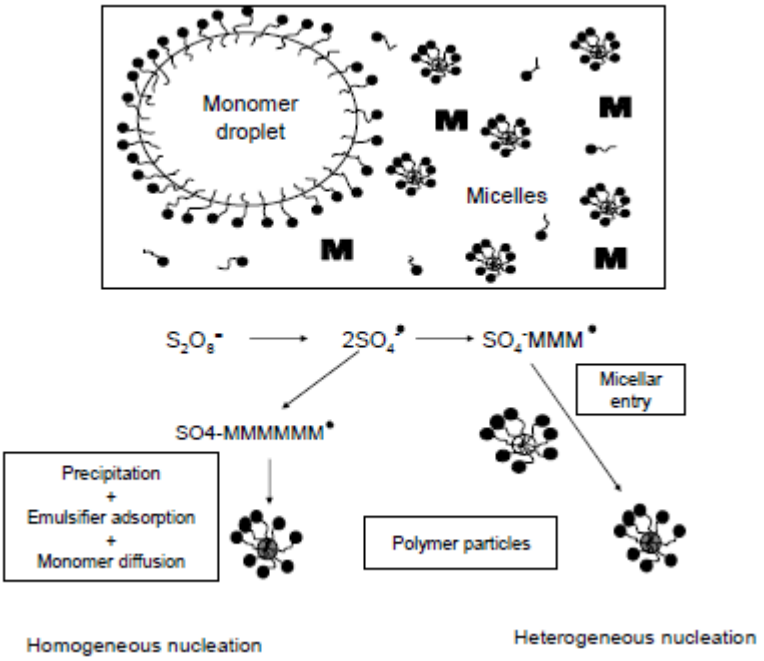

Figure I.10. Scheme of different nucleation mechanisms in emulsion polymerization

The first ab initio RAFT emulsion polymerization was reported by the CSIRO group[50], using butyl methacrylate (BMA) as a monomer and cumyl dithiobenzoate, highly reactive RAFT agent (Ctr >1000) and their experimental procedures were designed to avoid the presence of monomer droplets. High conversion was reached (95%) and a low PDI (1.22) with the Mn following the theoretical prediction. These results were an indication that the transportation of the RAFT from droplets to growing particles needs to be avoided. Later, Uzulina et al.[51] reported attempts to polymerize three different types of monomers: styrene (St), methyl methacrylate (MMA) and vinyl acetate using highly reactive dithio-RAFT agents (Z-phenyl and R=CH_2CO_2H or $C(CH_3)_2CONH_2$). They showed that when using amide functional RAFT agents, styrene was successfully polymerized, even if PDI was high,1.5 and 2. The other monomers used proved to be less successful. The nature of the RAFT agents appeared critical since more hydrophobic RAFT agents were unsuitable and led to phase separation. Nozari and Tauer[52] also studied the use of highly reactive RAFT agents (Ctr>10) for ab initio St polymerization and showed that the best control was achieved for the least hydrophobic dithiobenzoate agents. They prescribed this to the faster transportation of the more hydrophilic RAFT agents from monomer droplets to the growing particles. Furthermore, the PDI obtained from such systems was much higher than the ones found either in bulk or solution. Later on, the authors confirmed that the diffusion of the RAFT agent strongly depended on its water solubility, supporting their previous postulate of slow RAFT agent transportation[53].

Monteiro et al.[48] studied the seed polymerization of St mediated by cumyl dithiobenzoate as a RAFT agent. The polymerization was problematic and a high level of phase separation of a red monomer layer containing either RAFT agent or RAFT based oligomers was reported. They proposed that the excessive retardation was due to the exit of the R leaving groups from the RAFT agent out of the growing seed particles. For successful polymerization, the transport of the RAFT agent and its solubility were again discussed. Prescot et al.[54] used acetone to transport the oil soluble RAFT agent (PEPDTA) to the pre-existing seed particles. The acetone was removed by rotary evaporator and then St was added. The polymerization proceeded in a controlled manner, and the PDI was below 1.4 after the subtraction of the polymer in the seed. This showed a clear indication that the transportation of the RAFT agent is important and that once inside the particles, the RAFT agent can mediate the “living” behavior of the polymerization.

An aqueous heterogeneous polymerization process that avoids the transport issues between the monomer droplets and polymer particles, and allows the incorporation of water insoluble compound is miniemulsion polymerization[55].

I.4.2. Miniemulsion polymerization

Miniemulsion stands for submicron (d=50-500nm) monomer droplets in water dispersion prepared using efficient emulsification apparatus, stabilized against

diffusion degradation (Ostwald ripening) and droplet coagulation by using a water insoluble low-molecular weight compound (costabilizer, e.g. hexadecane) and an efficient surfactant. Generally, miniemulsions have broad droplet size distribution. The difference of the chemical potentials of the monomers in the droplets of radius r_1 and radius r_2 is:

$$\frac{\Delta\mu}{RT} = \frac{2\sigma\overline{V_m}}{RT} = \left(\frac{1}{r_1} - \frac{1}{r_2}\right) \qquad \textbf{(I. 5)}$$

If $r_1 > r_2$, then the chemical potential of the small droplets is larger than the one of the bigger droplets, therefore the monomer diffuses from the small droplets to the big ones. This effect is called Ostwald ripening and it is the source of the miniemulsion degradation by monomer diffusion. Oswald ripening is prevented by addition of low molecular weight water insoluble compound, named as costabilizer, or high molecular weight polymers, named as hydrophobes. Droplet stability increases with the amount of costabilizer added. Nevertheless it was shown that addition of costabilizer above 4wt% led to only a minor stability increase[55]. One of the most used costabilizer, highly effective in preventing Oswald ripening is hexadecane. Hexadecane remains in the particle after the polymerisation and evaporates in the atmosphere upon film formation. This can be avoided by using reactive costabilizers, like initiators and chain transfer agents or highly water insoluble reactive monomers[56]. When initiator is added in the miniemulsion, droplet nucleation occurs and ideally

case one to one copy is achieved, namely all the monomer droplets become polymer particles. Droplet nucleation occurs because the surface area of the monomer droplets is large and in ideal case no micelles are present in the system, thus the radicals add monomer units and after becoming hydrophobic enough enter the monomer droplets. After previously reported difficulties using ab initio and seeded emulsion polymerizations, it was expected that elimination of the need of the RAFT agent to be transported through the water phase would alleviate the encountered stability problems. However, when RAFT was implemented in miniemulsion, again several adverse phenomena were observed, namely inefficient droplet nucleation, loss of molecular weight control, high level of coagulum, thick red layers (phase separation) forming during polymerization (after initiation) and very slow polymerization rates. Primarily, stability issues were reported in RAFT miniemulsion polymerization by Brouwer et al.[57,58] when an anionic surfactant was used. Luo-Tsavalas-Schork attributed this to the “superswelling theory”[59]. This theory is based on an early work of Ugestal et al.[60] which describes the swelling capacity of the latex particles that contain polymers and oligomers which differ in swelling capacity. The main difference between standard polymerization and the one which involves highly active RAFT agent is that in RAFT polymerization there is a time interval early in the reaction where oligoradicals dominate in the MWD. This effect is neglected in FRP due to the presence of high molecular weights chains from the early stage of polymerization. Luo and co-workers claimed that the growing particles in RDRP will

have a lower chemical potential than non-nucleated droplets due to the "superswelling effect" of small oligomers. To reduce the chemical potential in the system, as previously discussed, there is diffusion of monomer from droplets to oligomeric particles. Ugelstad et al.[60,61] demonstrated with experimental and theoretical data that oligoradicals are very effective swelling agents and can cause high swelling of polymer particles with monomer. On the other hand, high molecular weight polymers swell monomer to a much lesser extent. Since the oligoradicals dominate the MWD early in the reaction, there will be a large amount of monomer transferred from droplets (high monomer chemical potential) to oligomeric particles (low monomer chemical potential), which will give rise to the colloidal instability and ultimately loss of molecular weight control. Luo et al. also showed that the superswelling equilibrium will be affected by the stabilizer concentration and length, initial droplet size, interfacial tension, and molecular weight of the control agent (RAFT agent) concentration. They concluded that larger particles, higher amount of costabilizer and lower molecular weight controlling agent concentrations would solve the issues encountered when performing ionically stabilized RAFT miniemulsion polymerization. Furthermore, Brouwer and the coworkers[57] using non-ionic surfactant Brij 98 supported Luo's finding and showed that the polymerization became well controlled in molecular weight and colloidal stability, however they observed retardation in polymerization rate. The tendency of non-ionic surfactants to better stabilize the miniemulsions, results from the fact that they produce larger

droplets/particles than anionic surfactants, and the extent of superswelling decreases with increasing droplet/particle size[59]. McLeary[62] applied the suggestions of Luo et al. and successfully performed ionically stabilized RAFT miniemulsion polymerization with reasonable conversion and low polydispersity using high amount of surfactant. Luo et al. further extended the research and following the recommendations (high amount of surfactant and costabilizer) they successfully polymerized A–C block copolymers (C block is a copolymer of A and B) with predictable results[63]. In this context, with a proper choice of the polymerization conditions this issue was easily overcome and miniemulsion was successfully used for the synthesis of block copolymers with living character[64–66].

I.5. Film Formation

Latex film formation is the process of transforming a stable dispersion of colloidal polymer particles into a continuous film. The film formation process shown in Figure I.11 involves mainly three steps (drying, particle deformation and polymer interdiffusion between particles) and has a pronounced influence on the final film properties. When a stable dispersion (latex) is deposited on a surface and subjected to evaporation, particles come together in close packaging (stage II). As the particles come into closer contact, they deform from their spherical shape in order to fill the void space around them and honeycomb structure is formed (stage III). Since the

interparticle voids are lost, the particle layer becomes optically transparent, since light is no longer scattered by heterogeneities in the refractive index. Transparency onset is generally used to define the point of film formation.

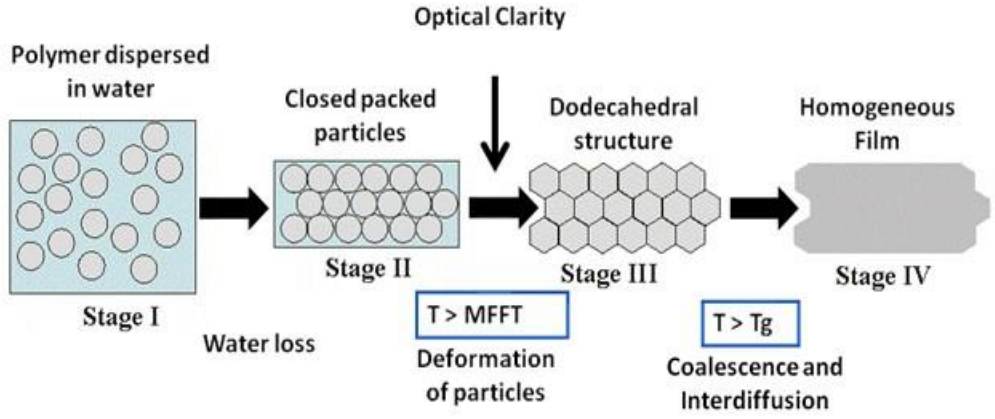

Figure I. 11. Waterborne emulsion/miniemulsion film formation stages.

The minimum temperature at which optical transparency is obtained is defined as "minimum film formation temperature" or "MFFT". Upon particle deformation, their surface come into intimate contact over large areas and above the polymer's Tg, interdiffusion of molecular chains across the boundary between particles occurs (Figure I.12). This leads to formation of continuous film which has increased mechanical strength (stage IV)[67].

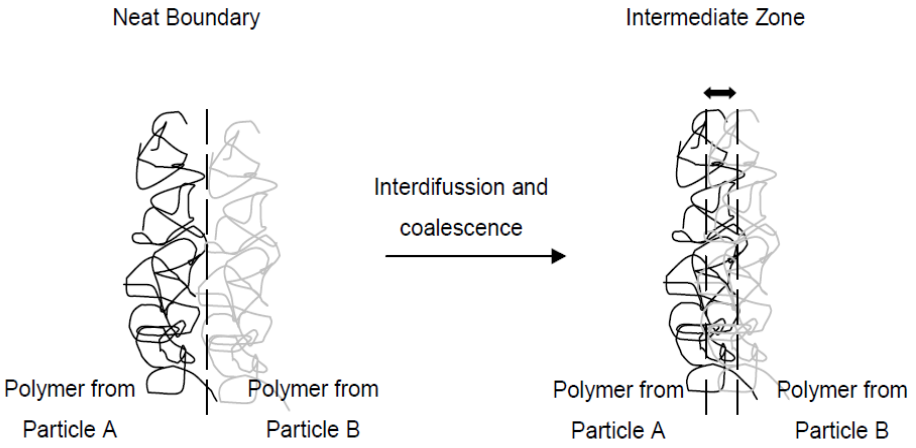

Figure I.12. Scheme of interdiffusion and entanglement formation at the polymer/polymer boundary between particles

Block copolymers of AB[63,65,68] and ABA type[65] have been successfully synthesized by RAFT miniemulsion polymerization and the nanostructured particle[69–71] morphology has been profoundly investigated. In contrast, the film formation from the nanostructured latex has not been explored. Films were generally cast from solution[72,73] and the phase separation was studied. Yang and coworkers[71] were the only authors who studied the morphology of the films obtained directly from the latex. They synthesized ABA triblock copolymers by RAFT miniemulsion polymerization starting from a macroRAFT agent. Casting of latex produced films exhibiting nanostructured morphologies which did not attain thermodynamic equilibrium even

after thermal annealing. This was attributed to the kinetic limitations on interparticle self-assembly of copolymers. However, there was a lack of information in the article on the film preparation and annealing conditions.

I.6. Application of block copolymers synthesized by RAFT

Since 1998 (the year of filing of the first RAFT patents)[50], more than 500 patent applications pertaining to RAFT polymerization have been filed by more than 100 companies, and the rate of patenting continues to increase. A survey of granted US patents in the field of RAFT[74] has been published by Thang et al. These patents cover multiple applications including polymer therapeutics, drug delivery[77], biosensors,[78], plastic solar cells, microelectronics, desalination membranes, cosmetics, lubricants, surfactants, paints and inks, thickeners for aqueous systems etc. Moreover block or star copolymers synthesized via RAFT polymerization have been used in optoelectronics[77] as well as rheology control agents[7]. Several patent publications deal with pressure sensitive adhesive[78–80] or adhesive masses based on triblock polymers synthesized with RAFT polymerization. Furthermore, patent publication dealing with temperature and pH responsive block copolymers has also been launched[81]. Nevertheless, all these polymers have been synthesized in bulk or solution and/or used as components to improve adhesions. Waterborne systems are more beneficial for the reasons discussed previously in the chapter. However, block

copolymers synthesized via RAFT polymerization are mostly described for specialty applications like dispersant additives in aqueous systems and not for big volume polymer applications in the industry. Orica Consumer Products for example produced amphiphilic reactive block copolymers as surfactants to produce latexes with controlled particle size[82]. Furthermore they extended their invention[83] to the possibility to produce stable latexes and encapsulate pigments like TiO_2.

In this thesis, among the different potential applications of waterborne block copolymers, the influence of temperature responsiveness of ABA and AB block copolymers on heat seal lacquers applications has been studied.

I.7. Heat sealing

Heat seal is a conventional technique used in packaging industry for joining polymer films or different substrates by polymer film. Numerous types of heat sealing techniques are available nowadays and include jaw-type bar sealers, rotatory sealers, bead sealers, hot knife or side-weld sealers etc. The operation mechanism includes pressing together two films between heated platens or dies to achieve fusion at the interface.

A key factor in heat sealing techniques is the proper control of process parameters such as: (i) platen temperature, (ii) dwell time, and (iii) pressure. In

commercial practices, to achieve high production rates, the dwell time which is the time of contact between the platens and films is very short, of the order of a second or less. The general mechanism or molecular processes which occur during heat sealing of a semi-crystalline polymer is schematically illustrated in Figure 1.13.

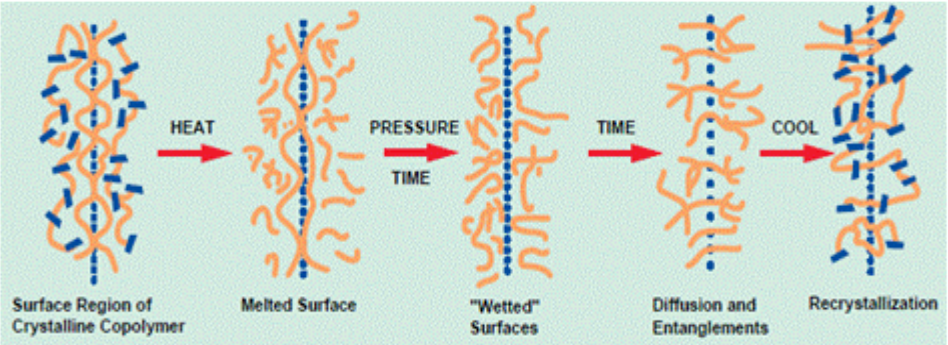

Figure I.13. Molecular processes involved in heat sealing of semicrystalline polymer films[86]

It generally involves several steps: initially two surfaces are brought together into intimate Van der Waals contact by means of pressure, then heat is applied through seal bars or hot wires causing the surface to melt and the application of slight pressure causes increased molecular contact or wetting of the molten film surfaces. When sufficient time is given, polymer chain segments from the opposite sides of the interface diffuse across the interface, and molecular entanglements between polymer molecules in the interfacial zone are created. Then the cooling leads to crystallization or stiffening of the the polymer, yielding a heat seal joint.

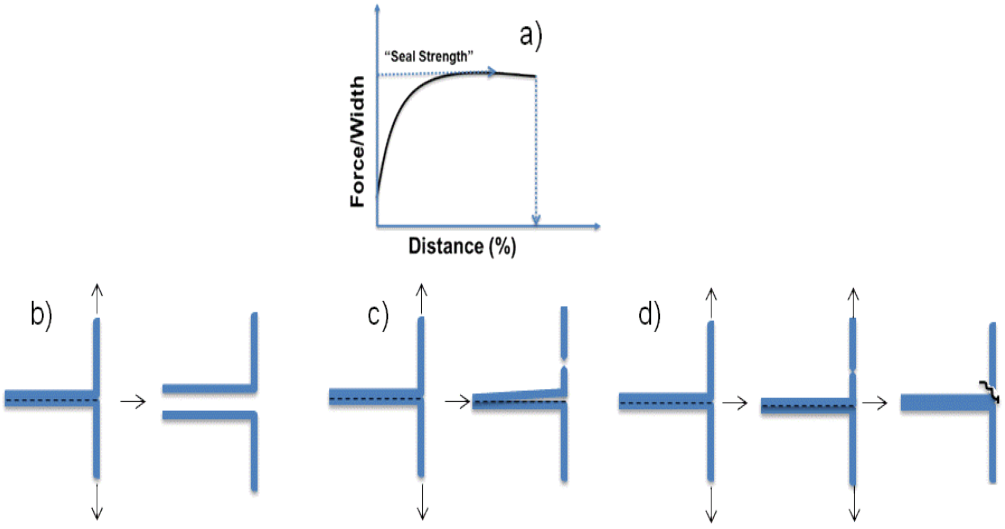

Figure I.14. Schematic illustration of T-peel test and the type of seal failures that can be observed a) force vs. extension curve b) peeling failure, c) peeling and tearing failure and d) tearing failure

T-peel tests are generally used for testing heat seals between thin films. The two legs of a test piece are pulled at a constant rate and force vs. extension curve is obtained as illustrated in Figure I.14. The seal strength is defined as maximum force/width value obtained (Figure I.14a). Failure of the test piece occurs at sufficient high extension. As an indicator of the toughness of the seal, generally the elongation of the test piece at failure (seal elongation) and the area under the curve (seal energy) are taken. Generally, three types of failure can occur; (i) peeling failure (ii) peeling and tearing failure and (iii) tearing failure, as illustrated in Figure I.14.

Lack of diffusion during seal formation generally results in peeling failure and clean separation of sealed surfaces occurs. This type of failure is caused by inadequate heating, by incompatibility of blend components in a sealant or by cross-linking at the surface before sealing and is sometimes a desirable property, e.g. in cereal liners. Tearing mode is the most common failure mode. In this type of failure, the interface between films is not separated and rupture of the film adjacent to the seal occurs. This suggests the maximum seal strength and the strength defined above, measures the bulk properties of the film rather than an interfacial property.

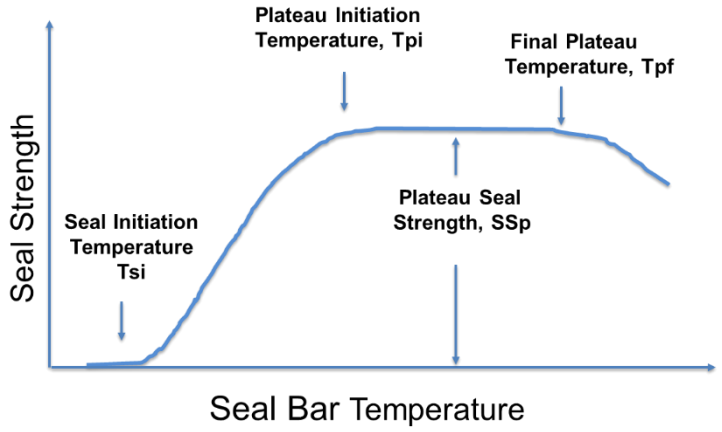

Figure I.15. Heat sealing curve, SS(T), relating sealing temperature and seal strength for semicrystalline polymers

The sealing curve (schematic plot of the apparent seal strength vs. platen temperature plot SS(T)) shown in Figure I.15 for a crystalline polymer, is described

with relatively universal terms. Seal initiation temperature Tsi, is the temperature at which a measurable but low level of seal strength is achieved. Peeling failure is observed when the seal bar temperature is substantially lower than the melting point of the polymer. As the sealing temperature increases, the seal strength levels off at Tpi, a plateau region begins after which the seal strength begins to drop off rapidly and seal distortions occur (Tpf).

Heat seal lacquers are useful coatings for lidding and other end-uses where a flexible substrate is coated at one side, stored, transported, or otherwise processed. Then this substrate is sealed to another surface at a later time with heat and pressure. These coatings can be melt-applied polymers such as polyethylene or polypropylene extruded onto the web, or they can be applied in the liquid state and solvent-based solutions or water-based dispersions.

The pioneering work on heat bar sealing applications of plastic films was done by Theller[84] who reported that interfacial temperature and dwell time are the primary factors which control the heat-seal strength on low density polyethylene films (LDPE). Moreover, he concluded that slight pressure was required to bring the two films surfaces into intimate contact and that higher pressures had little further effect on seal strength. Several other authors also studied the heat sealing process variables. The effect of heat sealing process variables like seal bar temperature, dwell time and

pressure on sealing properties (seal strength, seal elongation and seal energy) of polyethylene films was quantitatively determined by Meka and Stehling[85,86]. In their first paper [85] they used a finite element modelling technique to calculate the interfacial temperature as a function of time during the sealing of semi-crystalline polymer films. They estimated the required platen temperature for the highest possible heat seal strength of a semi-crystalline polymer, with the given dwell time and interfacial temperature by finite element analysis calculation/model. They found out that increasing the dwell time from 0.4 to 1.4 s at 130°C platen temperature, seal strength increases only by 10% and that at higher platen temperature, the effect of dwell time is even smaller. They also confirmed the earlier finding of Teller: the heat seal strength is primarily controlled by sealing temperature and dwell time but not pressure. However, they concluded that when two microscopically uneven heated surfaces are brought together, a small undetermined level of pressure should be required to bring the surfaces into intimate contact across a significant fraction of the film surface. The plot heat seal strength versus platen temperature was also established in their study. The effect of heat sealing temperature on the mechanical properties of oriented polypropylene (OPP)/cast polypropylene (CPP) laminate films was investigated by Tetsuya group[87]. They stated that the orientation of the films had great effect on the tensile strength of the seal. Furthermore an investigation on the failure criteria of the heat sealed part of the OPP/CPP heat seals made by impulse type heat sealing machine was done by the group of Tsujii[88], who found out that the

heat seals were stronger in the transverse direction as compared to the machine direction. Yuan et al.[89] further extended the research of bar sealing parameters on heat seal strength of OPP/ metallic cast propylene (MCPP) laminate film and based on the results developed a bar sealing process window. They found out that the highest achievable heat seal strength was at the plateau region with corresponding failure modes of delaminating, tearing or combined failure modes (delaminating and tearing).

Many packaging printers and converters prefer to print or coat liquid heat seal coatings, allowing them the flexibility to keep fewer substrates on hand and to apply a heat seal layer in-line over printed graphics. Additionally, a substrate with a thin, liquid- applied coating can be recyclable, which is an advantage over heat sealable substrates with extruded polyethylene or laminated films. In terms of production throughput, a relatively low seal initiation temperature and plateau initiation temperature of a coating allow for more packages to be sealed in a given time. However, a coating with a low seal temperature can also be prone to blocking in a roll or stack, where the pressure is high enough to cause the coating to stick to the layer above it at storage conditions. This then leads to difficulty in unwinding, surface defects, or equipment jamming during the converting process. Careful choice and formulation of the heat seal coating can go a long way in balancing these properties.

Liquid like heat seal coatings can be either solvent or water based. In water based heat-seal coatings semi-batch approach is generally used. By this process water-based dispersion with core shell morphology can be produced, where the core and shell properties can be tailored for a better balance of properties. Shell with higher Tg can encapsulate a core of lower Tg core and blocking can be reduced at storage conditions. Then when lacquers during the heat sealing process are exposed to heat and pressure, the Tg of the hard phase can be overcome, allowing the phases to undergo an inversion or be mixed[90]. This brings the softer core material into the continuous phase and allows the surface wetting and chain mixing necessary to form a good bond. Many companies have been dealing with patents for production of heat seal lacquers based on polymer dispersions with core shell morphology, where the core and shell have different Tg as explained above. Toagosei Co. Tokyo, U.S[91] patented a polymer for a heat-sensitive adhesive sheet that has non or low adhesive properties at ordinary temperature but exhibits adhesive properties upon heating and/or applying pressure and can be used without subjecting any release treatment to the adhesive layer. BASF Ludwigshafen[92] disclosed aqueous dispersions for heat-seal applications with high amounts of carboxylic resins, having high Tg. Such high glass transition temperature polymers are generally known as support resins and while providing good colloidal stability, tend to impart unacceptable moisture sensitivity in applications where exposure to moisture occurs. Furthermore they also investigated[93] the effect of polymer design and formulation on the performance of

water-based acrylic dispersions for heat seal lacquers. They investigated three different commercial styrene-acrylic dispersions with different compositions of hard and soft phases, and different pH and different substrates. Röhm GmbH, Darmstadt[94], patented an aqueous synthetic resin dispersion comprising latex of a core material with a glass transition temperature above 60° C and a shell material with a glass transition temperature below 80° C . They claimed that the aqueous dispersion has a low minimum film forming temperature which give films or coatings having relatively high block point and slight tackiness and hardness sufficient for technical use. Ashland[95] disclosed a method of using a heat activatable adhesive for laminating vinyl sheet to wood, that is heat activated at temperatures as low as 71° C and the laminate resists delamination at 88° C. Dow[96] patented a method for forming a heat sealable coating on at least one oriented polymer with a heat seal initiation temperature of less than 80°C. Lubrizol Advanced Materials[97], patented a heat sealable adhesive dispersions for plastic and metal containers for moderate to high moisture food products with minimum film formation temperature near or below 25°C and blocking resistance up to 50° C. Later on they extended their invention[98] to a heat sealable adhesive composition having even higher moisture resistence for food packaging and related uses and enhanced wetting at the heat seal temperature of 66-200 °C. Evonik Industries[99] disclosed aqueous binders for heat-sealable coatings which adhere on aluminium without use of any primer, permit good sealability of the

coated aluminium foil with respect to pSt and/or PVC, and moreover feature good blocking resistance even at temperatures above 40°C.

As described above all the patents literature for heat seal lacquers are dealing with the synthesis of high Tg shell and low Tg core morphology polymer dispersions to avoid blocking when in a roll or a stack. However, this limits the possibility of low seal temperature which is desired for higher production throughput. To overcome these obstacles in this PhD thesis a different approach is tried. Waterborne block copolymers dispersions of hard/crystalline and soft domain were synthesized. In this way we were able to design the Tg of the hard phase or the Tm of the crystalline domains in a such way to bring a low seal initiation temperature and at the same time to avoid blocking at room temperature.

I.8. Objective

The objective of this thesis is to develop a strategy to synthesize by means of RAFT in safe and environmentally friendly way waterborne dispersions of well-defined block copolymers which form nanophase separated particles containing crystalline/soft and hard/soft domains that provide temperature responsiveness. Next to the synthesis, it is intended to study the film formation behavior of the block copolymer dispersions in order to understand how temperature responsiveness can be applied to control morphology and the resulting material properties of the films.

Block copolymers with hard/soft domains and crystalline/soft domains were synthesized to explore the use of the Tg of the amorphous hard phase or the melting temperature of the crystalline phase as triggering temperature. To achieve stable waterborne dispersions of well-defined block copolymers, the synthesis was done in two reactions steps and carefully studied for the conditions of controlled polymerization. First, miniemulsion polymerization was used for the synthesis of the crystalline/hard domains. Then in the second step, the controlled polymerization was continued with 2EHA to form soft domains. The effect of the polymer architecture (diblock, triblock, different Mw of the blocks) on particle morphology and that of the particle morphology on film morphology and mechanical properties of the films were investigated. As the final step, the block copolymers were tested as heat seal lacquers to explore this as a potential application field for the temperature responsiveness.

I.9. Outline of the thesis

In **Chapter II**, the optimization, synthesis and characterization of ABA waterborne block copolymers containing hard-soft-hard domains consisting of polystyrene (pSt) as outer block and poly2-ethylhexyl acrylate (p2EHA) soft middle block by means of RAFT polymerization in two steps, will be shown.

In **Chapter III,** optimization and synthesis of AB waterborne block copolymers having hard-soft domains synthesized using styrene and 2EHA monomers will be described. These copolymers were synthesized for comparison purposes with the ABA block copolymers.

In **Chapter IV,** the synthesis and characterization of ABA waterborne block copolymers containing crystalline-soft-crystalline domains will be discussed. Long chain acrylate (stearyl acrylate-SA) and 2EHA were used for the synthesis of the crystalline/soft domains respectively.

In **Chapter V,** the morphology of the synthesized block copolymers obtained was analyzed by with TEM and AFM, and their mechanical properties were studied by DMTA.

In **Chapter VI** the application properties of the block copolymers as heat seal lacquers will be shown.

In **Chapter VII** the most relevant conclusions of the thesis will be presented.

In order to avoid repetition of the experimental and characterization techniques, a detailed description of the materials, synthetic procedures and characterization methods is given in the Appendix.

I.10. References

1 P. B. Zetterlund, Y. Kagawa, and and M. Okubo, *Chem. Rev.*, 2008, **108**, 3747–3794.

2 J. M. Asua, *J. Polym. Sci.*, 2004, **42**, 1025–1041.

3 M. Szwarc, *Nature*, 1956, **178**, 1168–1169.

4 M. Szwarc, M. Levy and R. Milkovich, *J. Am. Chem. Soc.*, 1956, **78**, 2656–2657.

5 J. Nicolas, Y. Guillaneuf, C. Lefay, D. Bertin, D. Gigmes and B. Charleux, *Prog. Polym. Sci.*, 2013, **38**, 63–235.

6 K. Matyjaszewski, *Macromolecules*, 2012, **45**, 4015–4039.

7 G. Moad, E. Rizzardo and S. H. Thang, *Chem. - An Asian J.*, 2013, **8**, 1634–1644.

8 M. R. Hill, R. N. Carmean and B. S. Sumerlin, *Macromolecules*, 2015, **48**, 5459–5469.

9 P. B. Zetterlund, S. C. Thickett, S. Perrier, E. Bourgeat-Lami and M. Lansalot, *Chem. Rev.*, 2015, **115**, 9745–9800.

10 J. Qiu, B. Charleux and K. Matyjaszewski, *Prog. Polym. Sci.*, 2001, **26**, 2083–2134.

11 W. A. Braunecker and K. Matyjaszewski, *Prog. Polym. Sci.*, 2007, **32**, 93–146.

12 B. Y. K. Chong, T. P. T. Le, G. Moad, E. Rizzardo and S. H. Thang, *Macromoleculars*, 1999, **32(6)**, 2071–2074.

13 J. Jennings, G. He, S. M. Howdle and P. B. Zetterlund, *Chem. Soc. Rev.*, 2016, **45**, 5055–5084.

14 J. B. McLeary and B. Klumperman, *Soft Matter*, 2006, **2**, 45–53.

15 J. Chiefari, Y. K. B. Chong, F. Ercole, J. Krstina, J. Jeffery, T. P. T. Le, R. T. A. Mayadunne, G. F. Meijs, C. L. Moad, G. Moad, E. Rizzardo and S. H. Thang, *Macromolecules*, 1998, **31**, 5559–5562.

16 G. Moad, E. Rizzardo and S. H. Thang, *Aust. J. Chem.*, 2005, **62**, 379–410.

17 S. R. S. Ting, T. P. Davis and P. B. Zetterlund, *Macromolecules*, 2011, 4187–4193.

18 B. Klumperman, E. T. A. Van Den Dungen, J. P. A. Heuts and M. J. Monteiro, *Macromol. Rapid Commun.*, 2010, **31**, 1846–1862.

19 W. Meiser, J. Barth, M. Buback, H. Kattner and P. Vana, *Macromolecules*, 2011, **44**, 2474–2480.

20 C. Barner-Kowollik, *Handbook of RAFT Polymerization*, WILEY-VCH Verlag GmbH & Co. KGaA, Weinheim, 2008.

21 D. J. Keddie, G. Moad, E. Rizzardo and S. H. Thang, *Macromolecules*, 2012, **45**, 5321–5342.

22 G. Moad, E. Rizzardo and S. H. Thang, *Polymer*, 2008, **49**, 1079–1131.

23 M. Benaglia, M. Chen, Y. K. Chong, G. Moad, E. Rizzardo and S. H. Thang, *Macromolecules*, 2009, **42**, 9384–9386.

24 J. Chiefari, R. T. A. Mayadunne, C. L. Moad, G. Moad, E. Rizzardo, A. Postma, M. A. Skidmore and S. H. Thang, *Macromolecules*, 2003, **36**, 2273–2283.

25 H. Fischer and L. Radom, *Macromol. Symp.*, 2002, **182**, 1–14.

26 Y. Zhao, B. Qi, X. Tong and Y. Zhao, *Macromolecules*, 2008, **41**, 3823–3831.

27 Y. Yu, X. Sun, R. Zhang, S. Yuan, Q. Lu and Z. Wu, *J. Polym. Res.*, 2017, **24**, 1–6.

28 R. Ma, R. Ma, L. Feng, L. Fan, Y. Liu, B. Xing, Y. Hou and F. Bao, *Colloids Surfaces A Physicochem. Eng. Asp.*, 2009, **346**, 184–194.

29 B. Y. K. Chong, J. Krstina, T. P. T. Le, G. Moad, A. Postma, E. Rizzardo and S. H. Thang, *Macromolecules*, 2003, **36**, 2256–2272.

30 F. S. Bates and G. H. Fredrickson, *Phys. Today*, 1999, **52**, 32–38.

31 M. C. Orilall and U. Wiesner, *Chem. Soc. Rev.*, 2011, **40**, 520–535.

32 Y. Mai and A. Eisenberg, *Chem. Soc. Rev.*, 2012, **41**, 5969–5985.

33 E. Helfand and Z. R. Wasserman, *Macromolecules*, 1978, 960–966.

34 M. W. Matsen and M. Schick, *Phys. Rev. Lett.*, 1994, **72**, 2660–2663.

35 M. W. Matsen and F. S. Bates, *Macromolecules*, 1996, **29**, 1091–1098.

36 F. S. Bates, *Science*, 1990, **251(4996)**, 898–905.

37 I. W. Hamley, *Interfaces Cryst. Viscoelasticity*, 1999, **148**, 113–137.

38 H. Takeshita, T. Shiomi, K. Takenaka and F. Arai, *Polymer*, 2013, **54**, 4776–4789.

39 S. Nakagawa, H. Marubayashi and S. Nojima, *Eur. Polym. J.*, 2015, **70**, 262–275.

40 R. M. Michell and A. J. Müller, *Prog. Polym. Sci.*, 2016, **54-55**, 183–213.

41 A. J. Müller, V. Balsamo and M. L. Arnal, *Nucleation and Crystallization in Diblock and Triblock Copolymers*, Springer-Verlag Berlin, Heidelberg, 2005.

42 Y. L. Loo, R. A. Register and A. J. Ryan, *Macromolecules*, 2002, **35**, 2365–2374.

43 B. Nandan, J. Y. Hsu and H. L. Chen, *Polym. Rev.*, 2006, **46**, 143–172.

44 M. J. Derry, L. A. Fielding and S. P. Armes, *Prog. Polym. Sci.*, 2016, **52**, 1–18.

45 D. Boschmann and P. Vana, *Macromolecules*, 2007, **40**, 2683–2693.

46 J. Y. T. Chong, D. J. Keddie, A. Postma, X. Mulet, B. J. Boyd and C. J. Drummond, *Colloids Surfaces A Physicochem. Eng. Asp.*, 2015, **470**, 60–69.

47 I. Uzulina, S. Kanagasabapathy and J. Claverie, *Macromol. Symp.*, 2000, **150**, 33–38.

48 M. J. Monteiro, M. Hodgson and H. De Brouwer, *J. Polym. Sci. Part A Polym. Chem.*, 2000, **38**, 3864–3874.

49 J. M. Asua, *Polymer reaction enginering*, Blackwell Oxford, 2007.

50 WO9801478, 1998.

51 I. Uzulina, S. Kanagasabapathy and J. Claverie, *Macromol. Symp.*, 2000, 33–38.

52 S. Nozari and K. Tauer, *Polymer*, 2005, **46**, 1033–1043.

53 S. Nozari, K. Tauer and A. M. I. Ali, *Macromolecules*, 2005, **38**, 10449–10454.

54 S. W. Prescott, M. J. Ballard, E. Rizzardo and R. G. Gilbert, *Macromolecules*, 2002, **35**, 5417–5425.

55 J. M. Asua, *Prog. Polym. Sci.*, 2002, **27**, 1283–1346.

56 B. T. Pérez-Martínez, L. Farías-Cepeda, V. M. Ovando-Medina, J. M. Asua, L. Rosales-Marines and R. Tomovska, *Beilstein J. Nanotechnol.*, 2017, **8**, 1328–1337.

57 H. De Brouwer, J. G. Tsavalas, F. J. Schork and M. J. Monteiro, *Macromolecules*, 2000, **33**, 9239–9246.

58 H. De Brouwer, J. G. Tsavalas, F. J. Schork and J. Michael, *Macromolecules*, 2001, **34(12)**, 3938–3946.

59 Y. Luo, J. Tsavalas and F. J. Schork, *Macromolecules*, 2001, **34**, 5501–5507.

60 J. Ugelstad and P. C. and Moerk, *Adv. Colloid Interface Sci.*, 1980, **13**, 101–140.

61 J. Ugelstad, K. H. Kaggerud, F. K. Hansen and A. Berge, *Makromol. Chemie*, 1979, **180**, 737–744.

62 J. B. Mcleary, M. P. Tonge, D. DE WET Roos, R. D. Sanderson and B. Klumperman, *J. Polym. Sci. Part A Polym. Chem.*, 2004, **42**, 960–974.

63 Y. Luo and X. Liu, *J. Polym. Sci. Part A Polym. Chem.*, 2004, **42**, 6248–6258.

64 L. Yang, Y. Luo and B. Li, *Polymer*, 2006, **47**, 751–762.

65 A. Bowes, J. B. Mcleary and R. D. Sanderson, *J. Polym. Sci. Part A Polym. Chem.*, 2007, **45**, 588–604.

66 Z. X. Wang, Q. H. Zhang, Y. T. Yu, X. L. Zhan, F. Q. Chen and J. H. Xiong, *Chinese Chem. Lett.*, 2010, **21**, 1497–1500.

67 J. L. Keddie and A. F. Routh, *Fundamentals of Latex Film Formation*, Springer, Dordrecht, 2010.

68 A. Butte, G. Storti and M. Morbidelli, *Macromolecules*, 2001, **34**, 5885–5896.

69 R. Wei, Y. Luo and Z. Li, *Polymer*, 2010, **51**, 3879–3886.

70 P. Froimowicz, B. Van Heukelum, C. Scholten, K. Greiner, O. Araujo and K. Landfester, *J. Polym. Sci. Part A Polym. Chem.*, 2014, **52**, 883–889.

71 L. Yang, Q. Han, Q. Song, H. Li, Q. Zhao, Y. Shen and Y. Luo, *Colloid Polym. Sci.*, 2017, **295**, 891–902.

72 Z. Wang, Q. Zhang, X. Zhan, F. Chen, G. Rao and J. Xiong, *J. Polym. Res.*, 2013, **20**, 1–13.

73 R. Wei, Y. Luo, W. Zeng, F. Wang and S. Xu, *Ind. Eng. Chem. Res.*, 2012, **51**, 15530–15535.

74 G. Moad, B. E. Rizzardo and S. H. T. A, *Aust. J. Chem.*, 2012, **65**, 985–1076.

75 Z. An, Q. Qiu and G. Liu, *Chem.Commun*, 2011, 12424–12440.

76 D. Smith, A. C. Holley and C. L. McCormick, *Polym. Chem.*, 2011, **2**, 1428–1441.

77 G. Moad, M. Chen, H. Matthias, A. Postma, E. Rizzardo and S. H. Thang, *Polym. Chem.*, 2011, **2**, 492–519.

78 US Patent 7 521, 2009.

79 US Patent 7 514 515, 2009.

80 US Patent 8 012 581, 2011.

81 US 7 718 193, 2010.

82 WO2003055919A1, 2003.

83 WO2006037161A1, 2006.

84 H. W. Theller, *Plast. Film Sheeting*, 1989, **5**, 66–93.

85 P. Meka and F. C. Stehling, *J. Appl. Polym. Sci.*, 1994, **51**, 89–103.

86 F. C. Stehling and P. Meka, *J. Appl. Polym. Sci.*, 1994, **51**, 105–109.

87 T. Tetsuya, U. S. Ishiaku, M. Mizoguchi and H. Hamada, *J. Appl. Polym. Sci.*, 2005, **97**, 753–760.

88 T. T. Hashimoto Yasuo, Ishiaku U.S, Leong Y.W. , Hamada Hiroyuki, *Polym. Eng. Sci.*, 2006, **46**, 205–214.

89 C. S. Yuan and A. Hassan, *Express Polym. Lett.*, 2007, **1**, 773–779.

90 J. W. Taylor and M. A. Winnik, *J. Coatings Technol. Res.*, 2004, **1**, 163–190.

91 US 6368 707 B1, 2002.

92 US 5385 967A, 1995.

93 J. Rigney, B. Corporation, F. Reinhold and B. Corporation, *SPE ANTAC Anaheim*, 2017, 1278–1282.

94 US 5306 743, 1994.

95 US 5837089A, 1998.

96 US 8,383,723 B2, 2013.

97 WO 2011/017388 A2, 2011.

98 US 2017/0009111A1, 2017.

99 US 2015/0191619, 2015.

Chapter II. Synthesis and characterization of hard-soft-hard ABA block copolymers

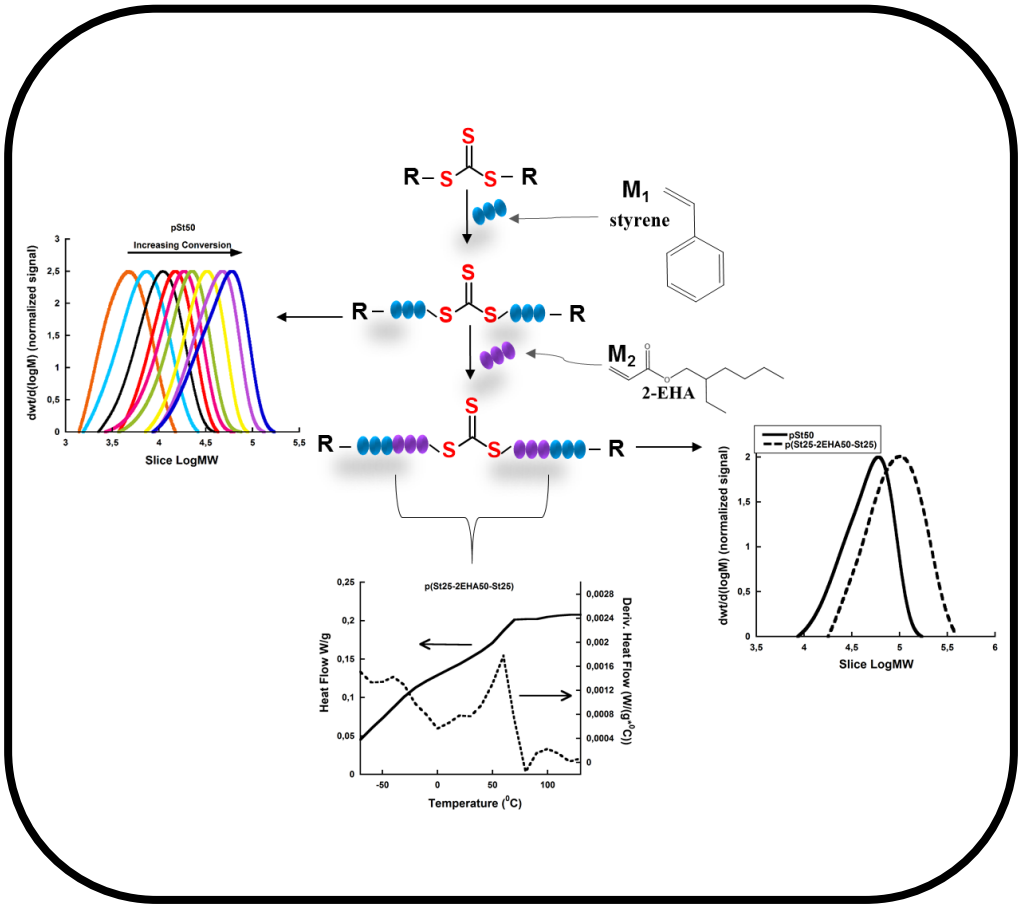

II.1. Introduction

As explained in the literature survey, compared to other living free radical polymerization methods RAFT has some advantages: (i) it can be applied to a wide range of monomers including functional monomers containing acid, hydroxyl or amino group[1], (ii) polymers with well controlled molecular weight and narrow polydispersity can be obtained; (iii) the polymerization conditions are very similar to conventional radical polymerization and (iv) the final polymers do not contain residues of metal ions. Taking into account the features of RAFT polymerization, the key point for successful experiments is the careful choice of the RAFT agent and the reaction conditions for the polymerization of the monomer of interest[2,3]. It is well known that the efficiency of RAFT agent in polymerization process is defined by the chemical nature of stabilizing Z and leaving R groups[4,5]. According to the literature data the most popular RAFT agents, especially in the polymerization of styrene and acrylates (MAMs, the more activated monomers) are thiocarbonylthio compounds[6,7]. In this context, these types of RAFT agents are less sensitive to hydrolytic and most other forms of degradation. Moreover, polymerization with this type of reagents generally displays much less discernible retardation. Polymers with predictable molecular weight, narrow molecular weight distribution, and controlled architectures (block copolymers, star polymers, etc.) continue to be of considerable interest in research

laboratories, since they are excellent model systems for establishing structure-property-performance relationships.

In this chapter, the synthesis of high molecular weight symmetric ABA block copolymers of styrene (St) and 2-ethylhexyl acrylate (EHA), containing hard (pSt) and soft (pEHA) domains by means of RAFT miniemulsion polymerization using a bifunctional symmetrical RAFT agent will be shown. Miniemulsion polymerization will be used for the A-block hard domains formation, followed by EHA feed to build the soft domains.

The motivation for synthesizing such type of block copolymers is because we would like to mimic the properties of thermoplastic elastomers and obtain polymers that would be temperature responsive. An important class of thermoplastic elastomers are microphase separated A-B-A type block copolymers, in which a physical crosslinking of a soft rubber phase B is caused by the hard high-Tg microphase. At high temperatures above the Tg of the hard phase A, the physical crosslinking is reversible and such ABA block copolymers can be easily processed like thermoplastic polymers. The most well-known commercial thermoplastic elastomers based on block copolymers are styrene-butadiene-styrene (SBS) block copolymers, in which the polybutadiene soft phase is physically crosslinked via polystyrene microphases.

Thus, we will use a bifunctional symmetrical RAFT agent and synthesize p(St-2EHA-St) block copolymers in emulsion polymerization and use the glass transition temperature of the hard pSt domain as triggering temperature.

Initially the effect of the type of initiators, temperature, molar ratio of RAFT agent to initiator and the targeted Mn on the polymerization kinetics of RAFT miniemulsion polymerization of styrene will be investigated. Once the optimal results will be achieved, the procedure for the formation of ABA block will be given. Variations were done on chemical composition and molecular weights of the block copolymers, and the polymerization kinetics and MWD's were studied. Finally, the thermal properties of the block copolymers will be studied both by TGA and DSC.

II.2. Experimental part

II.2.1. Materials

The materials used for the synthesis of hard-soft-hard block copolymers are given in the Appendix.

II.2.2. Synthesis Procedures

Synthesis of the first block: Batch Miniemulsion Polymerization

Polystyrene (pSt) "A" hard block was synthesized via RAFT miniemulsion polymerization at 30% solids content (s.c.) in water. To optimize the process, the following variables: (i) type of initiator, (ii) (RAFT):(Initiator) molar ratio, (iii) reaction temperature and (iv) targeted Mn were varied.

Table II.1. Recipe used for the synthesis of pSt homopolymers

Reactants	wt% BOM*
SA	8
Dowfax	2
Disponil A3065	1
$NaHCO_3$	0.16
n(DBTTC): n(Initiator)	
AIBN, KPS, WAKO-086	5:1
n(TBHP):n(AsAc)	
n(TBHP):n(RAFT)	5:1
n(TBHP):n(AsAc)	2:1
Other Reactants	
Water	70%
Styrene	26.7%

*BOM – Based on styrene monomer

The miniemulsion was prepared using the recipe shown in Table II.1 according to the following procedure. Initially the water phase was prepared by dissolving the surfactant Dowfax 2A (2 wt% based on styrene monomer, BOM), Disponil A3065

(1 wt% BOM) and $NaHCO_3$ (0.16 wt% BOM) in deionized water. The ingredients were mixed in a beaker using a magnetic stirrer for several minutes. The oil phase was prepared by dissolving the stearyl acrylate costabilizer (SA, 8 wt% BOM), RAFT agent (DBTTC) and initiator (in case when AIBN was used as initiator) in styrene. The mixture was stirred for 10 minutes until SA was dissolved in the monomer and a homogenous solution was produced. Then the organic phase was added to the water phase and the mixture was stirred magnetically for another 10 minutes. The coarse emulsion was then ultrasonicated for 15 min using Branson Digital Sonifier 450 (amplitude 70% and 50% duty cycle) under magnetic stirring in an ice-water bath to avoid overheating and possible initiation of the reaction. Once the miniemulsion was prepared, it was transferred to a jacketed batch reactor equipped with anchor type stirrer, a sampler inlet and a condenser. Furthermore, prior to polymerization the miniemulsion was purged with nitrogen for 30 min under agitation of 60 rpm to eliminate the dissolved oxygen and then the temperature was increased. When the desired temperature was reached, the agitation was increased to 100 rpm and time 0 was marked. Samples were taken at different time intervals and they were quenched with 1wt% hydroquinone (HQ) water solution to stop the polymerization. The reaction was performed for 360 min, then the temperature was decreased to 25°C, the final latex was collected and filtered. In addition, when water-soluble initiators were used, they were dissolved in water (2.5-2.9 wt%) and the solution was purged with nitrogen and added in one shot once the desired polymerization temperature was reached.

Furthermore, when the redox pair TBH/AsAc was used for initiating polymerisation, AsAc was added as a shot once the temperature was increased (70°C) and TBHP 6% solution was fed for 1h. The molar ratio of RAFT to TBHP was 5:1 and TBHP:As.Ac. molar ratio was 2:1.

Polystyrene polymers with different targeted Mn were synthesized using the recipe shown in Table II.1 and the equation shown below:

$$\overline{Mn_{theory}} = M_{RAFT} + \frac{x[M]oM_M}{[RAFT]o} \quad \text{(II.1)}$$

Where $\overline{Mn_{theory}}$ represents the predicted molecular weight, M_M is the molecular weight of the monomer, M_{RAFT} is the molecular weight of the RAFT agent, x is the conversion, $[M]o$ and $[RAFT]o$ are the initial moles of the monomer and the RAFT agent respectively. The amount of initiator was not considered in the calculation of the theoretical Mn due to the relatively small amount used compared to RAFT agent. This approach was also used by de Brouwer[8], who disregards the chains derived from the initiator in the calculation, due to the low efficiency of initiator systems such as AIBN in heterogeneous polymerizations. The amount of costabilizer used was also not included in the calculation of the targeted Mn.

Synthesis of the second block: Semi-batch emulsion polymerization

Polystyrene initial A block was used as a seed for the synthesis of the second middle B block. The B block was formed by feeding the monomer (2EHA) as a pre-emulsion for 3 h and polymerization was continued for 2 h batch wise to reach higher conversion. The preemulsion consisted of monomer, water and the emulsifiers (Dowfax 2A and Disponil A3065). The total amount of surfactants was kept constant 3 wt% based on all monomers. An additional amount of AIBN dissolved in monomer was added once the temperature was increased to 70°C to start the polymerization. The initiator added was calculated based on the amount of the moles of the RAFT agent present in the seed and was kept constant at a mol ratio of (RAFT):(Initiator) = 2:1. To remove the dissolved oxygen, the seed and the pre-emulsion were purged with nitrogen for 30 min prior to polymerization. The initiator dissolved in monomer was purged for 10 min too. Furthermore, nitrogen flow was kept during polymerization as well. At the end of the reaction, the temperature was decreased, and the latex was filtered and collected.

II.2.3. Characterization

Stability of the miniemulsion was assayed by Turbiscan LabExpert apparatus. The conversion of the monomers was followed gravimetrically. The monomer droplet and the final particle size of the latexes was measured by dynamic light scattering

(DLS). The molecular weights and the molecular weights distribution were measured using two different GPC instruments. Thermal stability of the block copolymers was measured using DSC and TGA. The detailed description of the characterization methods is provided in the Appendix.

II.3. Results and discussion

The synthesis of the block copolymers was mediated by S,S-Dibenzyl trithiocarbonate (DBTTC) RAFT agent. DBTTC is a symmetrical RAFT agent (Figure II.1) with good homolytic leaving groups, allowing the polymerization of ABA triblock copolymers in two sequential monomer addition steps.

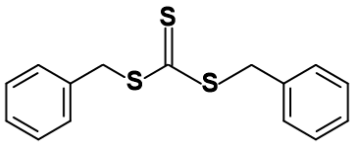

Figure II.1. Chemical structure of the DBTTC RAFT agent.

The symmetry of DBTTC guarantees that both arms are approximately the same length and composition. In the initial polymerization step, the monomer is inserted in between both leaving groups (R) and -S(C=S)- moiety and the -S(C=S)S- moiety stays in the middle of the polymer chain. In the second step, the first block is

extended by addition of a second monomer which builds in the middle and the first A blocks shift to the outside of the polymer chain (Figure II.2).

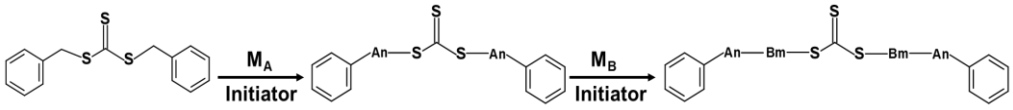

Figure II.2. Polymerization of the ABA block copolymers.

SA is a hydrophobic monomer and it is often used as a reactive costabilizer in miniemulsion polymerization to prevent Ostwald ripening[9]. It incorporates in the polymer backbone upon polymerization and stays in the film upon film formation, unlike the mostly used hexadecane costabilizer, which evaporates into the atmosphere and increases the volatile organic content of the latex. Thus, SA was used as a costabilizer for the synthesis of the initial pSt block. When homopolymerized pSA exhibits two transition temperatures; a melting temperature at around 51°C[10] and a Tg at around -100 °C[11]. Thus, according to the Fox equation[12], this costabilizer will reduce the Tg of the initial pSt block when copolymerizing with St. If the costabilizer amount does not exceed 10 wt%, pSA will not be able to crystallize.

Prior polymerization, the stability of the miniemulsion was investigated using the recipe shown in Table II.1 and using AIBN as an initiator, and the results are shown in Figure II.3. As it can be seen from the evolution of backscattered light (Figure II.3), the miniemulsion shows excellent stability during the whole 6 hours at 60 °C and no

separation or sedimentation is observed, thus this recipe was used for the synthesis of the initial pSt block.

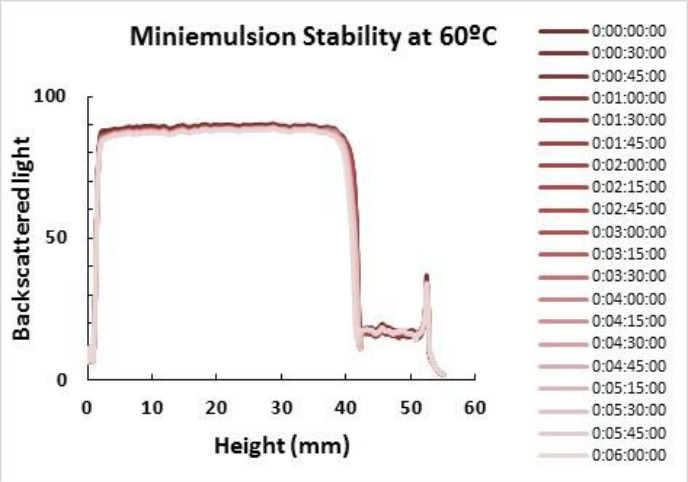

Figure II.3. Stability of the miniemulsion containing 2% Dowfax 2A1 and 1% of Disponil A3065.

As previously presented in the experimental method, four different parameters were investigated on the homopolymerization of styrene:

- Type of initiator
- Molar ratio of [RAFT]:[Initiator]
- Temperature
- Targeted Mn

II.3.1. Effect of the type of initiator on the RAFT miniemulsion polymerization of styrene

Both water soluble and oil soluble initiators are employed in miniemulsion polymerization[13]. The location where the initiators will fragmentate depends on the type of initiator used. This will influence the radical concentration in the different phases of the miniemulsion system. Even though in miniemulsion polymerization the nucleation mechanism is mostly by droplet nucleation, the type of initiator used may still influence the nucleation mechanism. Four different initiators were investigated in the homopolymerization of styrene using the recipe shown in Table (II.1).

<u>Water soluble initiators</u>:

Two water soluble thermal initiators were used: potassium persulfate (KPS), and WAKO-086 (decomposition of the initiators is shown on Figure II.4a and II.4b respectively).

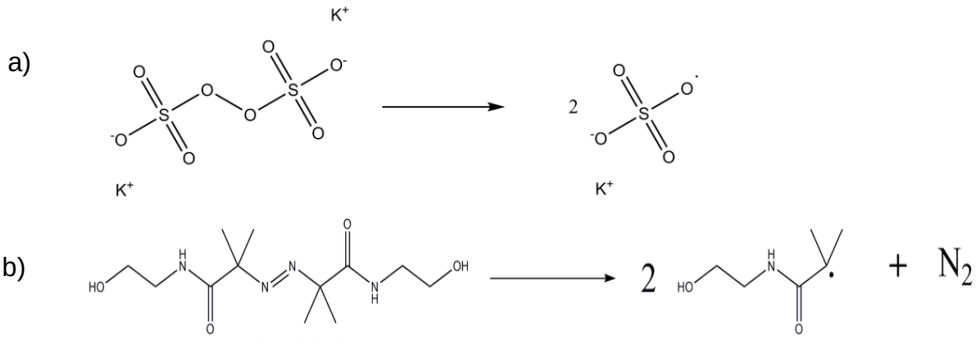

Figure II.4. Radial formation of a) KPS and b) WAKO-086.

KPS forms negatively charged hydrophilic sulfate radicals in the aqueous phase[14]. The radicals are too hydrophilic to directly enter the organic phase (monomer droplets), thus they first polymerize in the water phase until becoming sufficiently hydrophobic to enter the organic phase. WAKO-086 is nonionic and non-nitrile water soluble azo initiator having hydroxyl group at the end. The 10-hour life time temperature of KPS is 65 °C and of WAKO-086 is as high as 86 °C.

Oil soluble initiator:

AIBN- [2,2ˈ-Azobis(isobutyronitrile)] is an oil soluble thermal initiator that forms hydrophobic radicals in pairs in the organic phase (Figure II.5). Partitioning of AIBN in water is small and its contribution to the overall polymerization has been reported to be almost negligible [15]. The 10-hour life time temperature is 65 °C.

Figure II.5. Radical formation of AIBN[16].

Redox pair

Tert-butyl hydroperoxide/Ascorbic acid (TBHP/AsAc) is a redox couple (Figure II.6). TBHP distributes between aqueous and organic phases. AsAc is soluble in

water. The tert-butoxy radicals formed in the aqueous phase are hydrophobic enough to directly enter the organic phase[16].

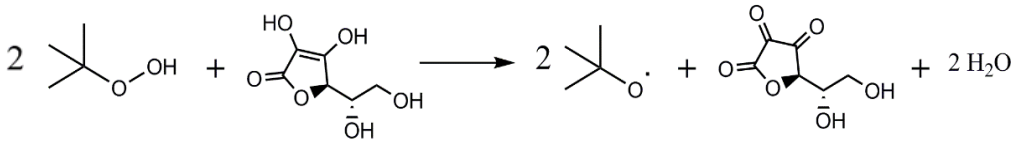

Figure II.6. Radical formation in TBHP/AsAc.[14,29].

Table II.2. Conversion, average particle size, Mn and PDI obtained at the end of reaction for pSt homopolymers synthesized using different types of initiators

Initiators	Conversion (%)	Droplet size (nm)	Particle size (nm)	Mn Theo. (g/mol)	Mn Obtained (g/mol)	PDI
WAKO-086	12.5	149.7	173.5	6,539	5,383	2.0
KPS	92.9	137.7	134.8	46,519	37,731	1.7
AIBN	71.1	122.0	145.0	35,652	35,053	1.4
TBHP/AsAc	95.9	131.1	133.0	47,967	35,407	1.9

The miniemulsion polymerization reactions of the initial pSt block were performed for 6h at 70°C targeting a Mn of 50,000 g/mol, with the four initiators presented above. The conversion-time profile and the evolution of Mn with conversion of the miniemulsion polymerization of styrene are shown in Figure II.7a and b. Moreover,

the droplets and the final particles size as well as Mn obtained at the end of the reaction are shown in Table II.2.

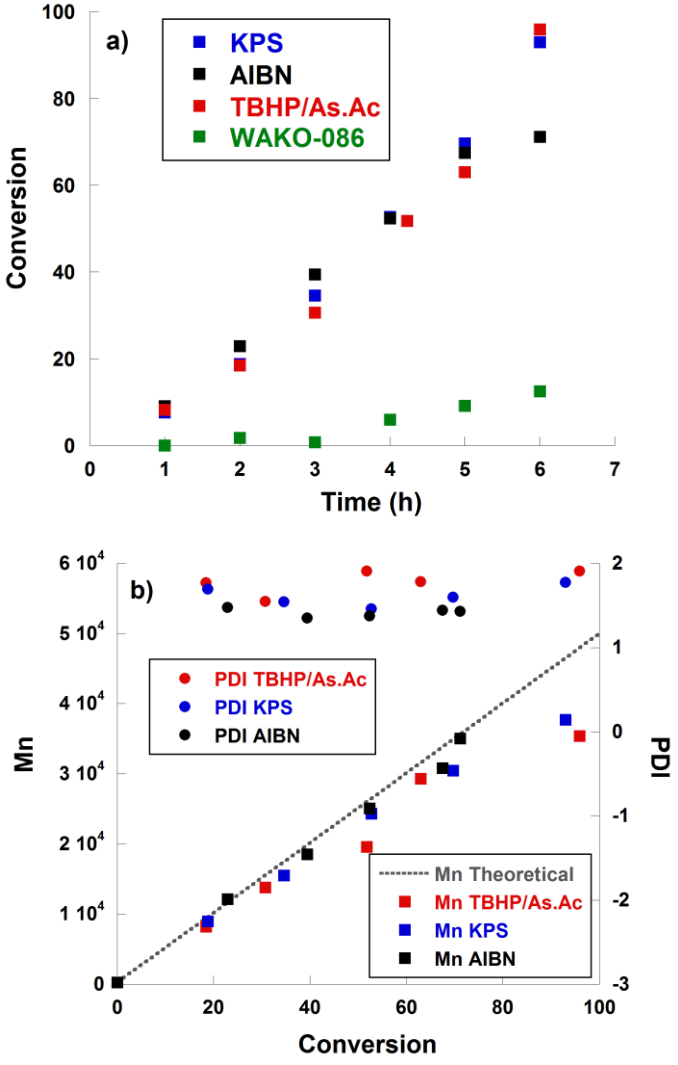

Figure II.7. The effect of initiator type used on a) conversion of styrene as a function of time and b) evolution of Mn of pSt with conversion.

It can be seen from the conversion evolution (Figure II.7a) that when the water soluble azo initiator WAKO-086 was used, a large inhibition time, for at least 3 h, and very low conversion was achieved (12.5%) at the end of reaction.

This is most likely due to the fact that this initiator has a high half life time temperature, leading to the formation of low stream of radicals at polymerization temperatures of 70 °C. Furthermore, it can be observed that the polymerization rate when using AIBN as an initiator is a bit higher than when using KPS or redox system TBHP/AsAc but only up to 70% conversion, above which a deviation from linearity is observed for AIBN. Moreover, at the end of the reaction higher conversion is achieved when using KPS compared to AIBN, even though these two initiators have similar decomposition temperatures compared to AIBN. This observation can be explained from the higher efficiency of KPS compared to AIBN. The free radicals of KPS produced in water phase enter monomer droplets and triggers the propagation reaction until another free radical of KPS enters the same latex particle, so the average number of free radical is $\bar{n}$ = 0.5, according to the Smith Edward theory[17].

By contrast decomposition of AIBN produces two radicals in pairs within a particle, thereby leading to enhanced bimolecular termination of two neighboring radicals so the number of initiating radicals is reduced significantly. The water-soluble

fraction of AIBN can also generate radicals but their contribution to the overall polymerization rate is almost negligible[15].

Moreover, highest conversion (Table II.2) achieved at the end of reaction is when using the redox system TBHP/As.Ac. as an initiator, which also leads to highest PDI obtained at the end of reaction. The redox initiator system TBHP/AsAc produced an augment of the radical availability, thus increasing the rate of polymerization substantially and achieving very high conversion.

No significant differences were observed in the droplet size (Table II.2), however it was noticed that lowest dd was obtained from the reaction where AIBN was used as an initiator. Most likely, even though in a very small quantity, being hydrophobic AIBN added to the overall stability of the miniemulsion. Furthermore, for WAKO-086 and AIBN a slight increase from the initial droplet size to the final particle size of about 20-30 nm was observed, while particle size was maintained almost constant during the miniemulsion polymerization with KPS and TBH/AsAc.

From the evolution plots of Mn versus conversion, a linear increase of Mn with conversion can be observed in all cases up till around 65% conversion which further on proceeds with deviation when KPS and TBHP/AsAc were used as initiators. Namely, lower Mn compared to the theoretical prediction is obtained above 65% conversion for these initiators, which could be attributed to chain transfer to polymer

or beta scission which is not characteristic only for polymerization of acrylates but also for styrene as shown by Chieferi et al.[18]. This has the overall effect of decreasing the molecular weight of the polymer and increasing the PDI. When AIBN was used as an initiator, the reaction proceeded with a low deviation from theoretical Mn and lowest PDI was obtained.

From the results above, it was decided to continue working with AIBN and investigate further other possible parameters that could affect the RAFT homopolymerization of St when using AIBN as an initiator.

II.3.2. The influence of different [RAFT]:[AIBN] molar ratio on the kinetics of the RAFT miniemulsion polymerization of styrene

According to the RAFT polymerization mechanism shown in chapter 1, the total amount of chains is regulated by the amount of RAFT agent, which successfully fragmentates and reinitiates the polymerization process, as well as by the amount of chains produced because of initiator decomposition[2,3]. The increase of initiator concentration and decrease of the RAFT amount will slow down the transformation of the RAFT into dormant polymer chains, resulting in higher probability of termination between two radicals (formation of dead chains) and as a result polymer with broader polydispersity will be obtained. According to the literature, to maintain a living/controlled character of process, the concentration of the RAFT agent should

exceed the one of the initiator and one should suppress the participation of radicals, formed because of initiator decomposition, in the side reactions like chain termination and reinitiation. Thus, the amount of initiator present in the system is of great importance to obtain controlled radical polymerization. In this context, the influence of several molar ratio of [RAFT]: [I] have been investigated while keeping the reaction temperature, type of initiator (AIBN) and targeted Mn (50,000 g/mol) constant, and the results are listed in Table II.3 and Figure II.8.

Table II.3. Conversion, average particle size, Mn and PDI obtained at the end of reaction for pSt homopolymers synthesized using different molar ratio of [RAFT]: [AIBN] at 70 °C

n[RAFT]: n[AIBN]	Conversion (%)	Droplet size (nm)	Particle size (nm)	$M_{n,Cal}$ (g/mol)	$M_{n,GPC}$ (g/mol)	PDI
5:1	71.1	122.0	145.0	35,652	35,053	1.4
7:1	56.3	161.3	151.3	28,290	24,891	1.4
10:1	38.9	137.0	155.4	19,662	22,314	1.3
0:1	98.3	79.16	100.4	-	729,284k	2.4

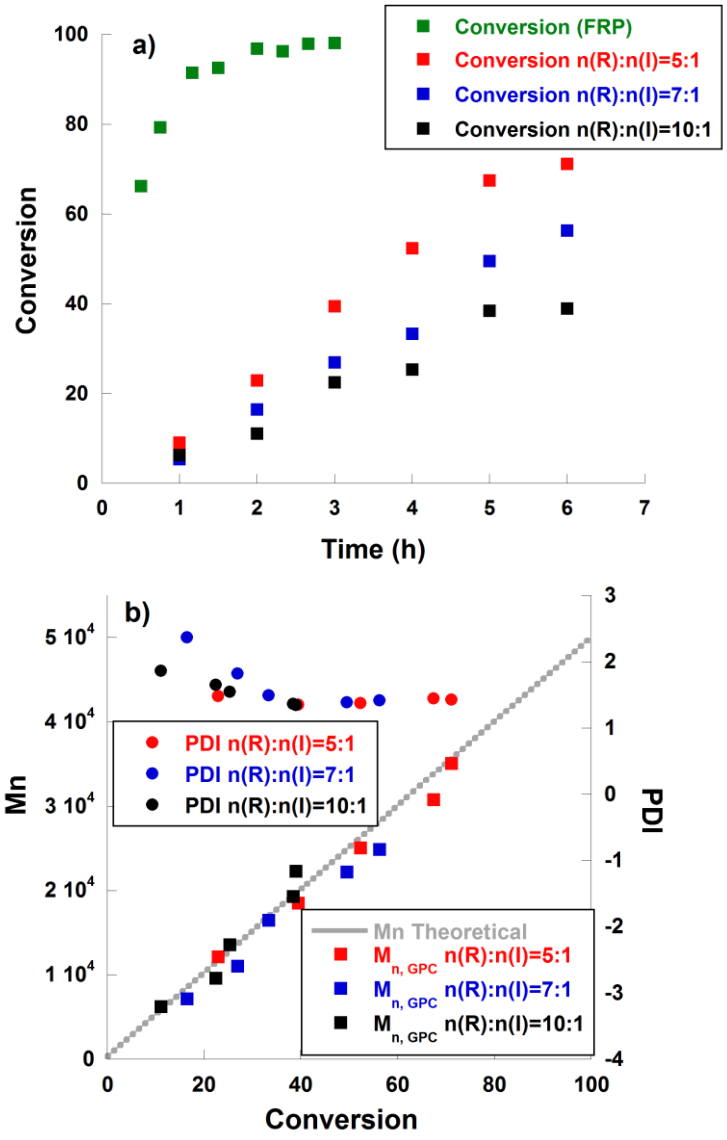

Figure II.8. The effect of [RAFT]: [I] on a) conversion of styrene as a function of time and b) evolution of Mn with conversion.

The results presented in Figure II.8a of the conversion-time profile show that the polymerization rate decreases as the ratio of [RAFT]: [AIBN] increases, which results from the decrease in free radicals concentration as $[AIBN]_0$ decreases. The results in Table II.3 also show that two times increase of [RAFT]: [AIBN] molar ratio led to decrease of pSt conversion from 71% to 38.9%, but without significant PDI change. The decrease of conversion while increasing the RAFT agent transformation into polymer form leads to a domination of dormant chains over the active ones. In turn, the polymerization rate is reduced, and the monomer conversion gets lower.

It is known that the RAFT agent addition changes the reaction conditions compared to the free radical process. As seen from the presented plots in Figure II.8a, the RAFT polymerization rate is relatively high, however lower than that of conventional free radical miniemulsion polymerization. The polymerization of St in absence of the RAFT agent reached almost full conversion in short time and later in the polymerization remained unchanged. On the other hand, when miniemulsion polymerization was performed in the presence of the RAFT agent, there was low conversion initially, then the conversion gradually increased and finally reached higher conversion after several hours. Moad [2] attributed RAFT retardation to several factors: (i) slow fragmentation of adduct ((PnS(Z)C-S*, 2) formed from initial RAFT agent RSC(Z)=S, 1, (ii) slow fragmentation of adduct (PmS(Z)C=S, 5) formed from the polymeric RAFT agent, (iii) specificity of the expelled radical (R*) to add to the

RAFT agent rather than to monomer and (iv) specificity for the propagating radical (Pn•) to add to the RAFT agent rather than monomer, effect especially pronounced as the ratio of [RAFT]:[AIBN] increases. Monteiro et al.[19,20] and Kwak et al.[21] on the other hand attributed retardation to cross-termination, i.e. the termination between the propagation free radical P* and intermediate P-(X*)-P. Furthermore, Zeterlung and coworkers[22] concluded that retardation is caused by cross-termination of very short radicals only. Even though the mechanism is still under investigation, it is clear that addition of the RAFT agent in to the system causes retardation.

From the Mn versus conversion plots (Figure II.9b) we can see that Mn grows linearly with monomer conversion following the predicted theoretical values for all molar ratio of [RAFT]:[AIBN] used. The good agreement of the predicted and experimental Mn values indicates that the miniemulsion polymerizations are well controlled and that there was a constant number of growing chains during the polymerization. However in order to reach a compromise between the conversion and time of reaction it was decided to further continue working with the molar ratio [RAFT]:[AIBN] = [5:1].

II.3.3. Effect of targeted Mn on the kinetics of the RAFT miniemulsion polymerization of styrene

Another important parameter that influences the control of molecular weight and dispersity is monomer to RAFT agent ratio or targeted Mn. Therefore, a study of the polymerization of styrene at various targeted Mn was carried out at 70°C using molar ratio [RAFT]:[AIBN] = 5:1. The results obtained are shown in Table II.4 and Figure II.9. As seen from Figure II.9, there is not a clear trend of the polymerization rates of the reactions where different Mn were targeted. Nevertheless, the highest conversion at the end of the reaction was achieved for the highest Mn targeted.

Table II.4. Conversion, average particle size, Mn and PDI at the end of reaction for pSt homopolymers synthesized targeting different Mn at 70 °C

Reactions	Conversion (%)	Droplet size (nm)	Particle size (nm)	$M_{n,Cal}$ (g/mol)	$M_{n,GPC}$ (g/mol)	PDI
pSt30	64.4	119.1	151.9	19,450	18,894	1.3
pSt50	71.1	122.0	145.0	35,652	35,053	1.4
pSt70	73.2	140.1	141.1	51,365	50,134	1.6

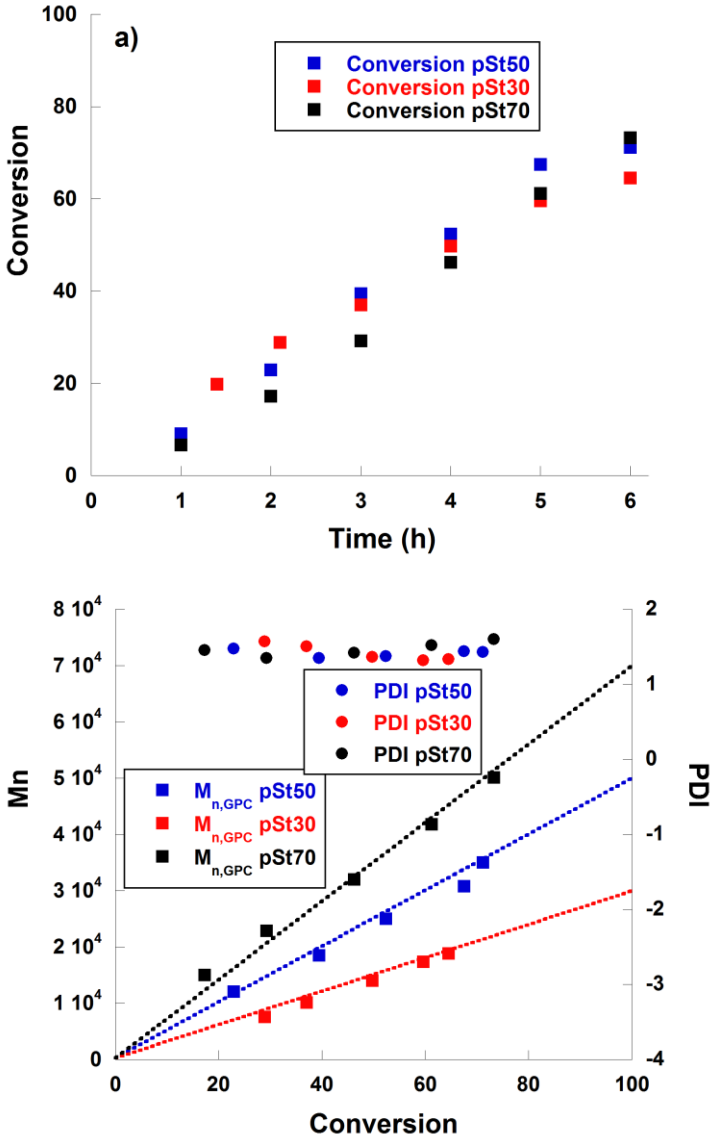

Figure II.9. The effect of targeted Mn on a) conversion of styrene as a function of time and b) evolution of Mn with conversion.

At the same time, the increase in targeted Mn resulted in an increase of PDI from 1.3 to 1.6. This was also observed by Yang et al. [23] who investigated the synthesis of pSt with high Mn using RAFT miniemulsion polymerization. They found out that to synthesize pSt with a high Mn and low PDI, semi-batch polymerization should be carried out, namely initially synthesizing a seed of pSt with lower Mn and then feeding the second monomer.

Moreover, it could also be observed that when lower Mn is targeted, i.e. when the level of DBTTC present in the miniemulsion is higher, smaller initial droplet size was obtained. DBTTC is very hydrophobic and acts also as a costabilizer and stabilizes the miniemulsion. Chern[24] and coworkers investigated the kinetics of RAFT miniemulsion of styrene using DBTTC as both RAFT and costabilizer and observed the same findings.

Furthermore, as seen from Figure II.9b, linear increase in Mn versus monomer conversion was obtained in all three cases, indicating that the reaction proceeded in a controlled manner.

II.3.4. Effect of temperature on the kinetics of the RAFT miniemulsion polymerization of styrene

RAFT miniemulsion polymerization of styrene using AIBN as an initiator was investigated at three different polymerization temperatures, namely 60°C, 70°C and

80°C, keeping constant the molar ratio of [RAFT]:[AIBN] = 5:1, and the results are shown in Table II.5.

Table II. 5 Conversion, average particle size, Mn and PDI at the end of reaction for pSt homopolymers synthesized at different polymerization temperatures for 6 hours.

Reactions	Conversion (%)	Droplet size (nm)	Particle size (nm)	$M_{n,Cal}$ (g/mol)	$M_{n,GPC}$ (g/mol)	PDI
pSt50-80°C	92.7	139.5	134.6	46,387	41,017	1.8
pSt50-70°C	71.1	122.0	145.0	35,652	35,053	1.4
pSt50-60°C	26.2	161.9	159.1	13,353	12,352	1.5

As can be seen in the Table II.5, at 60°C styrene polymerization reached only 26.2 % conversion in 6h. When the polymerization was performed at higher temperatures, higher conversion was obtained, namely 71.1% and 92.7% respectively for reaction temperature of 70 and 80°C.

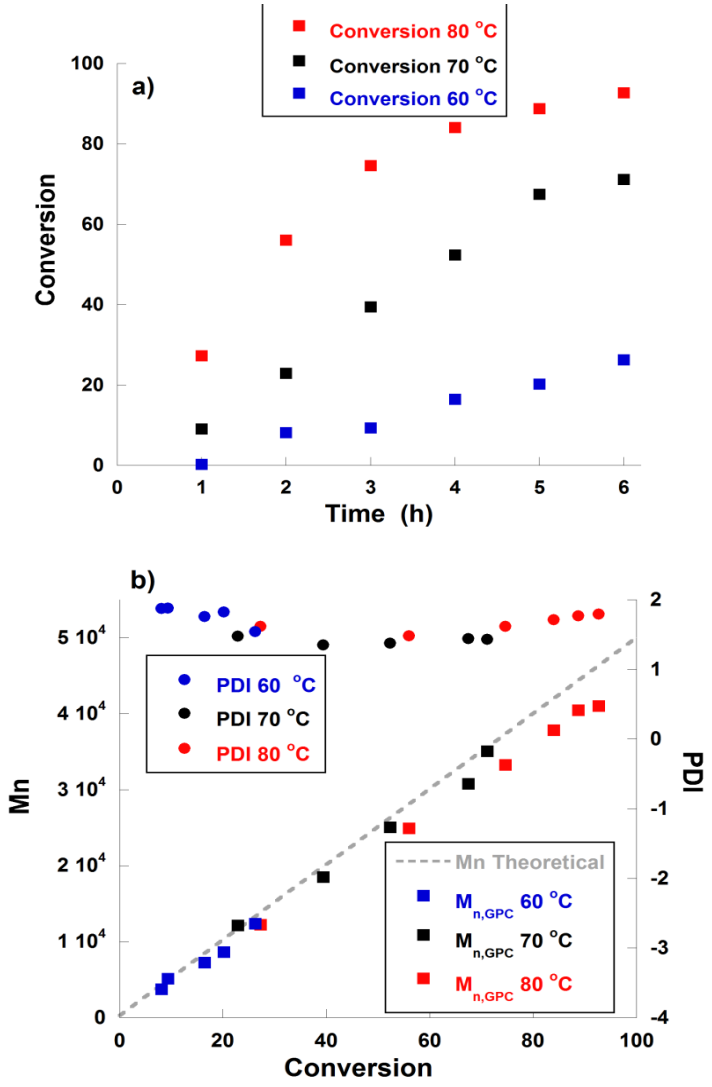

Figure II.10. The effect of temperature on a) evolution of conversion of styrene as a function of time and b) evolution of Mn with conversion of monomer.

It is perhaps worth emphasizing that the half-life time ($t_{1/2}$) of AIBN at increased temperature reduces substantially. In principle the $t_{1/2}$ of AIBN at 60°C, 70°C and 80°C is 1250 min, 300 min and 100 min respectively. In this context, the radicals stream at 60°C is very low and as a result low conversion is obtained. The effect of temperature on styrene free radical emulsion polymerization was studied by Chern at al.[25] using sodium persulfate as an initiator. They also observed that with increasing the temperature, the rate of polymerization increased rapidly.

Styrene can also polymerize in absence of initiator when T is above 60°C. Chern et al.[25] studied also the thermal polymerization of styrene in emulsion at 80°C without initiator and concluded that the conversion was insignificant compared to the polymerization performed at the same conditions in the presence of initiator. Thus, the thermal polymerization of styrene at 80°C could be excluded and the high conversion can be prescribed to the high radical stream generated by the added radical initiator AIBN. Independent of the reaction temperature, $M_{n,GPC}$ increased linearly with monomer conversion (Figure II.10b), in good agreement with the theory of controlled polymerization. Nevertheless, when the polymerization was performed at 80°C, deviation of $M_{n,GPC}$ compared to $M_{n,theoretical}$ at conversions above 60% were observed. Moreover, the PDI increased at higher conversions, which suggests that there is presence of irreversible termination due to monomer depletion.

II.3.5. Polystyrene hard domain synthesis

Once having chosen the optimized parameters, two pSt latexes targeting Mn of 30,000 and 50,000 g/mol were synthesized using AIBN as an initiator, n[RAFT]: n[AIBN] = [5:1] and at a temperature of 70°C, to serve as seeds for the later synthesis of the soft block of pEHA. The results of these synthesis are shown in Table II.6.

These reactions compared to the ones shown above were performed in a different institute and it was noticed that the obtained conversion of the homopolymers was higher.

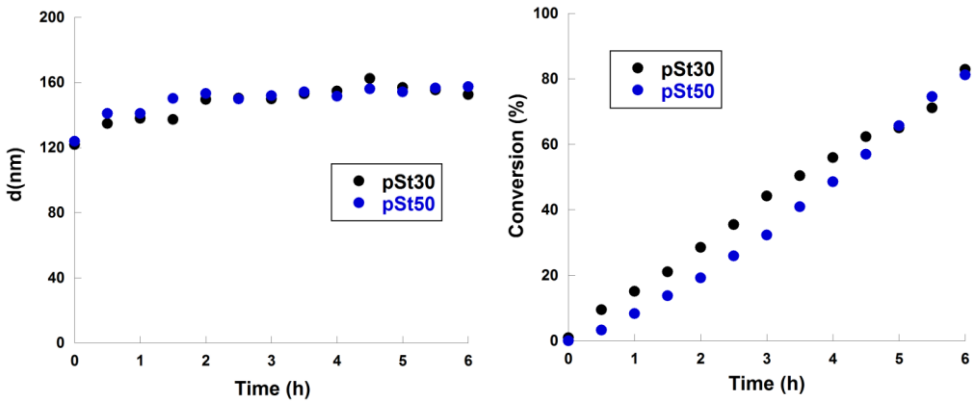

Figure II.11. Evolution of a) droplet/particle size evolution with time, b) St conversion versus time for the miniemulsion polymerizations carried out to obtain pSt30 and pSt50.

Technical grade monomers were used in both places and they contained 10 – 15 ppm of TBC inhibitor (4-tert-butylcatechol). The monomers were not distilled prior polymerization, thus most likely the difference in the amount of the inhibitor present in the monomer resulted in the difference of the conversion obtained. The evolution of the particle droplet-particle size is shown in Figure II.11.

It can be seen from the graph (Figure II.11) that dp initially increases with the progress of the Ostwald ripening process, and ultimately a relatively stationary particle size is achieved. The particle size at the end of the reactions was higher than the droplet size for about 30 nm in both pSt30 and pSt50, which is most likely the reason why the PDI obtained by GPC was higher at the end of reaction. Nevertheless, the conversion increased linearly with time and around 80% conversion was obtained for both pS30 and pSt50 after 6h. The reaction was stopped at 6h even though not full conversion was reached since a living system was desired for the extension of the initial block with the soft monomer.

To check the conversion reproducibility, three reactions were performed synthesizing pSt latexes with targeted Mn of 30,000 g/mol. It was shown that in all three cases the conversion points overlapped and the final conversion after 6h was around 80%, indicating that the reactions are reproducible (see Figure II.12).

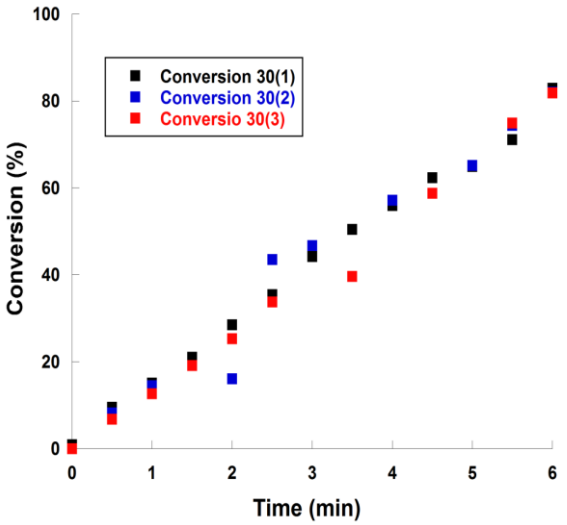

Figure II.12. Conversion of St versus time for pSt30 for three repeated reactions.

Mn for both pSt30 and pSt50 increased with conversion (Figure II.13a), following the theoretical prediction showing that the polymerization proceeded in well controlled manner. Moreover, the whole molecular weight distribution (Figure II.13a and II.13b) shifted to higher molecular weight with increasing the conversion. Therefore, it could be considered that the polymerization was living and well controlled.

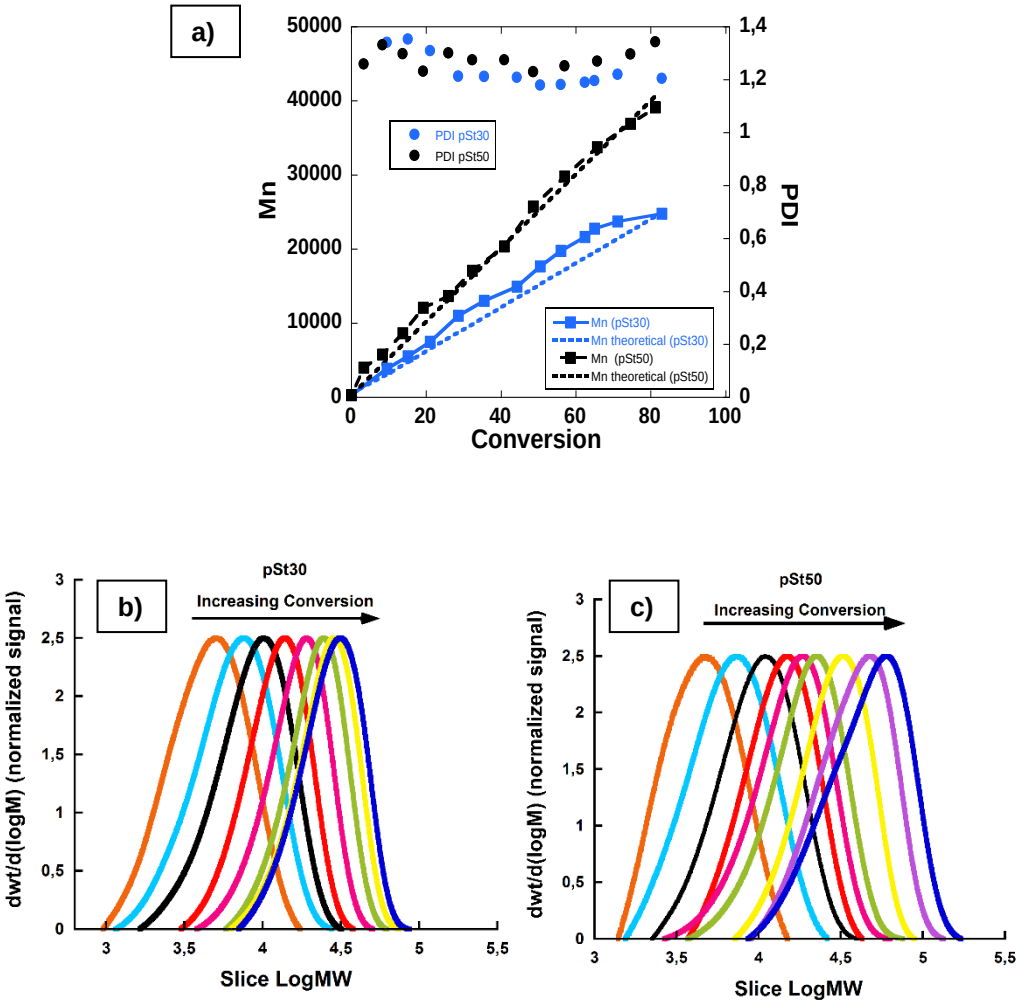

Figure II.13. a) Plots of the number-average molecular weight and polydispersity index vs monomer conversion for pSt30 and pSt50 and molecular weight distribution of b) pSt30 and c) pSt50 obtained by IR refractive index detector.

II.3.6. ABA block copolymer synthesis – Hard-Soft-Hard domains

Once the initial pSt blocks were formed with 30,000 and 50,000 g/mol of targeted molecular weight (pSt30 and pSt50), the extension with the second soft monomer proceeded. The optimization of this step was not done. Governed by the knowledge gained from the optimization process of the homopolymerization of pSt, AIBN was selected as an initiator and the reaction was performed at 70°C. A molar ratio of RAFT:Initiator was arbitrarily chosen to be 2:1, which was calculated based on the moles of RAFT present in the seed. When converted to wt% based on 2EHA (second monomer added) the amount of initiator ranged from 0.125-0.164%. Thus, the amount of the initiator used in the second step is relatively low and comparable to the one used in the first step. The second monomer was fed as a preemulsion for three hours with additional amount of initiator added. Four block copolymers were synthesized having different molecular weights, named through the text as: p(St25-2EHA50-pSt25) as an extension of pSt50 and p(St15-2EHA50-pSt15), p(St15-2EHA70-pSt15) and p(St15-2EHA100-pSt15) as extensions of pSt30. The results of these four block copolymers are shown in Table II.6. The numbers after the letters indicate the targeted molecular weight. The second monomer was fed without any removal of the unreacted monomers from the first step.

Table II.6. Conversion, average particle size, Mn and PDI at the end of reaction for pSt homopolymers and p(St-2EHA-St) block copolymers

Reactions	Conversion (%)	$M_{n,GPC}$ (g/mol)	PDI	dd (nm)	dp (nm)	dp (nm)	Conversion (%)	$M_{n,GPC}$ (g/mol)	PDI
	pSt Homopolymer					(St-2EHA-St) Block copolymers			
p(St25-2EHA50-pSt25)	81.2	39,119	1.34	119	157	177	84.0	73,854	1.45
p(St15-2EHA50-pSt15)	81.8	20,204	1.22	116	154	187	83.1	42,877	1.52
p(St15-2EHA70-pSt15)	82.0	20,044	1.29	130	161	187	95.2.	51,046	2.36
p(St15-2EHA100- St15)	82.0	20,044	1.29	130	161	207	96.3	72,203	2.6

Thus, the middle soft block is expected not to be pure poly(2-EHA) but rather a gradient polymer which incorporated still some styrene at the beginning of the polymerization of the second block and continues to grow into pure p(2-EHA) towards higher conversions. This gradient polymerization behavior was proven by GC analysis. However, for simplicity reasons this middle gradient block will be named as soft poly(2EHA) block throughout the text.

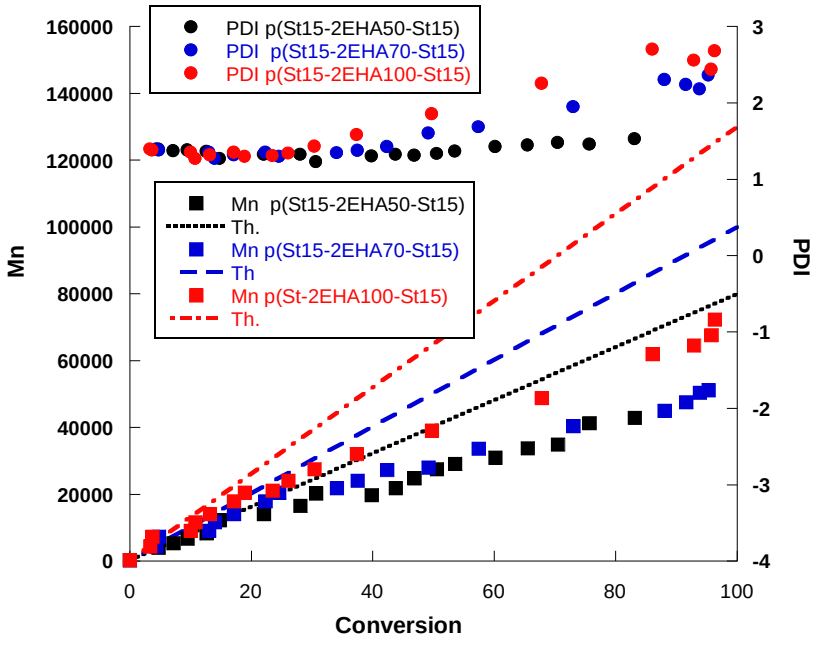

Figure II. 14. Evolution of the number average molecular weight and polydispersity index vs monomer conversion for different pSt-EHA-St compositions.

The evolution of the Mn versus total monomer conversion (determined by solids content measurements) for block copolymers with different Mn prepared from pSt30 seed is shown in Figure II.14. Mn grows linearly with conversion, however there is a visible negative deviation after the addition of the second monomer. The deviation gets more pronounced with the increase of the polymerized middle soft block. This is most likely due to the fact that the Mn's obtained from GPC were based on pSt standards and the Mark-Houwink constant of p2EHA was not taken into consideration. Equation II.2 presents how the molecular weights of two different polymers can be related using the Mark- Houwink equation. In the equation K_1, a_1 and K_2, a_2 represent the Mark-Houwink parameters for polymer 1 and 2 respectively, and M_1 and M_2 are the molecular weight of the polymers. Thus, as seen from the equation II.2 taking into considerations the constants for pSt (K=0.000158 a=0.704) and p2-EHA (K= 0.000124 and a=0.667) we were underestimating the real Mn.

$$K_1 M_1^{(1+a_1)} = K_2 M_2^{\wedge(1+a_2)} \qquad \text{(II.2)}$$

Furthermore, it can be seen, that all the final block copolymers have an overall conversion above 80% and the polydispersity index increased as the length of middle block was increased. Nevertheless, it should be noted that triblock copolymers were successfully formed, as is evident from the GPC curves (Figure II.15), where the MWD of the final block copolymer moved to higher molecular weights compared to initial pSt block.

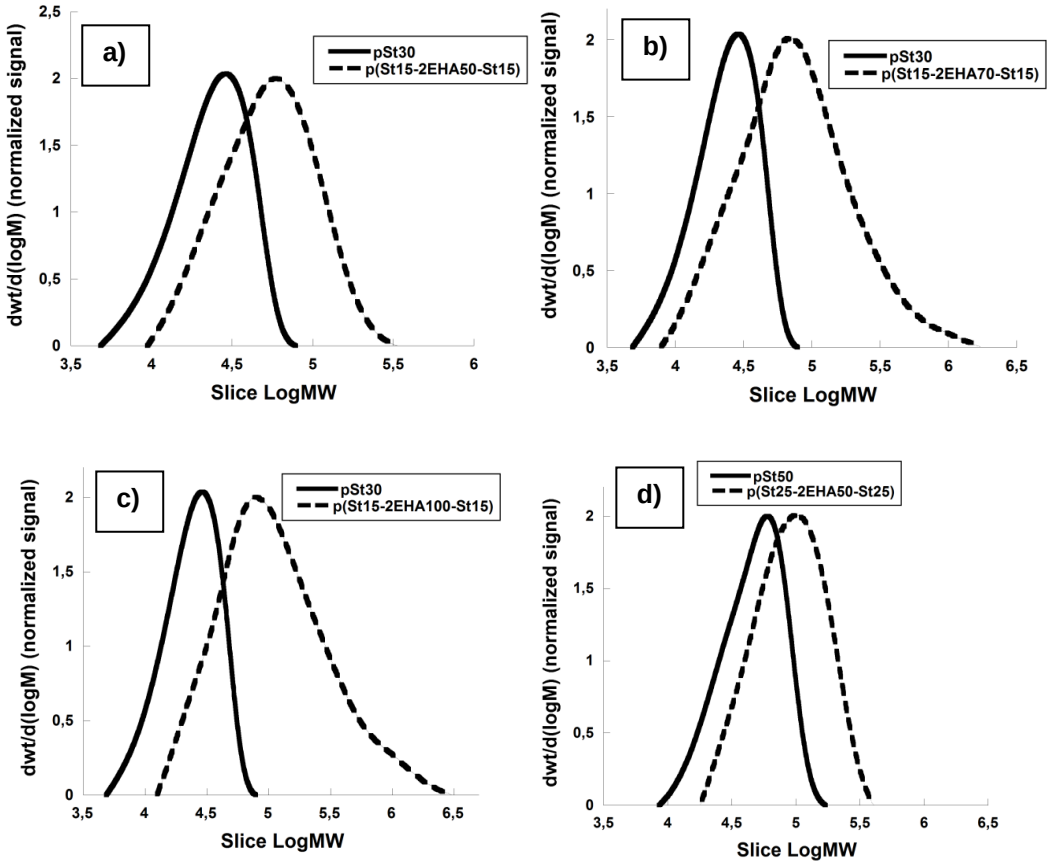

Figure II.15. MWD of the initial pSt homopolymer (solid line) and final block copolymers (dashed line) of different pSt-EHA-St compositions

Widening of the MWD in the region of high molecular weight is observed when higher molecular weight is targeted (for p(St15-2EHA70-St15) and p(St15-2EHA100-St15) Figure II.15b and c respectively). This is most likely due to branching reactions, characteristic for acrylates[26,27].

II.3.7. Thermal properties of the block copolymers

The glass transition temperatures (Tg) of the pSt homopolymers and pSt-2EHA-pSt block copolymers were determined by DSC analysis. The thermograms of the final block copolymers are shown in Figure II.16 and the Tg values obtained are presented in Table II.7.

Table II.7. Thermal properties of the p(St-EHA-St) block copolymers obtained by DSC

Material code	Tg_1 (ºC)	Tg_2 (ºC)
DSC analysis of the samples dried at 23 °C		
pSt30	58	-
pSt50	54	-
p(St25-2EHA50-pSt25)	-43	58
p(St15-2EHA50- pSt15)	-58	55
p(St15-2EHA70- pSt15)	-60	60
p(St15-2EHA100- pSt15)	-60	63

Polystyrene initial blocks with different Mn showed a single glass transition with very similar Tg values (58ºC for pSt30 and 54ºC for pSt50). Nevertheless, these Tg-values are much lower than the literature data Tg of pSt, which is around 100°C. This is attributed to the fact that stearyl acrylate was used as costabilizer.This monomer reacts with styrene and it incorporates in the chains and lowers the Tg of the polystyrene block. The theoretical Tg of the initial polystyrene block taking into account its conversion (82%), the amount of SA costabilizer (8% wt% based on

styrene) and its Tg (-100°)[11], predicted according to the Fox equation should be around 62 °C.

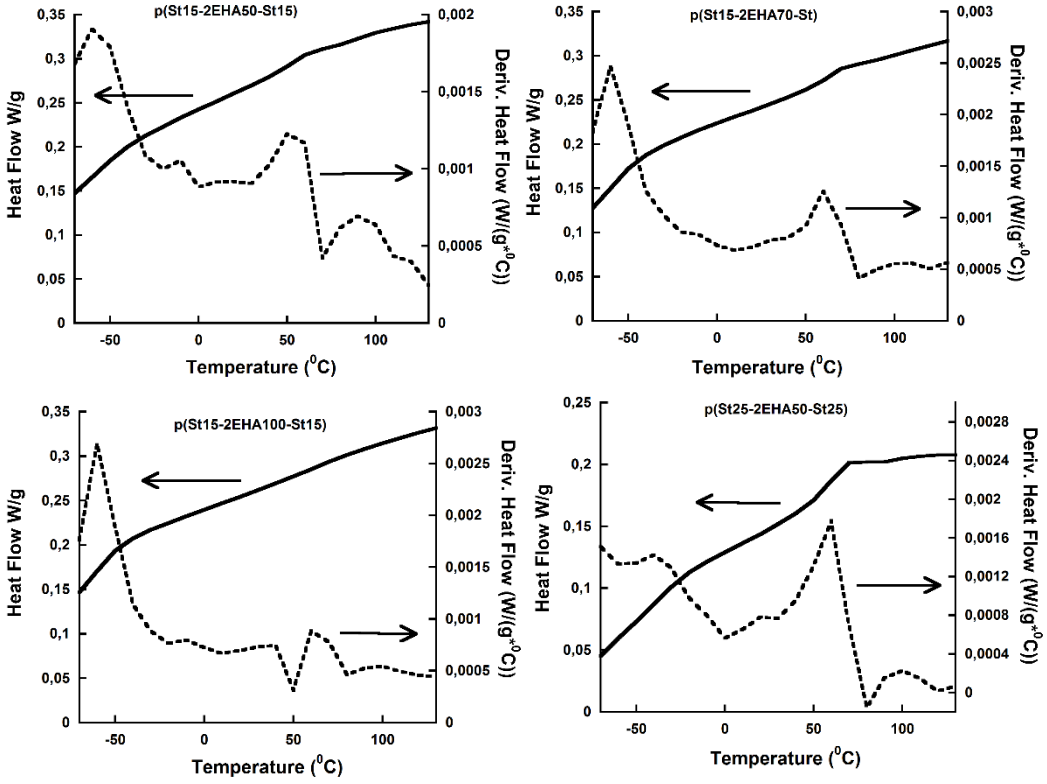

Figure II.16. DSC thermograms of the p(St-EHA-St) block copolymers measured at a heating rate of 10 °C/min.

This value is a bit higher compared to the experimental values obtained by DSC. However, the low molecular weight of the polymer has not been taken into account in this theoretical prediction by the Fox equation, which could be the reason for the difference in the experimental and theoretically obtained Tg as proven by Flory et al.[28]. Flory and Fox studied the dependence of second-order transition temperature of polystyrene on the molecular weight and concluded that Tg for high molecular weight polystyrene is 100 °C and it decreases linearly with 1/Mn. Therefore, both the presence of SA and the relatively low molecular weight pSt block can explain the Tg around 54-58ºC that have been found for the first block. On the other hand, the triblock copolymers exhibit two distinct transition temperatures. The lower transition temperature depending on the composition of the block copolymers ranges from -43 to -60 °C and it is associated with that of the soft block rich in p2EHA. The upper transition temperature ranges from 55 to 63 °C and corresponds to the Tg of the pSt initial block. Therefore, there is a clear indication of a two-phase system.

Table II.8. Thermal properties of the bloc copolymers obtained by TGA

Material code	Tonset (ºC)	Tmax (ºC)
TGA analysis performed in nitrogen atmosphere		
DBTTC	239.9	288.4
p(St25-2EHA50-pSt25)	372.7	413.8
p(St15-2EHA50- pSt15)	365.2	402.7
p(St15-2EHA70- pSt15)	364.0	397.7
p(St15-2EHA100- pSt15)	361.4	396.6

Furthermore, the thermal stability of the copolymers was studied by TGA (Figure II.17) in nitrogen atmosphere and the results are summarized in Table II.8. The temperature at 10% weight loss was taken as T_{onset}. T_{max} represents the maximum degradation temperature at which polymer back-bone starts degrading and was determined from the DTG thermogram. It can be seen from the results that as the styrene content in the block copolymers increased, there was a slight increase in T_{onset}. T_{max} on the other hand decreased as the length of the middle block increased.

On the other hand, DBTTC degradation starts at 240 °C and at 300 °C it is completely degraded. However, good thermal properties and a single step decomposition, comparable to all acrylic compolymers synthesized by free radical polymerization, is observed in all block copolymers.

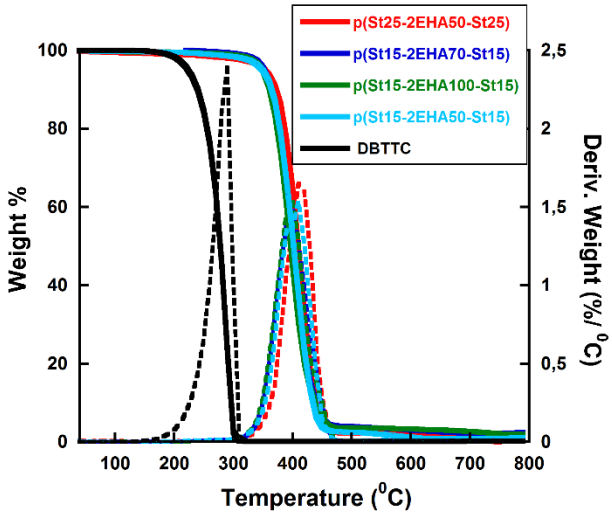

Figure II.17. TGA thermograms of the p(St-EHA-St) block copolymers measured at 10 °C/min in nitrogen

II.4. Conclusion

Waterborne ABA block copolymers of hard A block and soft B block were synthesized via two-step reversible addition fragmentation chain transfer polymerization, using S,S-dibenzyl trithiocarbonate bifunctional (DBTTC) RAFT agent. First, miniemulsion polymerization was used for the synthesis of the hard polystyrene domains where the reaction proceeded up to 80% conversion. Then in the second step 2EHA was fed to the system as a pre-emulsion and soft domains were formed containing a small fraction of styrene from the initial step. The effect of several reaction parameters including the type of initiator, molar ratio of RAFT:Initiator, temperature and targeted Mn on the homopolymerization of styrene were investigated. It was found out that from all the initiators used (water soluble, oil soluble and redox system), AIBN enabled lowest deviation from theoretical Mn and lowest PDI with reasonable conversion. The most suitable molar ratio of RAFT:Initiator was found to be 5:1 for a reaction temperature of 70°C, which led to linear increase in Mn and a reasonable PDI. Moreover, it was found out that when targeting higher Mn, the PDI index increased substantially and therefore the ABA block copolymers synthesis was focused on compositions in which the 2nd stage polymerization of the B-block proceeded only from the seed with targeted Mn of 50,000 and 30,000 g/mol of Poly2EHA. The successful formation of the block copolymer was proven by MWD shift and linear increase in Mn. However, it was also

observed that there is a negative deviation of the Mn obtained versus the theoretical Mn, which most likely originates from the fact that the Mn of the block copolymers was determined from the GPC running with pSt standards only. Thus, the Mark-Houwink constant of p2EHA was not considered.

Furthermore, the thermal properties of both the homopolymers and the block copolymers were investigated by DSC and it was shown that the initial PSt homopolymers show Tg lower than that of literature data of pSt synthesized by free radical polymerization. This was prescribed to the fact the stearyl acrylate was used as a costabilizer and to the low Mn of the blocks. On the other hand, good thermal stability and a single step decomposition was observed for the block copolymers studied by TGA.

II.5. References

1 F. Ganachaud, M. J. Monteiro, R. G. Gilbert, M. A. Dourges, S. H. Thang and E. Rizzardo, *Macromolecules*, 2000, **33**, 6738–6745.

2 G. Moad, J. Chiefari, Y. K. Chong, J. Krstina, R. T. A. Mayadunne, A. Postma, E. Rizzardo and S. H. Thang, *Polym. Int.*, 2000, **49**, 993–1001.

3 E. V. Chernikova and E. V. Sivtsov, *Polym. Sci. Ser. B*, 2017, **59**, 117–146.

4 J. Chiefari, R. T. A. Mayadunne, C. L. Moad, G. Moad, E. Rizzardo, A. Postma, M. A. Skidmore and S. H. Thang, *Macromolecules*, 2003, **36**, 2273–2283.

5 B. Y. K. Chong, J. Krstina, T. P. T. Le, G. Moad, A. Postma, E. Rizzardo and S. H. Thang, *Macromolecules*, 2003, **36**, 2256–2272.

6 G. Moad, E. Rizzardo and S. H. Thang, *Polymer*, 2008, **49**, 1079e1131.

7 G. Moad, G. Li, R. Pfaendner, A. Postma, E. Rizzardo, S. Thang and H. Wermter, in *Controlled/living Radical Polymerization*, ACS Sympos., 2006, pp. 514–532.

8 H. de Brouwer, J. G. Tsavalas and F. J. Schork, *Macromolecules*, 2000, **33**, 9239–9246.

9 B. T. Pérez-Martínez, L. Farías-Cepeda, V. M. Ovando-Medina, J. M. Asua, L. Rosales-Marines and R. Tomovska, *Beilstein J. Nanotechnol.*, 2017, **8**, 1328–1337.

10 E. Mehravar, J. R. Leiza and J. M. Asua, *Polymer*, 2016, **84**, 167–177.

11 E. Mehravar, J. R. Leiza and J. M. Asua, *Polymer*, 2016, **96**, 121–129.

12 T. G. Fox, *Bull. Am. Phys. Soc.*, 1956, **1**, 123.

13 J. M. Asua, *Prog. Polym. Sci.*, 2002, **27**, 1283–1346.

14 L. I. Ronco, R. J. Minari and L. M. Gugliotta, *Brazilian J. Chem. Eng.*, 2015, **32**, 191–199.

15 C. Autran, J. C. De La Cal and J. M. Asua, *Macromolecules*, 2007, **40**, 6233–6238.

16 S. Bilgin, R. Tomovska and J. M. Asua, *Polymer*, 2017, **117**, 64–75.

17 J. M. Asua, *Polymer Reaction Engineering*, Blackwell Publishing, 2007.

18 J. Chiefari, J. Jeffery, R. T. A. Mayadunne, G. Moad, E. Rizzardo and S. H. Thang, *Macromolecules*, 1999, **32**, 7700–7702.

19 M. J. Monteiro and H. De Brouwer, *Macromolecules*, 2001, **34**, 349–352.

20 H. De Brouwer, M. A. J. Schellekens, B. Klumperman, M. J. Monteiro and A. L. German, *J. Polym. Sci. Part A Polym. Chem.*, 2000, **38**, 3596–3603.

21 Y. Kwak, A. Goto, Y. Tsujii, Y. Murata, K. Komatsu and T. Fukuda, *Macromolecules*, 2002, **35**, 3026–3029.

22 S. R. S. Ting, T. P. Davis and P. B. Zetterlund, *Macromolecules*, 2011, 4187–4193.

23 L. Yang, Y. Luo and B. Li, *J. Polym. Sci. Part A Polym. Chem.*, 2005, **43**, 4972–4979.

24 R. I. Kusuma, C.-T. Lin and C.-S. Chern, *Polym. Int.*, 2015, 1389–1398.

25 C.-S. Chern, S.-Y. Lin and T. J. Hsu, *Polym. J.*, 1999, **31**, 516–523.

26 C. Plessis, G. Arzamendi, J. R. Leiza, H. A. S. Schoonbrood, D. Charmot and J. M. Asua, *Macromolecules*, 2000, **33**, 5041–5047.

27 N. Ballard and J. M. Asua, *Prog. Polym. Sci.*, 2018, **79**, 40–60.

28 T. G. Fox and P. J. Flory, *J. Appl. Phys.*, 1950, **21**, 581–591.

29 L. Da Cunha, P. Ilundain, R. Salazar, D. Alvarez, M. J. Barandiaran and J. M. Asua, *Polymer*, 2001, **42**, 391–395.

Chapter III. Synthesis and characterization of hard-soft AB block copolymers

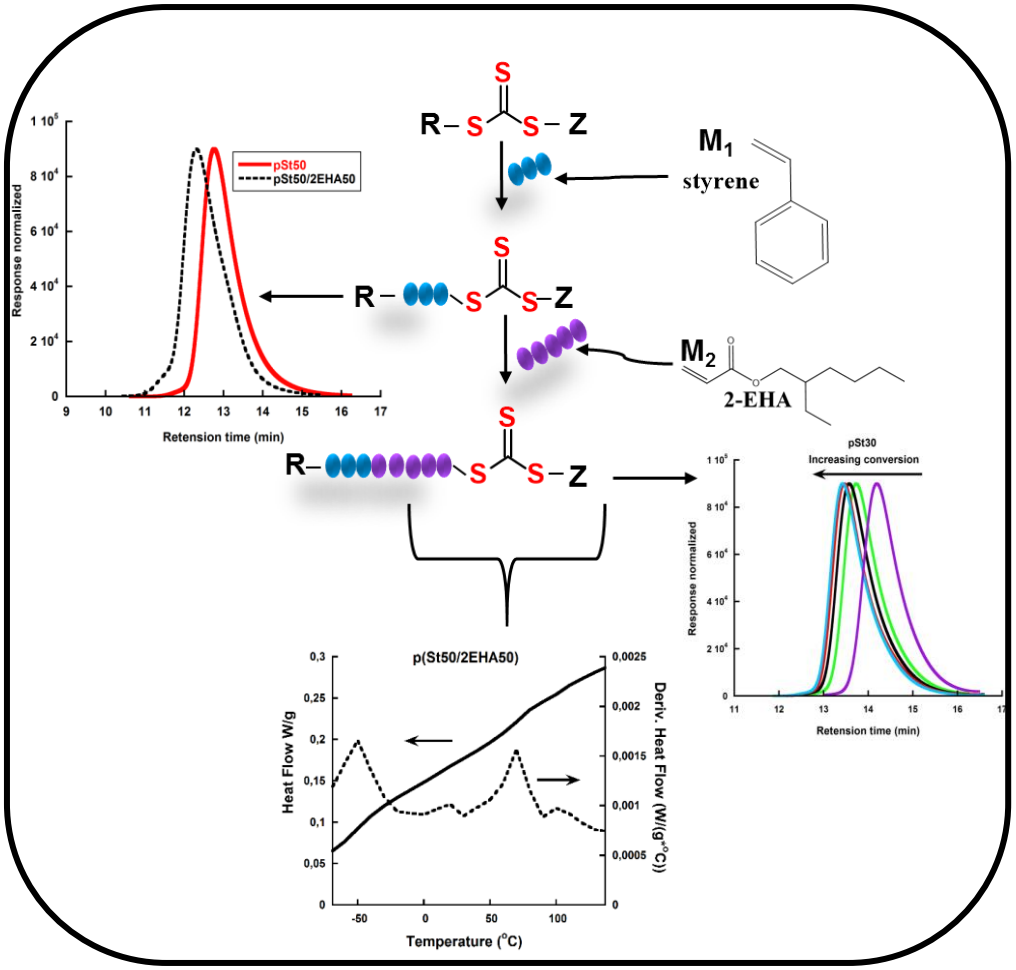

III.1. Introduction

As discussed in chapter I, RAFT polymerization provides the ability to control the polymerization of many unsaturated monomers polymerizable by free radical polymerization. The most important feature of RAFT polymerization is the selection of the RAFT agent (ZS(=S)SR), which should be done according to the monomers being polymerized and to the reaction conditions[1–3]. The effectiveness of the RAFT agents is determined by the substituents R(radical leaving group)[4] and Z(activating group Z)[5] and guidelines for selection of these groups have been proposed in Figure I.6, chapter I[6,7]. Aromatic dithioester (Z=aryl) are amongst the most active RAFT agents and have general utility in the polymerization of "more activated monomers", MAMs (like meth(acrylate), styrene, and acrylamides)[68]. However, these RAFT agents may give retardation, particularly when used in high concentrations and they are more sensitive to hydrolysis and decomposition. Trithiocarbonates RAFT agents on the other hand, where Z=S-$C_{12}H_{25}$ and/or R is a tertiary carboxylic acid[9] or cyanomethyl also provide good control over polymerization of MAMs, give substantially less retardation and have greater hydrolytic stability than dithioester[10].

A new class of RAFT agents developed by CSIRO and commercially available by BORON Molecular, which appear equivalent to the trithiocarbonates in their ability to control the polymerization of MAMs producing polymers with defined molar mass and

similarly low polydispersity, are the pyrazole-based RAFT agents[11,12]. Furthermore, unlike trithiocarbonates they are also able to control the polymerization of less activated monomers (LAMs), allowing the preparation of low polydispersity block copolymers of poly(MAM)-block-poly(LAM)[11]. In addition, they can be stored at ambient temperature and have distinct advantage over trithiocarbonates and the derived polymers that do not develop significant odor upon use or storage due to the absence of pathways that generate thiols.

Thus, in this chapter, both trithiocarbonate and dithiocarbamate-pyrazole based RAFT agents will be investigated for the synthesis of high molecular AB block copolymers containing hard (pSt) and soft (pEHA) domains. The hard A-block will be synthesized by RAFT miniemulsion polymerization, followed by feeding 2EHA to form the soft domains. The effect of the structure of RAFT agent and the molar ratio of RAFT agent to initiator on the polymerization kinetics of styrene will be initially investigated. Two trithiocarbonate and one dithiocarbamate-pyrazole RAFT agent will be explored as possible candidates for the synthesis of the first polystyrene block. Upon optimization of the polymerization process parameters of the initial block, the formation of AB block copolymers will be given. Variations were done on chemical composition and molecular weights of the block copolymers, and the polymerization kinetics and MWD's were studied. In addition, the thermal properties, studied by DSC of the initial homopolymers and the final block copolymers will be given.

The synthesis of such block copolymers was done to approach the properties of asymmetric AB thermoplastic elastomers and obtain polymers that would show temperature responsiveness. An important category of thermoplastic elastomers are the high molecular weight microphase separated AB block copolymers having mechanical properties like ordinary rubber, where the hard block is generally low molecular weight to minimize their negative impact on elasticity. As mentioned also in chapter II, when these materials are cooled from the melt, the hard blocks self-assemble into glassy domains that resist creep and viscous flow under load, whereas the elastic portion of the polymer remains amorphous and soft. However, as compared to the symmetric block copolymers (ABA) synthesized in chapter II, in this chapter the block copolymers were asymmetric (AB). The final goal was to see the effect of both configurations (ABA or AB) on the morphology of the latexes and films produced from both approaches, and on their final temperature responsive properties.

Thus, we used a monofunctional asymmetric RAFT agent and synthesized p(St-2EHA) block copolymers in emulsion polymerization and used the glass transition temperature of the hard pSt domain as triggering temperature.

III.2. Experimental part

Materials

III.2.1. The materials used for the synthesis of the hard-soft copolymers are given in Appendix.

Synthesis Procedures

III.2.2. **Synthesis of the first block: Batch miniemulsion polymerization of styrene**

AB hard-soft block copolymers were synthesized using the same procedure as for the synthesis of the ABA hard-soft-hard block copolymers. Thus, the procedure will be described only briefly. Polystyrene (pSt) “A” hard block was initially synthesized using asymmetric RAFT agent via RAFT miniemulsion polymerization at 30% solids content (s.c.) in water. The coarse emulsion was prepared by mixing the water phase with the oil phase. Water phase was prepared by dissolving the surfactant Dowfax 2A (2wt% based on styrene monomer, BOM), Disponil A3065 (1wt% BOM) and the buffer $NaHCO_3$ (0.16wt% BOM) in deionized water. The oil phase was prepared by dissolving stearyl acrylate costabilizer (SA, 8wt% BOM), RAFT agent, and initiator (AIBN) in styrene. After ensuring well mixing, the coarse emulsion was ultrasonicated for 15 min using Dr. Hielscher GmbH, 400 W (amplitude 70% and 50% duty cycle) under magnetic stirring in an ice-water bath to avoid overheating and possible initiation of the reaction.

The miniemulsion was then transferred to a jacketed batch reactor and purged with nitrogen for 30 min. under agitation to eliminate the dissolved oxygen. The temperature was increased to 70°C and when the desired temperature was reached, time 0 was marked. Samples were taken at different time intervals and they were quenched with 1wt% hydroquinone (HQ) water solution to stop the polymerization. The reaction was performed for 360 minutes, then the temperature was decreased to 25°C and the final latex was collected and filtered.

Synthesis of the second block: Semi-batch emulsion polymerization of 2EHA

AB block copolymers were synthesized by semi-batch emulsion polymerization using the A polystyrene block as seed. A pre-emulsion of 2EHA was fed for 3 h and the polymerization was continued for another 2 h batch wise to reach higher conversion and to form the second B block. The total amount of surfactants (Dowfax 2A and Disponil A3065) was kept constant, 3 wt% based on all monomers. Initiator (AIBN) was additionally added to start the polymerization. The initiator added was calculated based on the amount of the moles of the RAFT agent present in the seed and was kept constant at a mol ratio of (RAFT):(Initiator) = 2:1.

Characterization

Monomers conversion was followed gravimetrically. The monomer droplet size and the final particle size of the latexes was measured using dynamic light scattering (DLS). The molecular weights and the molecular weight distributions were measured using GPC. Thermal stability of the block copolymers was measured by DSC. The detailed description of the characterization methods is provided in Appendix.

III.3. Results and discussion

The synthesis of polystyrene “A” block was initially optimized investigating two different reaction parameters:

- Structure of RAFT agent
- Molar ratio of [RAFT]:[Initiator]

As seen in chapter II, where the synthesis and characterization of ABA hard soft hard block copolymers is shown, the most appropriate initiator for the styrene homopolymerization at a polymerization temperature of 70°C is AIBN. Thus, these reaction parameters (temperature and initiator) were not investigated in this chapter.

Influence of the structure of the RAFT agent on the RAFT miniemulsion polymerization of styrene

III.3.1. Three RAFT agents (Figure III.1), two trithiocarbonates (a,b) and one dithiocarbamate (c) were used to investigate the homopolymerization of styrene:

a) 2-(((dodecylthio)carbonothioyl)thio)propanoic acid (BM1430),

b) 4-cyano-4-(((dodecylthio)carbonothioyl)thio)pentanoic acid (BM1432),

c) 2-cyanobutanyl-2-yl 3,5-dimethyl-1H-pyrazole-1-carbodithioate (BM1542)

named through the text using only their commercial names; BM1430, BM1432, and BM1542 respectively. The homopolymerization of styrene was performed for 6 h targeting Mn of 50,000 g/mol and using a molar ratio of [RAFT]:[AIBN] = 5:1 at 70°C. The conversion obtained at the end of reaction, droplets and final particles size as well as final Mn are shown in Table III.1.

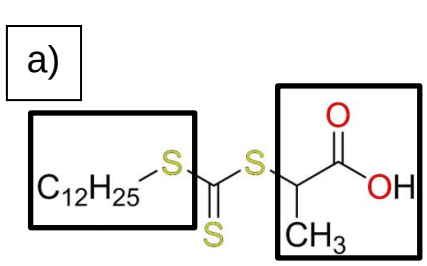

BM1430

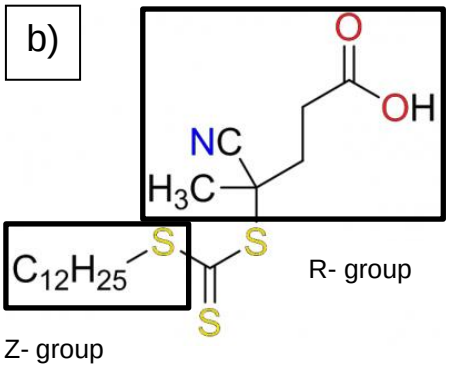

BM1432

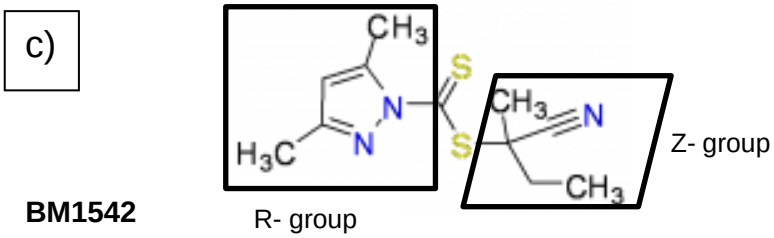

BM1542

Figure III.1. Chemical structures of the RAFT agents used for the synthesis of the polystyrene A block, a) 2-(((dodecylthio)carbonothioyl) thio) propanoic acid (BM1430), b) 4-cyano-4-(((dodecylthio)carbonothioyl)thio)pentanoic acid (BM1432), and c) 2-cyanobutanyl-2-yl 3,5-dimethyl-1H-pyrazole-1-carbodithioate (BM1542).

Table III. 1 Conversion, average droplet and particle size, theoretical Mn, Mn and PDI obtained after 6 h of reaction for pSt homopolymers synthesized using different types of initiators.

RAFT Agent	Conversion (%)	Droplet size (nm)	Particle size (nm)	Mn Theo. (g/mol)	Mn Obtained (g/mol)	PDI
BM1430	60	114.5	126.6	33444	41167	1.3
BM1432	0	120.7	-	-	-	-
BM1542	93.9	148.0	110.1	47014	40557	3.9

Both trithiocarbonate RAFT agents used had the same activating group Z (-$SC_{12}H_{25}$) based on non-volatile dodecane-thiol and different radical leaving group R (-$CH(CH_3)$-COOH and -$C(CH_3)CN$-CH_2-CH_2-COOH). Even though in small quantities, one could also expect that the activating group provides additional stabilization in the miniemulsification process. From the conversion-time profile shown on Figure III.2a, it can be seen that no conversion was achieved in 6 h when BM1432 was used as a

RAFT agent. This RAFT agent has a tertiary cyanoalkyl "R" group (-C(CH_3)CN-CH_2-CH_2-COOH) which is known to be a good free radical leaving group and good initiating radical[4]. BORON Molecular highly recommends this RAFT agent for styrene polymerization, and the literature data shows that it has been very effective with methacrylates[4,10,13]. However, no literature data could be found for styrene polymerization. According to our experiments, BM1432 RAFT agent did not initiate the RAFT miniemulsion polymerization of styrene and thus it was not further investigated. Furthermore, when BM1430 was used to mediate the polymerization, almost linear increase of conversion versus time was achieved up to 5 h, above which only a slight increase in conversion was obtained. As seen from Table III.1 the conversion reached at 6 h was 60%.

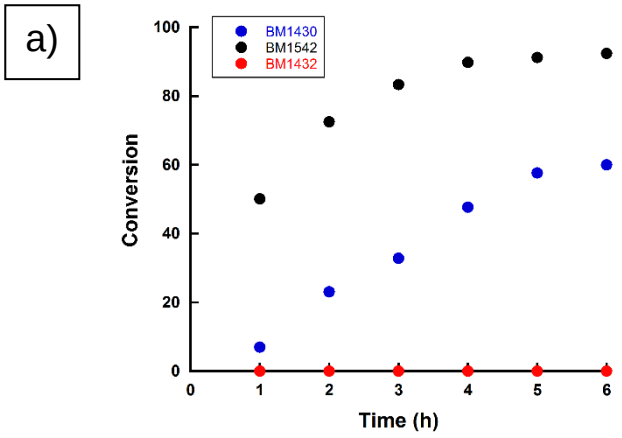

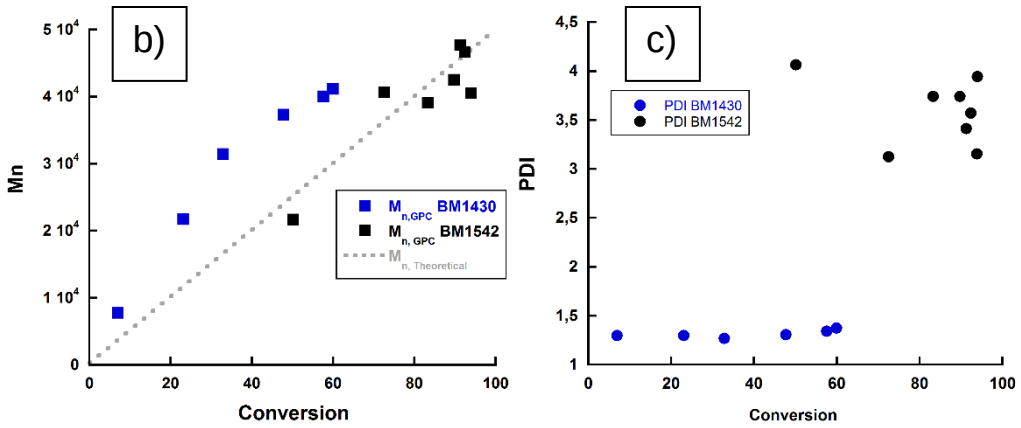

Figure III.2. The effect of RAFT agent on a) evolution of conversion of styrene as a function of time, b) evolution of Mn with conversion of monomer and c) evolution of PDI with monomer conversion

From the Mn versus conversion plots (Figure III.2b) we can see that the experimentally measured values were higher than the theoretical predicted ones at all conversion for BM1430 RAFT agent. This suggests that the RAFT agent role was not fully reached[14]. A number of proposals have been put forward that suggest ways in which thiocarbonylthio groups are lost or stored during the RAFT process. The fate of intermediate species 2 and 4 (Figure I.3 shown in Chapter I), their lifetimes, and concentrations as well as rates of fragmentation to R* and Pn* are subjects of intense debate[15–21]. Nevertheless, regardless of the mechanism involved, from the data obtained, one could conclude that the number of participating trithiocarbonyl group is not in accordance to the targeted ones.

On the other hand, the polymerization of styrene in the presence of tertiary dithiocarbamate RAFT agent (BM1542) reached around 50% conversion in one hour, almost full conversion in 4 h and later the polymerization remained unchanged (Figure III.2a). Moreover, this RAFT agent provided only limited control as indicated by high PDI obtained through the reaction. The final PDI was 3.9 as shown in Table III.1. One could also observe that the Mn obtained was not far from the predicted values. However, the very high PDI makes this RAFT agent not suitable for the polymerization of the initial polystyrene block. Gardiner et al.[11] investigated this RAFT agent for the polymerization of styrene, methyl acrylate and N,N-dimethylacrylamide in microwave reactor using 1,1'-azobis-1-cyanocycloxexane (ACHN) as initiator and concluded that its activity was similar to the corresponding trithiocarbonates. The polymerization of styrene was performed using toluene as solvent and the conversion achieved was only 68% for 48 h. Although the polydispersity obtained was very low (1.07), the reasons for such a long reaction time were not discussed. No literature data has been found to show the activity of this RAFT agent in minimemulsion polymerization. From the investigated RAFT agents, it can be concluded that BM1430 provided the best controlled reaction and it was further used for the synthesis of the AB-block copolymers.

The influence of different [RAFT]:[AIBN] molar ratio on the kinetics of the RAFT miniemulsion polymerization of styrene

III.3.2.

As previously discussed both in chapter I and chapter II, the amount of initiator present in the system is of great importance to obtain controlled radical polymerization. The total amount of chains is regulated by the amount of RAFT agent which successfully fragmentates and reinitiates the polymerization process as well as the amount of chains produced because of initiator decomposition[22,23]. However, higher conversion, requires a constant supply of initiator derived radicals as seen by Thomas et al.[14], who investigated the kinetics and molecular weight control of acrylamide polymerization via RAFT process. In this context, to obtain the highest conversion and still keep the reaction under control, the influence of several molar ratio of [RAFT]:[AIBN] have been investigated. The reaction was performed at 70°C targeting Mn of 50,000 g/mol with BM1430 as RAFT agent and the results are listed in Table III.2 and Figure III.3.

Table III.2. Conversion, average droplet and particle size, theoretical Mn, Mn and PDI obtained at the end of reaction for pSt homopolymers synthesized using BM 1430 at different molar ratios of [RAFT]:[AIBN] at 70°C.

[RAFT]:[AIBN]	Conversion (%)	Droplet size (nm)	Particle size (nm)	Mn, Theo. (g/mol)	Mn Obtained (g/mol)	PDI
4:1	72.0	98.6	115.3	36,129	42,912	1.37
5:1	59.9	114.5	126.6	30,126	41,167	1.37
7:1	56.6	107.4	126.5	28,478	42,043	1.28
10:1	48.3	78.0	116.0	24,377	37,530	1.26

The conversion vs time profile results shown in Figure III.3a show that the polymerization rate decreased as the ratio of [RAFT]:[AIBN] increased. From the results shown in Table III.2, we can see that when the [RAFT]:[AIBN] molar ratio was increased two times (from 5:1 to 10:1), the conversion of styrene decreased only slightly, namely from 59.9 to 48.3. Moreover, the PDI was not changed tremendously; it decreased from 1.37 to 1.26. Highest conversion was achieved when higher stream of radicals were added in the system (n[RAFT]:n[AIBN] =4:1). From the Mn versus conversion plots (Figure III.3b) we can see that for all the different n[RAFT]:n[AIBN] ratios used, the experimentally measured values were higher than the predicted ones. This is an indication that the utilization of the RAFT agent was indeed reduced largely by a constant factor in all the cases not depending on the initiator concentration present

in the system. In addition, the PDI increased at higher conversions for all the different molar ratios used, due to the irreversible termination because of monomer depletion.

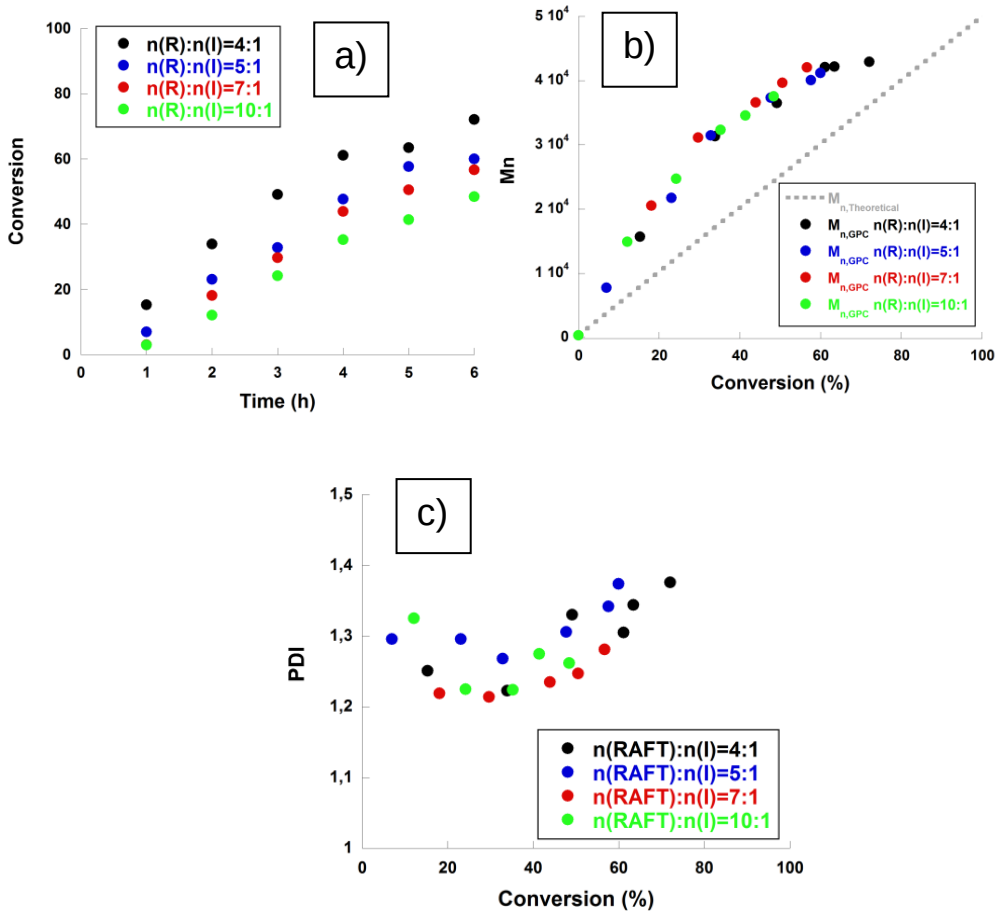

Figure III.3. Miniemulsion polymerization using RAFT Agent BM 1430: the effect of [RAFT]:[AIBN] on a) conversion of styrene as a function of time, b) evolution of Mn with conversion and c) PDI with conversion

As it has been mentioned, the polystyrene (containing small amounts of stearyl acrylate) will constitute the hard domain of the hard-soft block copolymer, therefore a high Tg is expected from it. However, the Tg of the polystyrene block is dependent on its length below a critical molecular weight and therefore we see dependence to the monomer conversion. Thus, to reach a compromise between the conversion, reaction time and Tg of the polymer, it was decided to further continue working with the molar ratio of [RAFT]:[AIBN] = 4:1.

III.3.3. Synthesis of polystyrene blocks: Hard domains

After optimization of the synthesis parameters, two pSt latexes targeting Mn of 30,000 and 50,000 g/mol using BM1430 as RAFT agent, AIBN as initiator, n[RAFT]:n[AIBN]=4:1 and a reaction temperature of 70°C were prepared and the results are shown in Figure III.4. These will be later used as seeds for the synthesis of the hard-soft block copolymers. From the conversion vs time plots, it can be seen, that an almost linear increase was achieved for both homopolymers (pSt30 and pSt50) up to 4 h, above which conversion slows down. After 6 h of reaction conversions of 72% and 74% were reached for pSt50 and pSt30 respectively (Figure III.4a). Even though not full conversion was achieved, the reaction was stopped due to the fact that living blocks were desired, able to be further extended with the second soft monomer. Mn for both pSt30 and pSt50 increased with conversion, but for both cases it was seen that the obtained values were higher than the theoretical predictions, effect more

pronounced for the higher Mn targeted (Figure III.4b). The molecular weight distribution (Figure III.4c and III.4.d) shifted to higher molecular weight up to 5 h after which only a small shift was observed as a result of the enlargement of low Mn chains.

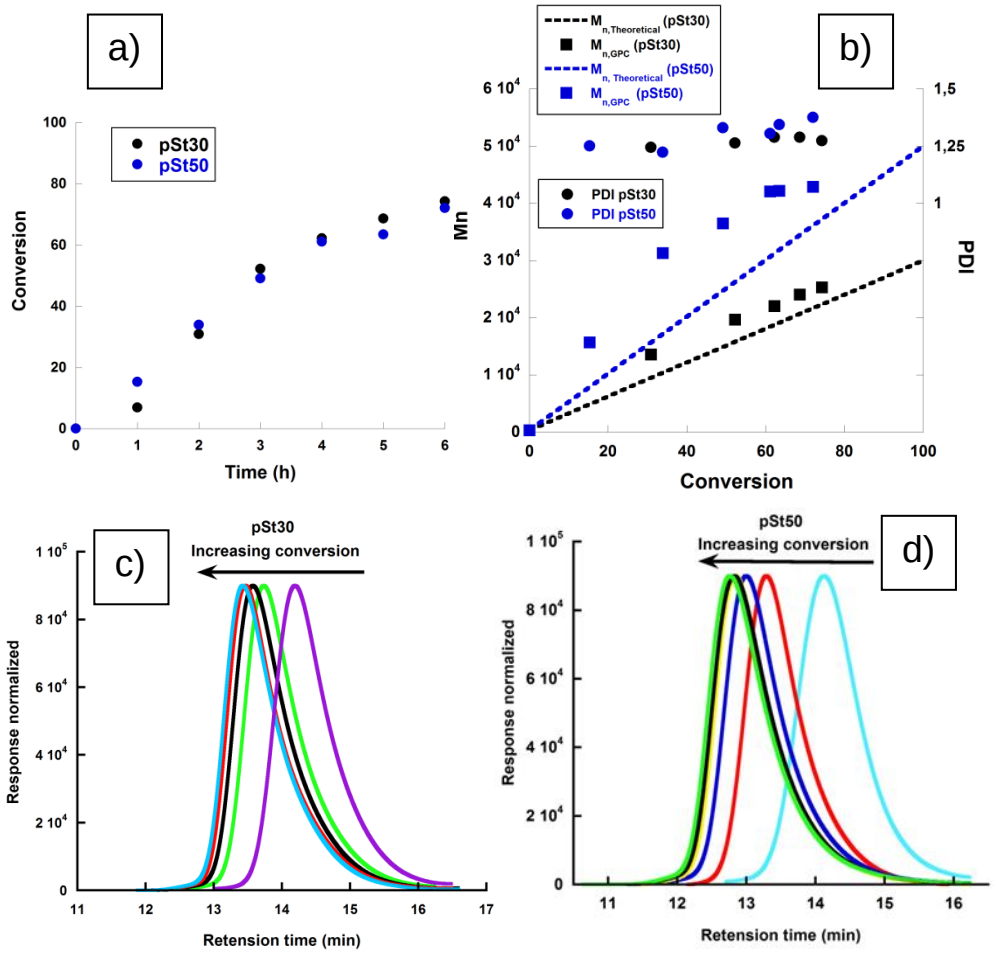

Figure III.4. Miniemulsion polymerization using RAFT Agent BM 1430: a) St conversion versus time, b) number-average molecular weight and polydispersity index vs monomer conversion for pSt30 and pSt50 and molecular weight distribution of c) pSt30 and d) pSt50 obtained by IR refractive index detector in GPC.

Synthesis of AB block copolymers: Hard-Soft domains

III.3.4

The pSt30 and pSt50 initial blocks were extended with the second soft 2EHA monomer to form AB block copolymers. The second monomer was fed as a pre-emulsion for 3 h with additional amount of initiator (AIBN) added in the system. The molar ratio of [RAFT]: [AIBN] was 2:1 and it was calculated based on the moles of RAFT agent present in the seed. Four block copolymers were synthesized with different target molecular weights, named through the text as: p(St50/2EHA50) as an extension of pSt50, p(St30/2EHA50), p(St30/2EHA70) and p(St30/2EHA100) as extensions of pSt30. The numbers after the letters indicate the targeted molecular weight divided by 1000. The results from the synthesis of the block copolymers are shown in Table III.3. Since the second block was fed without any removal of the unreacted styrene from the initial block, the second B block was a gradient block with more styrene units incorporated close to the A block and with an end of the chain richer in 2EHA. Nevertheless, the B block will be named as p(2EHA) through the text for simplicity reasons. From the evolution of Mn versus total monomer conversion (determined by solids content measurements), the block copolymers prepared from pSt30 seed (Figure III.5a) showed a linear increase of Mn. Nevertheless, the Mn started to negatively deviate from the theoretical prediction once the second monomer was added. As explained in chapter II, this is most likely due to the difference in the Mark-Houwink constants of pSt and 2EHA[24] (the GPC results are based on pSt standards). This effect

was less pronounced for pSt50/2EHA50 block copolymer, since this polymer was richer in pSt compared to the block copolymers starting from a pSt30 seed.

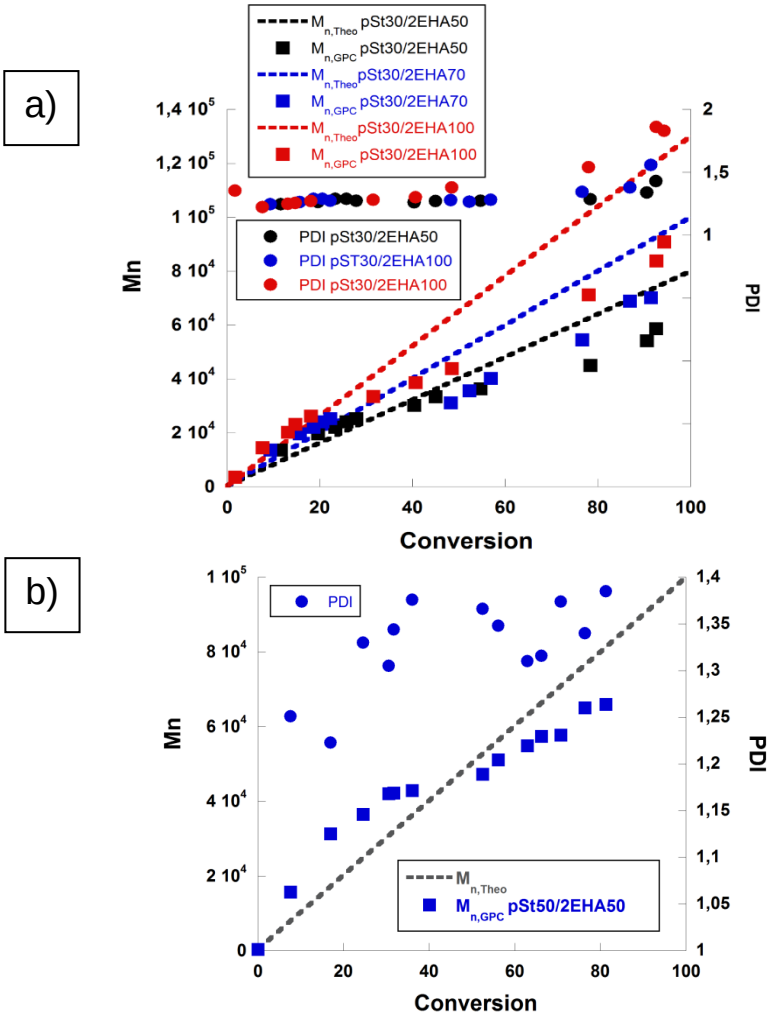

Figure III. 5 Evolution of the number average molecular weight and polydispersity index vs monomer conversion for a) pSt30/2EHA50; pSt30/2EHA70 and pSt30/2EHA100 and b) pSt50/2EHA50 block copolymers

Table III.3. Conversion, average particle size, Mn and PDI at the end of reaction for pSt homopolymers and p(St/2EHA) block copolymers

Reactions	Conversion (%)	$M_{n,GPC}$ (g/mol)	PDI	dd (nm)	dp (nm)	dp (nm)	Conversion (%)	$M_{n,GPC}$ (g/mol)	PDI
	pSt Homopolymers					(St/2EHA) Block copolymers			
p(St5/2EHA50)	72.0	36,121	1.37	98.6	115.3	150.4	81.2	65,980	1.38
p(St30/2EHA50)	74.2	22,364	1.27	100.6	121.1	160.6	92.53	58,611	1.42
p(St30/2EHA70)	74.2	22,364	1.27	100.6	121.1	165.0	91.4	70,103	1.55
p(St30/2EHA100)	78.1	23,509	1.27	89.9	126.2	171.3	94.2	90,834	1.83

The overall conversion of the block copolymers was above 90% except for the pSt50/2EHA50, which reached 81% conversion (Table III.3). Moreover, as seen from the Table, PDI increased with increasing the targeted Mn, most likely due to branching reactions which are characteristic for acrylates[25–27].

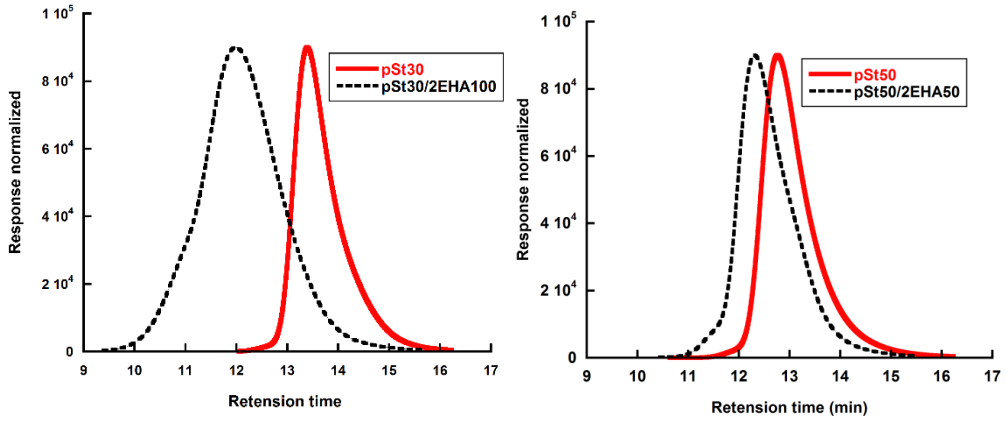

Figure III.6. MWD of the initial pSt homopolymer and the final block copolymers for pSt30/2EHA100 and pSt50/2EHA50.

The MWDs presented in Figure III.6 indicate that the block copolymers have been successfully formed, since not only the average Mn but all the MWD for the AB block copolymers shifted to higher molecular weights compared to the initial pSt block. Furthermore, it could be seen that the MWD for pSt30/2EHA100 broadened in the second step which is in good agreement with the high PDI obtained.

Thermal properties of the block copolymers

DSC measurements were performed to determine the glass transition temperatures (Tgs) of the pSt precursor polymers and pSt-2EHA block copolymers and the results obtained are shown in Figure III.7 and Table III.4.

III.3.5

Table III.4. Thermal properties of the p(St-EHA) block copolymers obtained by DSC

Material code	Tg_1 (ºC)	Tg_2 (ºC)
DSC analysis of the samples dried at 23 °C		
pSt30	-	67.3
pSt50	-	61.0
p(St30-2EHA50)	-60.5	79.6
p(St30-2EHA70)	-60.5	78.3
p(St30-2EHA100)	-61.6	79.5
p(St25-2EHA50)	-50.4	69.9

A single glass transition temperature was obtained for both initial pSt30 and pSt50 A blocks having different Mn. The Tg values were similar to each other (67.3 ºC for pSt30 and 61.0ºC for pSt50), however much lower than the Tg of pure pSt (100°C) shown in the literature data. As explained in the experimental part and as well elaborated in chapter II, stearyl acrylate was used as a costabilizer to prevent Oswald ripening in the miniemulsion. The Tg of the polystearyl acrylate is low (-110°C)[28].

Thus, when this monomer is copolymerized with styrene, we can expect that the Tg is substantially reduced compared to pure polystyrene. In addition, apart from the effect of the costabilizer comonomer, the low molecular weight of the polystyrene precursor could also have an influence[29] to decrease the Tg of the polystyrene block compared to the literature value of pure polystyrene.

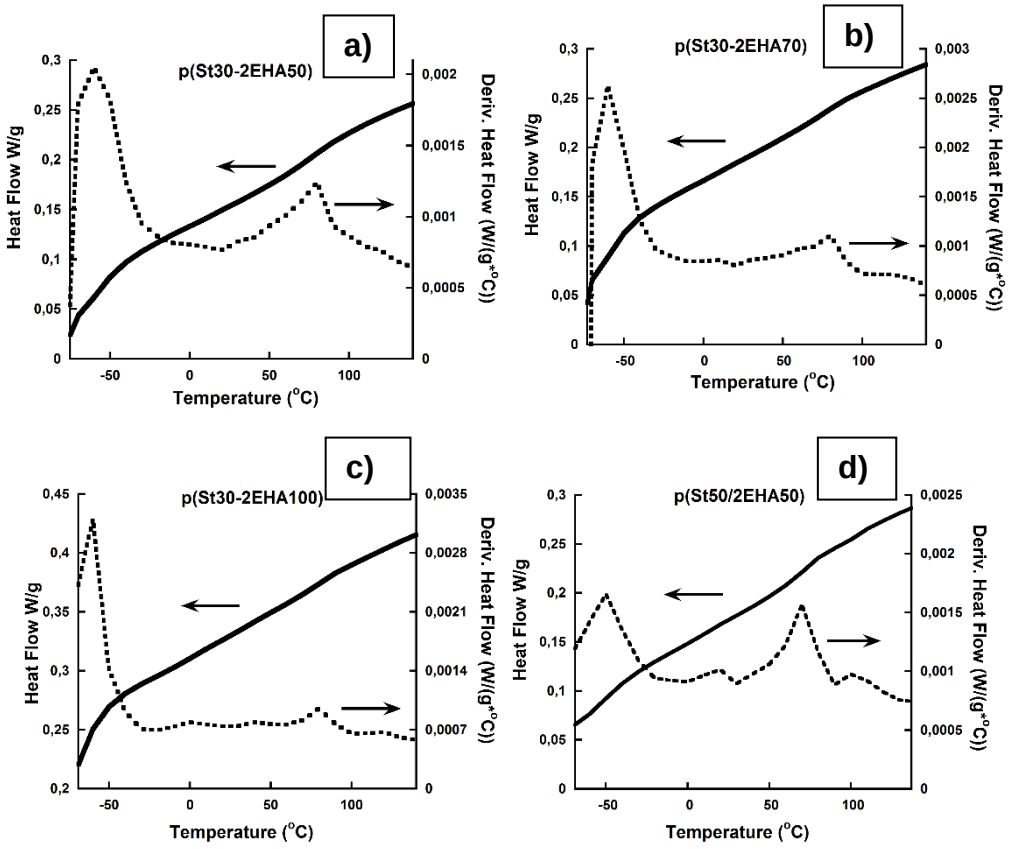

Figure III.7. DSC thermograms of the p(St-EHA) block copolymers measured at a heating rate of 10 °C/min

The DSC results of the AB block copolymers on the other hand showed two distinct Tg's, a lower one in the range of -50 to -60°C, corresponding to the soft block composed mainly of p2EHA, and an upper one in the range of 70 to 80°C, associated with Tg of the hard polystyrene domain. Moreover, from the first heat flow derivative we can clearly see that for the block copolymers formed from pSt30, the area under the peak of the lower Tg was much higher than the one of the higher Tg. On the other hand, the peaks are almost the same for the pSt50/2EHA50 block copolymer. This is an indication of two-phase systems with different proportion of soft and hard domains.

III.4. Conclusions

In summary, two-step reversible addition fragmentation chain transfer polymerization and an asymmetric RAFT agent were used to synthesize a series of waterborne AB block copolymers containing hard and soft domains. The synthesis of the hard-polystyrene domains was done using miniemulsion polymerization and a conversion up to ~74% was obtained. These precursor miniemulsion polymers later served as a seed for the second polymerization of 2EHA soft block. The effect of three RAFT agents and several molar ratios of RAFT to Initiator were investigated on the polymerization of the first styrene block. It was observed that from both tritiocarbonate and dithiocarbamate-pyrazole based RAFT agents, the 2-(((dodecylthio)carbonothioyl)

thio)propanoic BM1430 mediated the mini emulsion polymerization of styrene in the most controlled way. Successful formation of the AB block copolymers was proven by MWD shift and a linear increase of Mn versus conversion. Nevertheless, a negative deviation of the Mn obtained with GPC versus the theoretical prediction was observed. The reasons behind this finding are explained in chapter II and originate from the fact that the Mn of the block copolymers obtained with GPC is measured using pSt standards only. DSC measurements showed that pSt precursor polymers exhibit a single Tg lower than 100° (Tg of high molecular weight pSt synthesized by free radical polymerization) because of the reactive comonomer stearyl acrylate used as costabilizer in the miniemulsion and due to the low Mn obtained. The block copolymers on the other hand showed two Tg corresponding to the soft and hard domains.

III.5. References

1 T. Roshan, E. Rizzardo, J. Chiefari, J. Krstina, G. Moad, A. Postma and S. H. Thang, *Macromolecules*, 2000, **33**, 243–245.

2 C. Barner-Kowollik, J. F. Quinn, T. L. U. Nguyen, J. P. a Heuts and T. P. Davis, *Macromolecules*, 2001, **34**, 7849–7857.

3 M. S. Donovan, T. A. Sanford, A. B. Lowe, B. S. Sumerlin, Y. Mitsukami and C. L. Mccormick, 2002, **35**, 4570–4572.

4 B. Y. K. Chong, J. Krstina, T. P. T. Le, G. Moad, A. Postma, E. Rizzardo and S. H. Thang, *Macromolecules*, 2003, **36**, 2256–2272.

5 J. Chiefari, R. T. A. Mayadunne, C. L. Moad, G. Moad, E. Rizzardo, A. Postma, M. A. Skidmore and S. H. Thang, *Macromolecules*, 2003, **36**, 2273–2283.

6 G. Moad, A. E. Rizzardo and San H. Thang, Aust. J. Chem., 2005, **58**, 379–410.

7 G. Moad, E. Rizzardo and S. H. Thang, *Polymer*, 2008, **49**, 1079–1131.

8 G. Moad, E. Rizzardo and S. H. Thang, *Aust. J. Chem.*, 2006, **59**, 669–692.

9 J. T. Lai, D. Filla and R. Shea, *Macromolecules*, 2002, **35**, 6754–6756.

10 E. Rizzardo, M. Chen, B. Chong, G. Moad, M. Skidmore and S. H. Thang, *Macromol. Symp.*, 2007, **248**, 104–116.

11 J. Gardiner, I. Martinez-Botella, J. Tsanaktsidis and G. Moad, *Polym. Chem.*, 2016, **7**, 481–492.

12 J. Gardiner, I. Martinez-Botella, T. M. Kohl, J. Krstina, G. Moad, J. H. Tyrell, M. L. Coote and J. Tsanaktsidis, *Polym. Int.*, 2017, **66**, 1438–1447.

13 G. Moad, Y. K. Chong, A. Postma, E. Rizzardo and S. H. Thang, *Polymer*, 2005, **46**, 8458–8468.

14 D. B. Thomas, A. J. Convertine, L. J. Myrick, C. W. Scales, A. E. Smith, A. B. Lowe, Y. A. Vasilieva, N. Ayres and C. L. McCormick, *Macromolecules*, 2004, **37**, 8941–8950.

15 C. Barner-Kowollik, M. L. Coote, T. P. Davis, L. Radom and P. Vana, *J. Polym. Sci. Part A Polym. Chem.*, 2003, **41**, 2828–2832.

16 M. L. Coote, *Macromolecules*, 2004, **37**, 5023–5031.

17 B.-K. Christopher, Q. J. F, M. D. R and D. T. P, *J. Polym. Sci. Part A Polym. Chem.*, 2001, **39**, 1353–1365.

18 Y. Kwak, A. Goto, Y. Tsujii, Y. Murata, K. Komatsu and T. Fukuda, *Macromolecules*, 2002, **35**, 3026–3029.

19 M. J. Monteiro and H. De Brouwer, *Macromolecules*, 2001, **34**, 349–352.

20 A. R. Wang and S. Zhu, *Macromol. Theory Simulations*, 2003, **12**, 663–668.

21 A. Ah Toy, P. Vana, T. P. Davis and C. Barner-Kowollik, *Macromolecules*, 2007, **37**, 744–751.

22 G. Moad, J. Chiefari, Y. K. Chong, J. Krstina, R. T. A. Mayadunne, A. Postma, E. Rizzardo and S. H. Thang, *Polym. Int.*, 2000, **49**, 993–1001.

23 E. V. Chernikova and E. V. Sivtsov, *Polym. Sci. Ser. B*, 2017, **59**, 117–146.

24 E. Lathova, D. Lath and J. Pavlinec, *Polym. Bull.*, 1993, **30**, 713–718.

25 N. Ballard and J. M. Asua, *Prog. Polym. Sci.*, 2018, **79**, 40–60.

26 C. Plessis, G. Arzamendi, J. R. Leiza, H. A. S. Schoonbrood, D. Charmot and J. M. Asua, *Macromolecules*, 2000, **33**, 5041–5047.

27 S. Hamzehlou, Y. Reyes, R. Hutchinson and J. R. Leiza, *Macromol. Chem. Phys.*, 2014, **215**, 1668–1678.

28 E. Mehravar, J. R. Leiza and J. M. Asua, *Polymer*, 2016, **96**, 121–129.

29 T. G. Fox and P. J. Flory, *J. Appl. Phys.*, 1950, **21**, 581–591.

Chapter IV. Synthesis and characterization of crystalline-soft-crystalline ABA type block copolymers

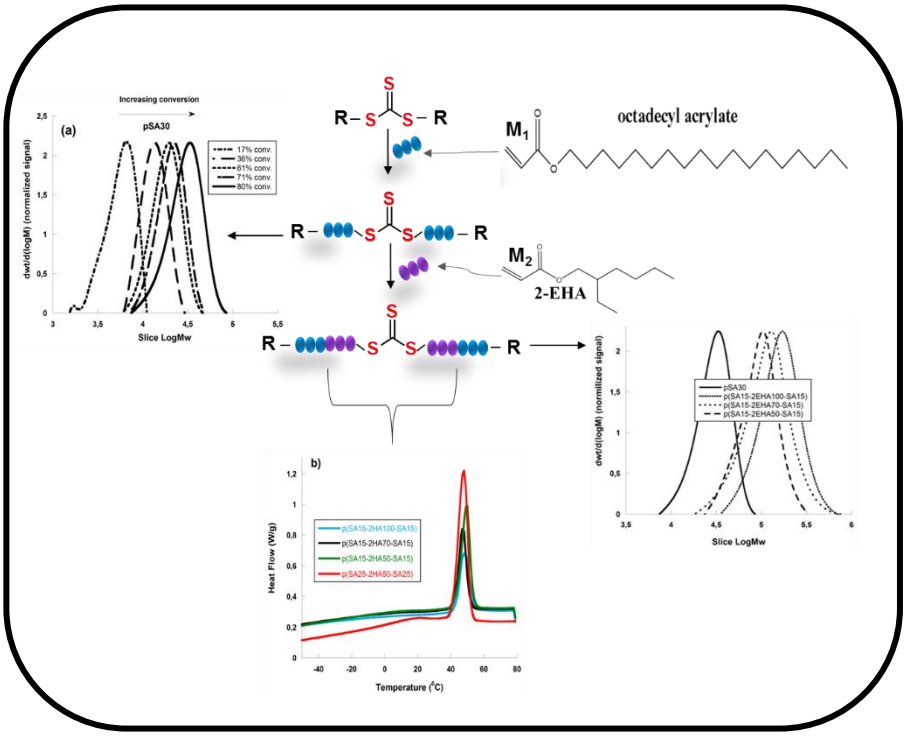

IV.1. Introduction

The properties of poly n-alkyl (meth)acrylate polymers have been of continuing interest since they were initially investigated by Rehberg et al. in 1940's[1]. In these types of polymers the long n-alkyl side chains crystallize, unlike conventional crystalline polymers whose backbone crystallizes[2–4]. The melting-crystallization transition in the n-alkyl (meth)acrylate monomers, which occurs at the melting temperature (Tm), can be controlled by side-chain length and causes significant changes in the physical properties of the polymer[2,5–9]. The longer the side-chain of the polymer, the more side chain carbons are able to crystallize which increases the energy required to melt the polymer (ΔH_f) as well as crystallite size distribution, which at the end influences Tm and its breadth. The n-alkyl side chains in poly (n-alkyl) (methyl) acrylate pack in hexagonal crystalline lattice, as shown by wide angle X-Ray scattering (WAXS)[10], with a distance between side chains of 4.85 Å. End to end packing and interdigitating packing formation of poly (n-alkyl) acrylates based on X-Ray scattering (SAXS) studies was suggested by Plate et al.[10] and Hsieh et al.[11]. Moreover, Plate et al. showed that due to bulkiness of the main chain in poly (n-alkyl) methacrylates, they show reduced crystallinity compared to poly (n-alkyl) alcrylates. Rehberg et al.[1] on the other hand showed that the glass transition temperature (Tg) dropped with the increase of the side chain up to 8-10 carbon atoms and that crystallinity appeared for side chains reaching a certain critical value of n>11. Monomers with relatively long side chains $(CH_2)n$ ($10 \leq n \leq 22$)

are commercially available and they have been used for the synthesis of waterborne latex particles containing crystalline domains for various applications. One of the widely used long chain monomer is octadecyl acrylate (commercially known as stearyl acrylate). Waterborne semicrystalline temperature-responsive pressure sensitive adhesives[12,13], coatings[14,15] and paints[16] based on stearyl acrylate have been already reported in the literature. Moreover, Popadyuk et al.[17] synthesized pSA based thermoresponsive latexes for fragrance encapsulation and release. Zhang et al.[18] synthesized poly(perfluoralkyl acrylate-co-stearyl acrylate) using miniemulsion and investigated their macrostructure and surface properties.

Furthermore, and regarding the controlled polymerization of SA monomer, homo and block copolymers based on stearyl acrylate and produced by Atom Transfer Radical Polymerization (ATRP) have also been reported[19–21]. However, they were synthesized either in bulk or solution polymerization. The literature referring to the synthesis of block copolymers containing pSA by Reversible Addition Fragmentation Chain Transfer polymerization (RAFT) in water media remains scarce.

In this sense, in this chapter waterborne ABA block copolymers of stearyl acrylate (SA) and 2-ethylhexyl acrylate (2EHA), containing crystalline A block and soft middle B block, were synthesized via two-step RAFT polymerization, using S,S-dibenzyl trithiocarbonate (DBTTC) bifunctional RAFT agent. The synthesis of the block

copolymers was done in two steps. First miniemulsion polymerization was used for the synthesis of the pSA block, which forms crystalline domains. Then in the second step semi-batch emulsion polymerization was used for the synthesis of the p2EHA mid-block, which forms soft domains. 2EHA was fed in the system and soft domains were formed. Different MWs of the blocks were targeted and the effect on the kinetics and MWD's was studied. Moreover, the thermal properties of both the initial pSA and the final block copolymers were analysed with different experimental techniques.

IV.2. Experimental part

IV.2.1. Materials

The materials used for the synthesis of crystalline-soft-crystalline block copolymers are given in Appendix I.

IV.2.2. Synthesis Procedures

Synthesis of the first block: Batch Miniemulsion Polymerization

SA miniemulsion was prepared according to the following procedure. The oil and the aqueous phase were prepared separately. First the aqueous phase was prepared by dissolving the surfactant disodium lauryl sulfosuccinate (DSLS) (2 wt% Based on monomer =BOM) and $NaHCO_3$ (0.16 wt% BOM) in deionized water. This mixture was

heated up and kept at 40°C under magnetic stirring (800 rpm) for 10 min until homogeneous solution was produced. SA is a solid monomer at room temperature, so to form a good dispersion of this monomer in the aqueous phase, melted SA where AIBN and the RAFT were previously dissolved, was added to the preheated aqueous phase and stirred under high magnetic agitation for 15 min at 40°C. The resultant emulsion was then ultrasonicated using a Branson Sonifier 450 for 15 min (amplitude 70%) under magnetic stirring in an ice water bath to avoid overheating and possible reaction. To narrow down the droplet size distribution, the miniemulsion was additionally passed through a high-pressure Niro-Soavi homogenizer. Two cycles were used with a pressure of 6 MPa in the first valve and 60 MPa in the second valve. The total solids content of the miniemulsion was 30 wt% and a (RAFT):(Initiator) molar ratio of 5:1 was used in all cases.

The miniemulsion was then transferred to a 1L commercial calorimetric glass jacketed reactor (RTCal™, Mettler-Toledo) equipped with a mechanical anchor stirrer, a platinum resistance thermometer, a nitrogen inlet and sampling tube. The conversion of SA was followed online using the following formula:[15]

$$X_{SA}(t) = \frac{\int_0^t Qr(t)dt}{\int_0^\infty Qr(t)dt} = \frac{\int_0^t Qr(t)dt}{\Delta Hp * Mo} \quad (1)$$

where Qr(t) is the heat generated, ΔHp is the enthalpy of the SA homopolymerization (ΔHp = -88 kJ mol^{-1}, measured in the calorimeter reactor for full conversion and confirmed by ^{1}H NMR) and Mo is the mass of the SA initially added in the reactor. Prior to increasing the temperature, the miniemulsion was purged with nitrogen for 30 min to remove the dissolved oxygen. Then the temperature was increased to 70°C and the resulting miniemulsion was polymerized under nitrogen. Once the polymerization of SA started, samples were taken at different time intervals for conversion determination and GPC analysis and they were quenched with 1 wt% hydroquinone water solution.

Synthesis of the second block: Semibatch emulsion polymerization

PolySA (pSA) initial A block latex was used as a seed for the synthesis of the second middle block. The second monomer (2EHA) was fed as a pre-emulsion for 3h and left 1h batchwise to reach higher conversion. The pre-emulsion was prepared by mixing the monomer, water and the emulsifier. The total amount of the surfactant was kept constant, 2 wt% based on all monomers. Additional amount of AIBN dissolved in monomer was added once the temperature was increased to 70°C to start the polymerization. The initiator added was calculated based on the amount of the moles of the RAFT agent present in the seed and was kept constant at (RAFT):(Initiator) =2:1 for all block copolymers. To remove the dissolved oxygen, the seed and the pre-emulsion were purged with nitrogen for 30 min prior to polymerization. The initiator

dissolved in monomer was purged for 10 min. Furthermore, nitrogen flow was kept during polymerization as well. At the end of the reaction, the temperature was decreased, and the latex was filtered and collected. Coagulum amounts lower than 0.5 wt% were collected in all the cases.

IV.2.3. Characterization

The conversion of the monomers was followed both gravimetrically and by NMR. The monomer droplet and the final particle size of the latexes was measured by dynamic light scattering (DLS). The molecular weights and the molecular weights distribution were measured using two different GPC instruments. Thermal stability of the block copolymers was measured using DSC and TGA. The detailed description of the characterization methods is provided in Appendix.

IV.3. Results and discussion

IV.3.1. A block homopolymer synthesis: Crystalline domains

Homopolymers of pSA (A-crystalline block) were synthesized with two different molecular weights using trithiocarbonate DBTTC RAFT agent. The calorimeter reactor was used for the polymerization of the initial pSA blocks due to the large inhibition time and in order to stop the reaction at around 80% conversion. Table IV.1. describes the

experimental conditions used for the homopolymerization of SA, and the results obtained after the polymerization.

Table IV.1. The experimental recipes, conversion (x), theoretical Mn for the conversion achieved ($M_{n,theory}$), Mn measured by SEC ($M_{n,SEC}$), diameter of the droplets (dd) and particles (dp) for the pSA homopolymers.

Run	Target (g/mol)	Monomer SA (g)	RAFT (mol x 10^4)	x(%)	$M_{n,\ theory}$ (g/mol)	$M_{n,SEC}$[a] (g/mol) RI signal	PDI	dd (nm)	dp (nm)
pSA30	30 k	120	40.39	80.0	24.1 k	27.0 k	1.19	171	176
pSA50	50 k	120	24.14	78.2	39.1 k	42.2 k	1.17	188	190

[a]calculated based on Mark- Houwink constant for pSA

From Table IV.1. it can be seen that the SA miniemulsion droplet size and the final particle sizes were almost identical, indicating efficient droplet nucleation and no issues with colloidal stability, meaning that no superswelling[26] occurred under the synthesis conditions. SA is an extremely hydrophobic monomer and often used as a costabilizer in miniemulsion polymerization to prevent Ostwald ripening.[22,23] Higuchi and Misra [24] were the pioneers to consider Ostwald ripening kinetics in the two-component disperse phase miniemulsion system. They showed that only a small amount of an extremely hydrophobic compound in the dispersed phase dramatically retarded the Ostwald ripening process due to equalization of the concentrations of the major component (e.g., monomer) in droplets of different sizes, as a consequence of the osmotic pressure effect.

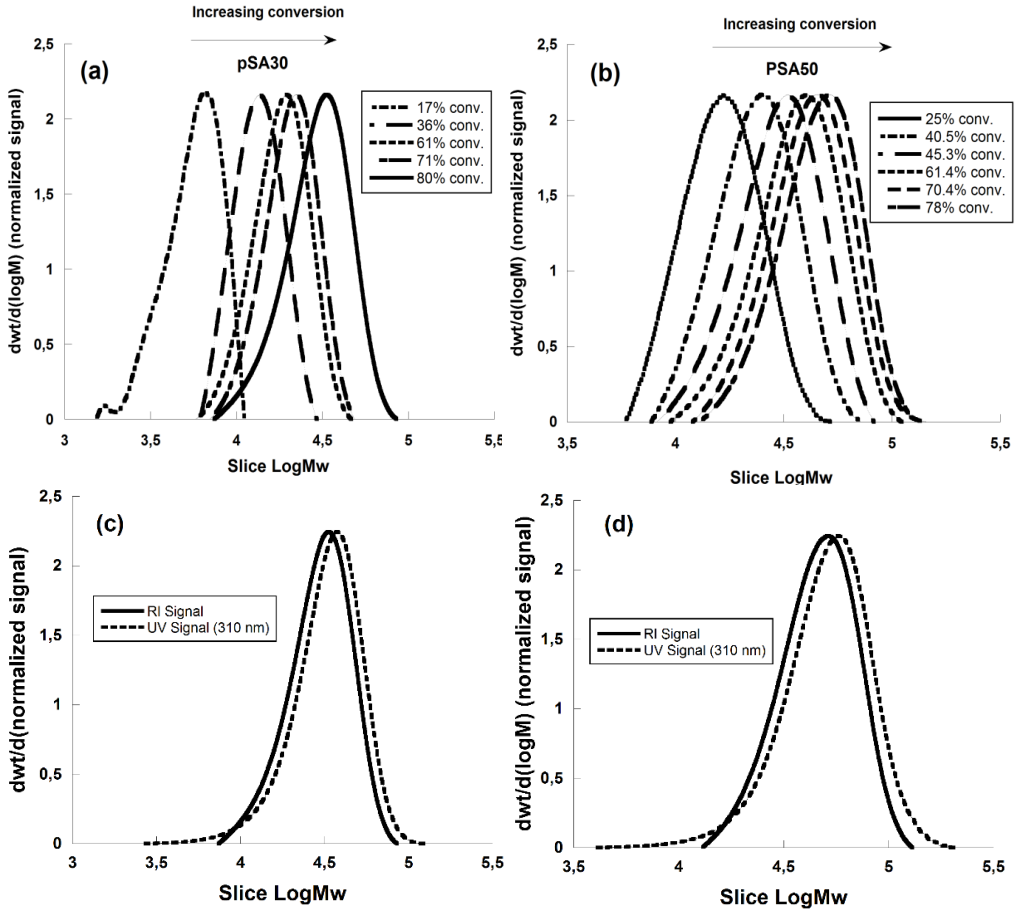

Figure IV.1. Evolution of MWDs with conversion for a) pSA30 and b) pSA50 (RI detector) and final MWD based on UV and RI detectors for c) pSA30 and d) pSA50.

Lin et al.[25] modelled the Ostwald ripening rate of styrene minemulsions stabilized by homologues of n-alkane costabilizers, with n ranging from 10-32. They found out that the effectiveness of n-alkenes as costabilizer increases with increasing n-alkane

molecular weight. Thus, no additional co-stabilizer was necessary in the miniemulsion as SA served as both monomer and costabilizer and the apparent colloidal stability of the miniemulsion was excellent. Furthermore, a monomodal particle size distribution was obtained in both pSA30 and pSA50, demonstrating that the primary nucleation mechanism was droplet nucleation. Secondary nucleation is highly undesired in RAFT polymerization because the newly formed particles would not contain any RAFT agent and as a result the polymerization in these particles will not be controlled.[27] Moreover, the polymerization of pSA proceeded with good control or livingness as evidenced by the MWD's shifting to higher molecular weight with increasing conversion (Figure IV.1.(a and b)). In order to investigate the presence of the trithiocarbonate group through the MWD both RI and UV detector systems were used for the SEC analysis. The UV detector was set to 310 nm, which corresponds to the maximum absorption wavelength of the trithiocarbonate unit in the RAFT agent.[28] As it can been seen from Figure IV.1. (c,d) the overlay of the RI and UV shows that the RAFT agent was incorporated throughout the whole distribution.

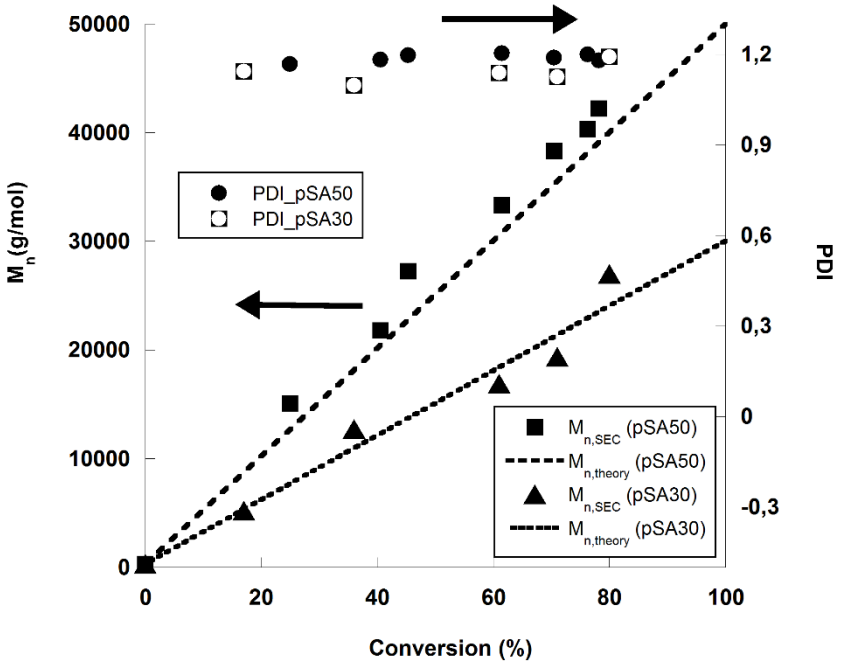

Figure IV.2. Evolution of Mn's and PDI's for RAFT miniemulsion polymerization of pSA30 and pSA50.

Another confirmation for the livingness of the system as discussed in previous chapters is the linear increase of the Mn with conversion, following the theoretical prediction. As it can be seen in Figure IV.2, the experimental M_{nSEC} values followed the predicted ones and the polydispersities at the end of the reaction were very low, remaining constant throughout the reaction, which indicates that the chains bear the RAFT agent at the end of the reaction.

IV.3.2. ABA block copolymer synthesis Crystalline-Soft-Crystalline domains

Block copolymers of ABA type where A is the crystalline block formed from pSA and B is a soft copolymer based on 2EHA units, still containing small amounts of the non-reacted SA, were then prepared by seeded semi- batch emulsion polymerization. The homopolymer pSA latexes with around 80% conversion served as seed for the second block polymerization.

Table IV.2. The experimental recipes, conversion (x), theoretical Mn for the conversion achieved ($M_{n,theory}$), Mn measured by SEC ($M_{n,SEC}$), diameter of the particles (dp) for the pSA-2EHA-SA block copolymers.

Run	Target Mn (g/mol)	Amount of seed (g)	Monomer 2EHA (g)	x (%)*	$M_{n,\ theory}$ (g/mol)	$M_{n,SEC}$ (g/mol) RI signal	PDI	Final particle size (nm)
p(SA15-2EHA50-SA15)	80 k	135 (pSA30)	66.01	99.6	79.7 k	83.5 k	1.23	195
p(SA15-2EHA70-SA15)	100 k	100 (pSA30)	68.46	100	100 k	96.5 k	1.39	200
p(SA15-2EHA100-SA15)	130 k	100 (pSA30)	97.80	92.8	120.7 k	140.8 k	1.28	236
p(SA25-2EHA50-SA25)	100 k	200 (pSA50)	58.70	81	81.0 k	81.0 k	1.21	209

*Determined by combination of NMR and gravimetrically

Formation of the ABA block copolymers and extension of the pSA block was proven by shifting of the MWD to higher Mn's as shown in Figure IV.3. In Figure IV.3 the MWD of the initial pSA30 block and the final MWDs of the block polymers are presented. The properties of the final block copolymers are shown in Table IV. 2.

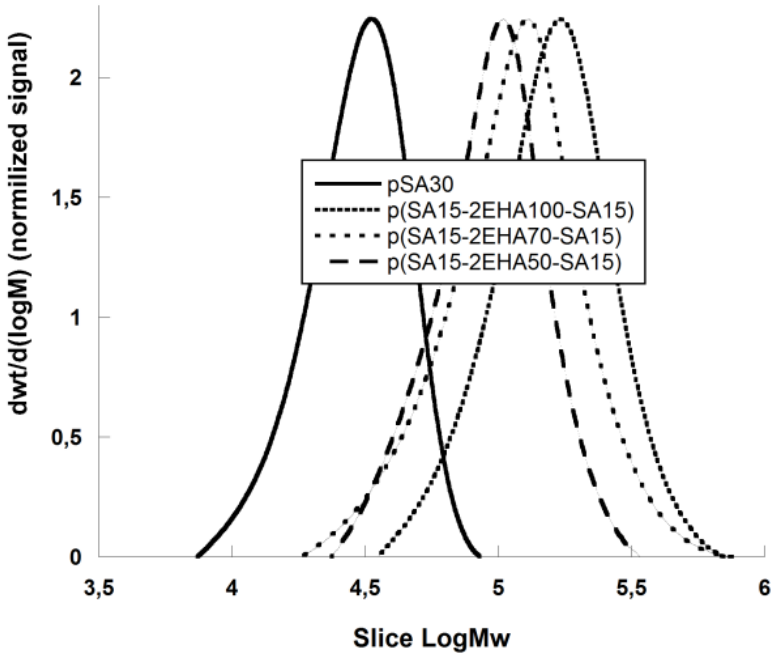

Figure IV.3. GPC Analysis: Extension of the pSA block and formation of ABA blocks (RI detection)

It can be seen from the table that the final overall conversion is very high (above 92 %) except for the case when higher Mn initial pSA homopolymer latex was used (run- p(SA25-2EHA50-SA25)). This is most likely due to the lower amount of the initiator added in the second step, which is referred to the lower amount of RAFT agent bearing chains for pSA50. The obtained Mn's are very close to the theoretical ones for the obtained conversion and the PDI indexes are rather low indicating that the reaction proceeded in a controlled manner.

It has to be pointed out that B block was not be pure P2EHA, as SA conversion was not 100%l in the first block. However due to the high SA concentration in the particles while 2EHA was being fed slowly, a gradient polymer will be formed in the second step, containing more monomer units of SA located closely to the preformed pSA homopolymer in the chain and more 2EHA units as it moves further away from the PSA block.

IV.3.3. Thermal properties of the block copolymers

The thermal properties of the homo and block copolymers were analyzed by means of DSC and TGA. The DSC of the pSA homopolymer (a) and p(SA-2EHA-SA) (b) block copolymers are shown in Figure IV.4. The DSC of the pSA homopolymers (Figure IV.4a) reveal a single big endothermic peak at around 49°C attributed to the melting of the crystalline domains and a smaller peak at 30°C attributed to the crystals of the unreacted monomer still present in the initial pSA block.[29]

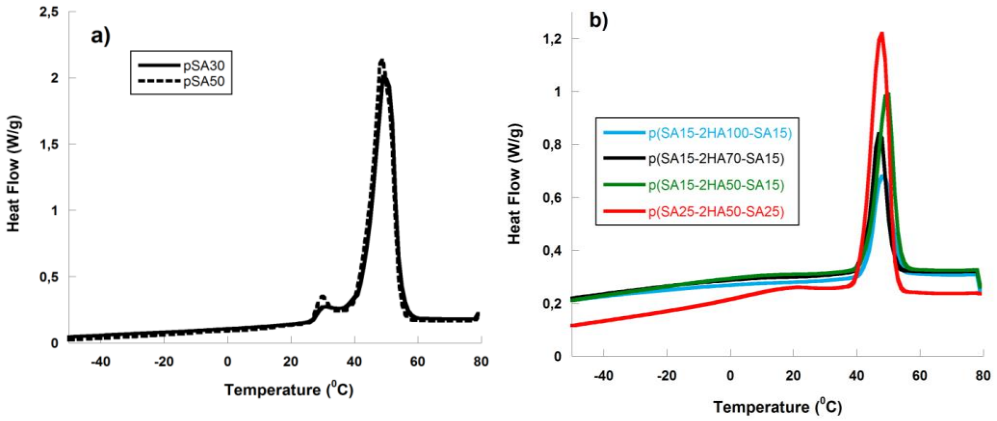

Figure IV.4. First heating DSC scans of the a) initial A-Block homopolymers pSA and b) final ABA block copolymers with different compositions.

Additionally, the DSC thermograms shown in Figure IV.4b show a single endothermic peak decreasing as the length of the middle soft block is increasing and the absence of the peak at 30°C indicating that the SA monomer had copolymerized with 2EHA in the second step.

Melting temperatures, heat of fusion and the degree of crystallinity obtained from the DSC curves are summarized in Table IV.3.

Table IV.3. Melting temperatures and crystallinity of the synthesized homo and block copolymers. In the case of the XRD measurements, they were carried out after drying the sample at 23ºC and at 60ºC.

Name	Tm (°C) 1st run	Tm (°C) 2nd run	ΔH_f (J/g) 1st run	ΔH_f (J/g) 2nd run	% cryst. by DSC (btpw)[a]	% cryst. by DSC (bpSA)[b]	% cryst. by XRD (23ºC) (btpw)[a]	% cryst. by XRD (60ºC) (btpw)[a]
pSA30	49.8	47.2	85.8		39.3	49.1	62.7	
PSA50	48.5	46.3	90.4		41.5	51.8	59.6	
p(SA15-2EHA50-SA15)	49.6	46.6	26.1	26.4	11.9	39.6	8.3	14
p(SA15-2EHA70-SA15)	47.1	46.4	18.7	19.2	8.5	35.4	5.5	8.5
p(SA15-2EHA100-SA15)	47.9	46.1	15.9	11.4	7.3	37.4	4.6	7.1
p(SA25-2EHA50-SA25)	47.8	44.8	40.2	39.8	18.4	41.6	21	27

[a] **Based on total polymer weight**

[b] **Based on pSA block**

As it can be seen from the table, no significant difference between the first and the second heating run is evident in the obtained heats of fusion. So, the first run was taken for the calculation of the degree of crystallinity. The heats of fusion of pSA initial blocks, not including the area of the crystals originating from the unreacted monomer, were 85.8 J/g for pSA30 and 90.41 J/g for pSA50 leading to 39.3 and 41.5% of crystallinity respectively. The degree of crystallinity was calculated based on the heat of fusion (expressed in J/g) of the sample, determined by DSC (from the first heating cycle) and the heat of fusion of a 100% crystalline pSA (218 J/g)[19]. The degree of crystallinity and the melt enthalpy of the block copolymers decreased with incorporation of 2EHA units, as also observed by Lu's group who synthesized poly(SA-b-styrene-b-SA) triblock copolymers by atom transfer radical polymerization[30].

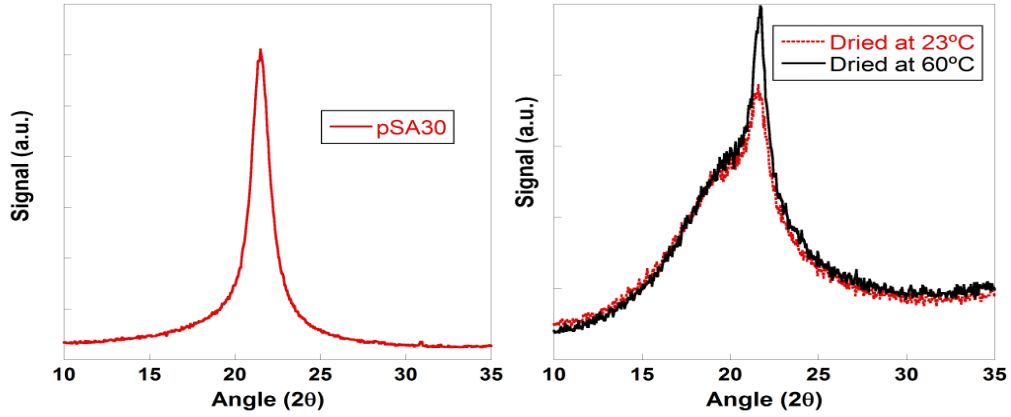

Figure IV. 5 XRD results of the a) the precursor block pSA30, b) the block copolymer p(SA15-2EHA50-SA15).

The decrease in the overall degree of crystallinity (% crystallinity based on total polymer weight) could be predicted by the addition of the non-crystallizable 2EHA monomer units. However, the crystallinity of the pSA block itself also decreased when it was linked to the soft 2EHA block, due possibly to the hindrance imposed by this block. Nevertheless, the length of the middle soft block did not affect the change in crystallinity obtained, as in all the cases a decrease in crystallinity of about 10% from the pSA homopolymer to the block copolymers was obtained. WAXS measurements were also performed and crystallinity was calculated based on the method explained by Monteil group[31]. The WAXS measurements of the pSA homopolymers (pSA30 in Figure IV.5a) showed a single diffraction peak at 2Θ=21.5° which is equivalent to a crystal lattice spacing of 0.42 nm. This is attributed to the crystalline state formed by the long alkyl side chain of SA.[10] Furthermore, the WAXS measurements of the block copolymers cast at two different temperatures (Figure IV.5b) showed the diffraction peak of the pSA crystalline block and an amorphous halo originating from the amorphous middle block. As it can be seen from the crystallinity results calculated from the XRD measurements shown in Table IV.3, samples cast at 60°C for 96h hours showed higher crystallinity. This was not seen in the DSC results, since no difference was observed between the heat of fusion of the first and second cycle. Most likely there was not enough time for substantial re-arrangement of the crystalline domains to show higher crystallinity in the second heating of the DSC. Regarding the values of the crystallinity obtained from the WAXS measurements, it can be seen that the values for

the homopolymers were higher than the values obtained from DSC. From the crystallinity values obtained by WAXS for the block copolymers, the same trends observed by DSC can be seen too.

Thermal stability of the block copolymers and DBTTC was studied by TGA (Figure IV.6) in nitrogen atmosphere and the data obtained are summarized in Table IV.4. As it can be seen from the graphs, DBTTC degradation starts at 240 °C and at 288°C it is completely degraded. Tonset is defined as the temperatue at 10% of weight

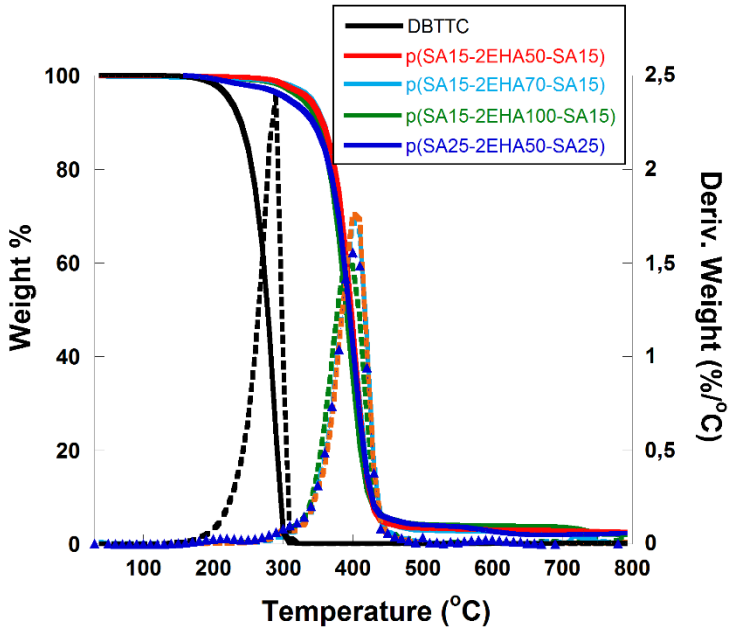

Figure IV.6. TGA thermograms of the ABA block copolymers measured at 10 °C/min in nitrogen atmosphere

loss. However, good thermal properties and a single step decomposition, comparable to other acrylic compolymers synthesized by free radical polymerization, is observed in all block copolymers.

Table IV.4. Degradation temperatures of the block copolymers and DBTTC.

Reaction	T_{onset}(°C)	T_{max}(°C)
p(SA15-2EHA50-SA15)	357.1	404.1
p(SA15-2EHA70-SA15)	357.5	403.8
p(SA15-2EHA100-SA15)	350.5	396.9
p(SA25-2EHA50-SA25)	343.8	403.4
DBTTC	239.9	288.42

IV.4. Conclusion

In this chapter, ABA block copolymers of stearyl acrylate (SA) and 2-ethylhexyl acrylate (2EHA) containing crystalline A block and soft middle B block, were synthesized via two-step RAFT mediated miniemulsion polymerization, using DBTTC RAFT agent. First, miniemulsion polymerization was used for the synthesis of PSA forming the crystalline domains and the reaction was stopped at around 80% conversion. Linear increase of Mn versus conversion and MWD shifting to higher molecular weights with conversion was obtained indicating that the reaction was of well

controlled manner. Then in the second step 2EHA was fed to the system as a pre-emulsion and polymerization was continued to form the soft mid-block. This was proven by GPC analysis, which showed MWD's shift of the block copolymers compared to the initial pSA seed. Thermal properties of the pSA initial A blocks and the final ABA block copolymers were investigated by means of DSC analysis. The DSC thermograms of the A block revealed an endothermic peak at 49°C originating from the melting of the crystalline domains and a smaller one at 30° attributed to the crystalls of the unreacted monomer present in the block. When the block copolymers where analyzed by DSC, the melting of the SA monomer units did not show anymore, indicating its full conversion, but the crystallinity of polySA block was reduced by the incorporation of the 2EHA units. Moreover good thermal properties and a single step decompostition was shown from the TGA analysis.

IV.5. References

1 C. E. Rehberg and C. H. Fisher, *J. Am. Chem. Soc.*, 1944, **66**, 1203–1207.

2 E. F. Jordan, D. W. Feldeisen and a. N. Wrigley, *J. Polym. Sci. Part A Polym. Chem.*, 1971, **9**, 1835–1852.

3 E. F. Jordan, *J. Polym. Sci. Polym. Chem.*, 1972, **10**, 3347–3366.

4 E. F. Jordan, *J. Polym. Sci. Part A-1 Polym. Chem.*, 1971, **9**, 3367–3378.

5 K. A. O'Leary and D. R. Paul, *Polymer.*, 2006, **47**, 1245–1258.

6 K. A. O'Leary and D. R. Paul, *Polymer*, 2006, **47**, 1226–1244.

7 Z. Mogri and D. R. Paul, *Polymer*, 2001, **42**, 2531–2542.

8 Z. Mogri and D. R. Paul, *Polymer*, 2001, **42**, 7765–7780.

9 K. O'Leary and D. R. Paul, *Polymer*, 2004, **45**, 6575–6585.

10 N. a. Platé and V. P. Shibaev, *J. Polym. Sci. Macromol. Rev.*, 1974, **8**, 117–253.

11 B. and M. Hsieh, H.W.S., Post, *J. Polym. Sci. Part B Polym. Phys.*, 1976, **14**, 1241–1255.

12 A. Agirre, C. D. Las Heras-Alarcón, T. Wang, J. L. Keddie and J. M. Asua, *ACS Appl. Mater. Interfaces*, 2010, **2**, 443–451.

13 E. Mehravar, M. A. Gross, A. Agirre, B. Reck, J. R. Leiza and J. M. Asua, *Eur. Polym. J.*, 2018, **98**, 63–71.

14 E. Mehravar, J. R. Leiza and J. M. Asua, *Polymer*, 2016, **96**, 121–129.

15 E. Mehravar, J. R. Leiza and J. M. Asua, *Polymer*, 2016, **84**, 167–177.

16 E. Mehravar, J. Leswin, B. Reck, J. R. Leiza and J. M. Asua, *Prog. Org. Coatings*, 2017, **106**, 11–19.

17 N. Popadyuk, A. Popadyuk, A. Kohut and A. Voronov, *Int. J. Cosmet. Sci.*, 2016, **38**, 139–147.

18 Q. Zhang, Q. Wang, J. Jiang, X. Zhan and F. Chen, *Langmuir*, 2015, **31**, 4752–4760.

19 F. Dutertre, P. Y. Pennarun, O. Colombani and E. Nicol, *Eur. Polym. J.*, 2011, **47**, 343–351.

20 S. Qin, J. Saget, J. Pyun, S. Jia, T. Kowalewski and K. Matyjaszewski, *Macromolecules*, 2003, **36**, 8969–8977.

21 G. Street, D. Illsley and S. J. Holder, *J. Polym. Sci. Part A Polym. Chem.*, 2005, **43**, 1129–1143.

22 B. T. Pérez-Martínez, L. Farías-Cepeda, V. M. Ovando-Medina, J. M. Asua, L. Rosales-Marines and R. Tomovska, *Beilstein J. Nanotechnol.*, 2017, **8**, 1328–1337.

23 A. Agirre, J. Nase, E. Degrandi, C. Creton and J. M. Asua, *J. Polym. Sci. Part A Polym. Chem.*, 2010, **48**, 5030–5039.

24 W. I. Higuchi and J. Misra, *J. Pharm. Sci.*, 1962, **51**, 459–466.

25 C. T. Lin and C. S. Chern, *J. Taiwan Inst. Chem. Eng.*, 2015, **49**, 240–246.

26 Y. Luo, J. Tsavalas and F. J. Schork, *Macromolecules*, 2001, **34**, 5501–5507.

27 H. de Brouwer, J. G. Tsavalas and F. J. Schork, *Macromolecules*, 2000, **33**, 9239–9246.

28 D. Boschmann and P. Vana, *Macromolecules*, 2007, **40**, 2683–2693.

29 R. Montenegro and K. Landfester, *Langmuir*, 2003, **19**, 5996–6003.

30 X. Zhu, Y. Gu, G. Chen, Z. Cheng and J. Lu, *J. Appl. Polym. Sci.*, 2004, **93**, 1539–1545.

31 F. Brunel, G. Billuart, P. Y. Dugas, M. Lansalot, E. Bourgeat-Lami and V. Monteil, *Macromolecules*, 2017, **50**, 9742–9749.

Chapter V. Morphological and mechanical properties of waterborne block copolymers

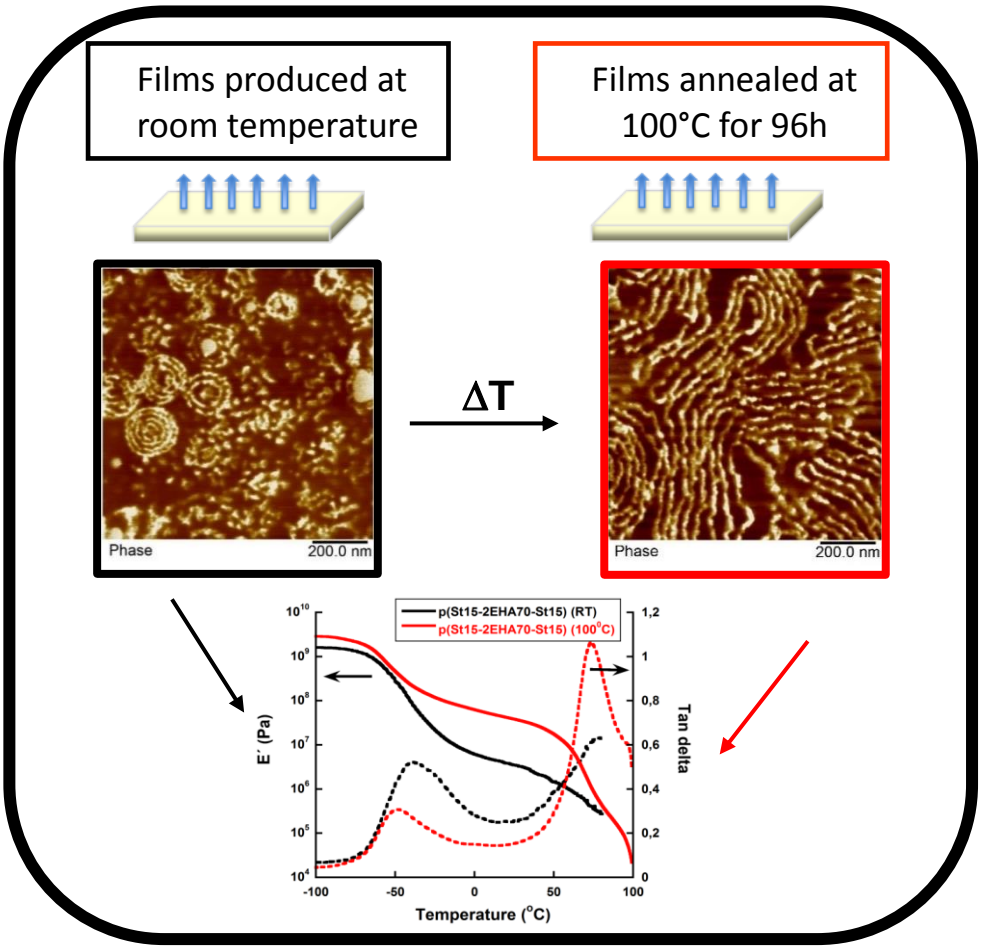

*Part of this chapter has been published in *Polymer 158 (2018) 327–337*

V.1. Introduction

The preparation of macromolecules of well-defined architecture is not only a synthetic challenge, but it is also of high interest for the design of novel polymeric materials providing superior combinations of properties. In this context, controlled radical polymerization, including the three different methods well explained in chapter I (NMP, ATRP and RAFT), has in the past years emerged as a technique of choice to prepare block, graft or comb copolymers of precise molecular and chemical structure. The above mentioned type of materials are increasingly involved in traditional structural materials[1] as well as in higher added value applications such as core-shell functional nanoparticles[2], organic/inorganic nanoparticles[3] or block copolymer lithography[4,5]. Block copolymers self-assembling capability and resulting regular nanostructures are indeed highly appreciated to develop materials with unique combinations of properties.

Emulsion polymerization is a process greatly appreciated from an industrial viewpoint because it is simple and solvent-free and thus it is very attractive for the synthesis of such types of structural materials. From an application perspective, block copolymers directly obtained as a stable latex form should produce useful nanostructured films, compatibilizers or even nanostructuring agents to be blended with homopolymers[1]. An extra advantage of the polymerization in water dispersed systems is the possibility to obtain these nanostructures directly inside latex particles,

a possibility not offered by the conventional solution or bulk block copolymers synthesis.

In order to obtain such nanostructured polymer particles dispersed in water, several approaches can be found in literature. For instance, Okubo and coworkers reported two main approaches to prepare nanostructured polymer particles. In the first approach multilayered polystyrene/poly(methyl methacrylate) composite microparticles were prepared by the so-called solvent-absorbing/releasing method[3,6,7], using either polystyrene-g-polymethyl methacrylate graft copolymers or polystyrene-b-polymethyl methacrylate block copolymers as compatibilizers. In the second approach, they used two-step ATRP miniemulsion polymerization process to prepare poly(i-butyl methacrylate)-b-polystyrene nanostructured latex particles. Later on Nicolas et al.[8] produced stable latexes with up to 27 wt% solids of diblock and triblock copolymers by NMP comprising a poly(n-butyl acrylate) first/central block and polystyrene second/outer block. For this purpose, they used (mini)emulsion polymerization, and monofunctional or difunctional water-soluble alkoxyamine initiators. They studied the direct self-assembly of block copolymers within latex particles in films dried at room temperature, the morphological changes of the films after annealing and in solvent cast films. Thermal properties of the films were studied using DSC, however no particle morphology nor mechanical properties of the films were provided.

RAFT miniemulsion polymerization has also been used as a method for the synthesis of water dispersed particles containing block copolymers of AB[9–11] and ABA type[9]. However, the mechanical and morphological properties of the polymer latexes and the films cast at different conditions were scarcely explored. Wei et al.[12] prepared nanostructured particles of styrene (St) and butadiene block copolymers by RAFT polymerization. They studied the morphology of the latex and observed changes in morphology with increasing the BD segment. However, the authors did not provide any film morphology nor mechanical properties in the article. Xiong and coworkers[13] developed a binary monomers RAFT miniemulsion copolymerization kinetic modelling to predict and produce p(St-b-St/Bd) copolymers with different well-defined structure and composition for controlled RAFT radical copolymerization. They also synthesized the block copolymers and analyzed the morphology of films cast from toluene solution. Lamellae, cylinders and disordered morphologies were observed. However, no particle morphology nor morphology of the films casted directly from the latex was given. Wei et al.[14] synthesized gel-free styrene-butadiene-styrene triblock copolymer latex and showed the morphology and mechanical properties of the polymer films cast from THF solutions only. Later on Landfester and coworkers[15] synthesized highly symmetric poly(styrene)-block-poly(butadiene-stat-styrene)-block-poly(styrene) copolymer in a non-stop one-pot RAFT polymerization in miniemulsion and observed core shell particles. The shell became bilayer as the butadiene content was increased. The equilibrium morphology of the obtained block

copolymers though was not provided nor was the high polymerization times of both blocks discussed. Furthermore, Yang and coworkers[16] synthesized ABA triblock copolymers by RAFT miniemulsion polymerization starting from a macroRAFT agent previously prepared by solution polymerization. They analyzed the particle and film morphologies and observed that the thermodynamic equilibrium was not attained by thermal annealing of the film.

Block copolymers composed of different incompatible polymer segments connected by covalent bonds, spontaneously form microphase-separated structures ranging from several nanometers to 100 nm in length. In general, bulk block copolymer self-assembly into phase-separated structures (e.g. spherical, cylindrical, lamellar and bicontinuous structures) is governed by both the enthalpic interaction between the blocks, quantified by the Flory-Huggins interaction parameter χ and the total degree of polymerization of the copolymer, N. Generally, if the product of χ and N exceeds 10.5, then the block copolymers phase separate into domains whose morphology depends on the relative volume fractions of the blocks[17]. In addition to block volume fraction, phase separated morphology can be influenced by confinement effects. The morphologies obtained under confinement spaces are affected by two factors (i) the ratio of the size of the confined space (D) to the equilibrium domain spacing of microphase-separated structures (Lo) and (ii) the interfacial energy between polymer segments of the block copolymer and the external matrix[18]. Such confinement effects have been observed within particles

prepared by controlled precipitations methods and can lead to new and useful morphologies inaccessible in bulk block copolymer systems[19]. In this context, block copolymers, which form a lamellar structure in bulk films, can form onion-like structures and three-dimensionally arranged spherical domains in a 3D confinement system[20].

In this chapter, the effect that confined phase separated particle morphology has on film formation process of ABA and AB block copolymers composed of hard A and soft B block copolymers dispersed in water, will be studied. In addition, the morphological properties of ABA crystalline-soft-crystalline block copolymers will be investigated. Morphological properties were studied by means of microscopic techniques (AFM and TEM), both of the particles in the latex form, as well as after film formation and different thermal post-treatments. Films were annealed at temperatures well above the Tg of the hard phase or Tm of the crystalline domains to study the bulk morphology of the films after complete particle coalescence. Moreover, the films were dissolved in THF, which is a good solvent for both blocks to gain knowledge about the equilibrium morphology. Finally, DMTA studies of the films annealed at different temperatures, were performed to correlate the morphology changes with the mechanical properties of the block copolymers.

V.2. Experimental

V.2.1. Materials

THF (99.9% GPC, Scharlab) was used as solvent for dissolving the films casted directly from the latex at room temperature.

V.2.2. Characterization

Morphologies of latex particles, latex films obtained at room temperature as well as annealed and solvent cast films were studied by atomic force microscopy (AFM) and/or transmission electron microscopy (TEM). The latex films were prepared by casting the latex into silicone molds and letting them dry for a week at room temperature. Annealed films were obtained by casting the latex and letting it dry at room temperature for 48 h and then annealing the film at 100°C for 96 h for p(St-2EHA-St) or p(St-2EHA) and at 60°C for 96 h for p(SA-2EHA-SA) block copolymers. Solvent cast films on the other hand were prepared by redissolution of the films in tetrahydrofuran followed by drying at room temperature for p(St-2EHA-St) or p(St-2EHA) and additionally 20 h at 100°C for p(SA-2EHA-SA) block copolymers. Mechanical properties were studied using DMTA measurements. NMR spectroscopy was used to determine the content of hard and soft block in the block copolymers. The detailed description of the characterization methods is provided in Appendix.

V.3. Results and discussion

Before analyzing the morphological and mechanical properties of the synthesized block copolymers, it should be reminded that the polymerization reaction in the first blocks was stopped at around 80% conversion. The unreacted monomer was not removed prior to the formation of the second block. Therefore, the homopolymers of the first block (either hard-pSt, or semi crystalline-pSA) were used as seeds that were extended with soft monomer (2EHA) and block copolymers with different compositions were formed. If one aims at the preparation of well-defined and pure block copolymers, unreacted monomer should be removed prior sequential monomer addition. However, in our studies the removal of unreacted monomer was disregarded, because it is very difficult to distill off monomers with high boiling point without destroying the formed latex. Therefore, it was decided not to remove the non-reacted A-monomer as the easiest and more up-scalable protocol for the synthesis of the waterborne block copolymer latexes. In this context, one should always take into consideration that the inner soft block will contain small amounts of the hard phase A-block monomer units.

V.3.1. Morphology of the ABA hard-soft-hard block copolymers

ABA block copolymers having hard-soft-hard domains were synthesized initially synthesizing the hard-polystyrene domains. Two stable pSt latexes were synthesized targeting different Mn of 30,000 and 50,000 g/mol. Four block copolymers were formed from these initial seeds, named through the text as p(St15-2EHA50-St15), p(St15-2EHA70-St15), p(St15-2EHA100-St15) and p(St25-2EHA50-St25). The numbers after the letters indicate the targeted Mn. The summary of the synthesis of the ABA hard-soft-hard block copolymers and the results obtained are described in detail in chapter II. Due to the complexity of our system, i.e. mixed monomer sequence arising from the presence of unreacted monomer (initial block: styrene + stearyl acrylate and middle block: styrene + 2-ethylhexylacrylate), it was not possible to determine the interaction parameter χ and also not possible to precisely determine the volume fraction of each microphase. Moreover, due to the difficulties in measuring the Lo values, the evaluation of the degree of confinement and determination of the equilibrium 3D microphase-separated structures was hard. Nevertheless, an estimate of the volume fraction of each component in the block copolymers was made based on the compositional information derived from NMR. An assumption was made that the weight fraction of monomers is equal or close enough to the volume fraction and the results are shown in Table V.1. The theory in Figure V.1 is for diblock copolymers but it can be used as an estimate for triblocks.

Table V.1. Block copolymer composition results determined by 1H NM spectroscopy and theoretical morphology predicted based on AB block copolymers model

Sample	Mole Fraction		Weight Fraction		Theoretical morphology
	% St	%2EHA+SA	%St+SA	%2EHA	
p(St25-2EHA50-St25)	61.0	39.0	40.6	59.4	L/G
p(St15-2EHA50-St15)	55.3	44.7	35.7	64.3	G/C
p(St15-2EHA70-St15)	35.6	64.4	20.8	79.2	S/C
p(St15-2EHA100-St15)	33.2	66.8	19.2	80.8	S

S-Spheres,**G**-Gyroid, **C**-Cylinders, **L**-Lamellae,

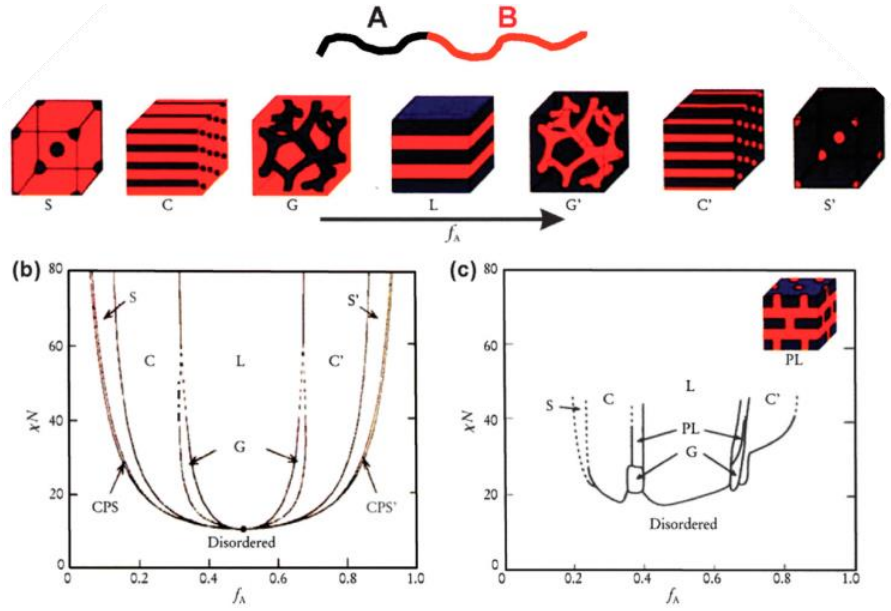

Figure V.1. Equilibrium morphologies of AB diblock copolymers in bulk: S and S' = body-centered-cubic spheres, C and C' = hexagonally packed cylinders, G and G' = bicontinuous gyroids, and L = lamellae. (b) Theoretical phase diagram of AB diblocks predicted by the self-consistent mean-field theory, depending on volume fraction (f) of the blocks and the segregation parameter, χN; CPS and CPS' = closely packed spheres. (c) Experimental phase diagram of polystyrene-b-polyisoprene copolymers, in which fA represents the volume fraction of polyisoprene, PL = perforated lamellae [21]

The volume fractions were used as an indication for the bulk state microphase separated morphology. As seen from the schematic represented equilibrium morphologies in Figure V.1. for AB hard soft block copolymers, the morphology changes with increasing the volume fraction f_A of the A block at a fixed $\chi N>10.5$. When the volume fraction of hard domain (like polystyrene) is small (<20 vol %) spheres of polystyrene dispersed in an elastic matrix are formed which then change to cylinders or gyroids as the pSt content increases. When the volume fractions of the both components are about equal (40-60 vol%), the two-component form alternating lamellae. As the polystyrene content increases an inverse morphology is formed and a continuous polystyrene phase forms in which either gyroid, cylinders or spheres of soft domains are dispersed. According to the diagram shown above, the predicted morphology based on the volume fractions obtained from NMR results suggest that the block copolymers phase separation will be in the region from spheres (p(St15-2EHA100-St15)) to lamellas (p(St25-2EHA50-St25)). The predictions are given in the Table V.1.

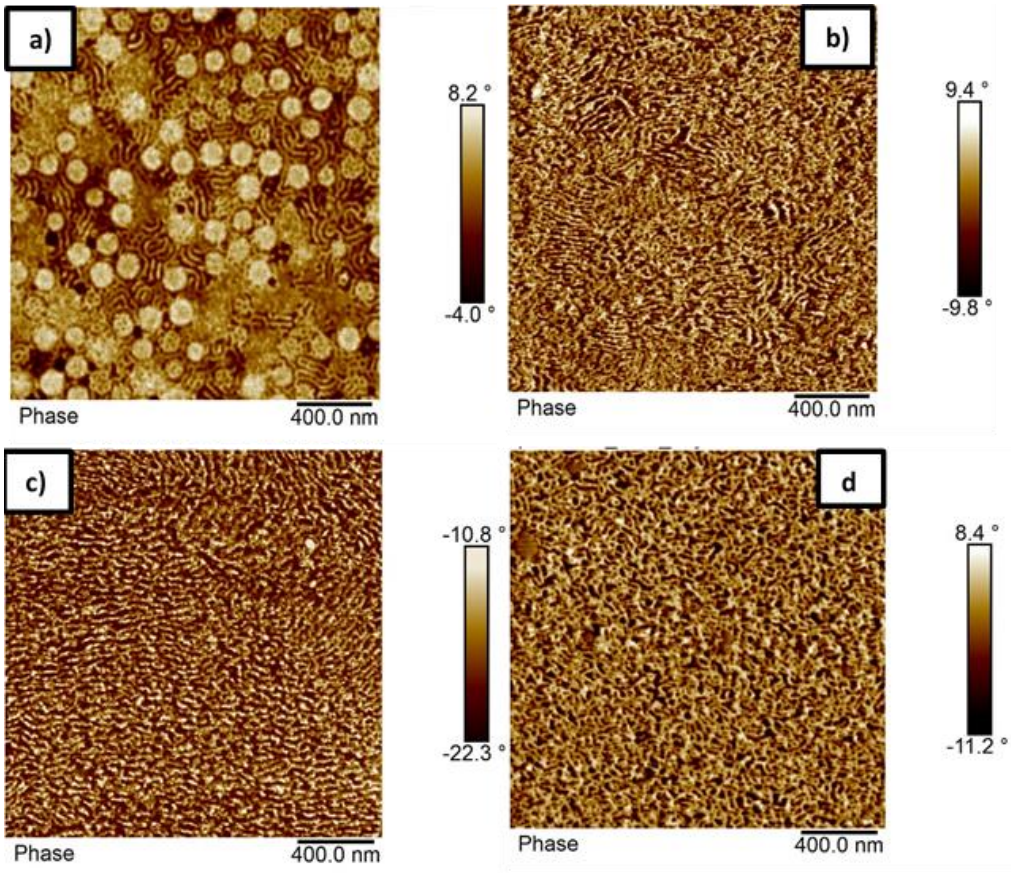

Figure V.2. AFM phase images of the sample p(St15-2EHA50-St15) a) top surface of the film dried at room temperature, b) cross-section of the film dried at room temperature, c) cross-section of the film dried at 100 °C and d) cross section of a film cast from THF-solution.

The morphology of the block copolymer with composition p(St15-2EHA50-St15) studied with AFM is shown in Figure V.2. The top surface of the polymer film prepared by drop casting of the latex at room temperature (Figure V.2a) reveals the presence of spherical particles with hard shell (shown as bright regions) that are smaller than

the particle size obtained by DLS (187 nm) dispersed in a nanophase separated continuous matrix, which formed most likely as a result of particle coalescence. The AFM imaging performed on a room temperature dried film, on a fresh cut through the thickness of the latex film, (Figure V.2b) showed no presence of particles and instead an extended nanophase separated pattern was visible. The most likely reason for observing a regular structure already at room temperature is the fact that this sample had substantial amount of unreacted monomer (as shown in chapter II) acting as a plasticizer and causing particles to coalesce already at room temperature. On the other hand, the sample annealed at 100 °C (Figure V.2c) showed even higher ordering compared to the sample obtained at room temperature. No significant difference in morphology was seen though between the films annealed at higher temperature and the ones cast from THF solution, indicating that equilibrium morphology was already reached by thermal treatment of the films. According to the diagram for AB block copolymers, the sample p(St15-2EHA50-St15), based on its volume fraction should phase separate either in cylinder or gyroid structure depending on the interaction parameters. However, based on the picture we assume it is gyroid.

The self-assembly of the block copolymer with composition p(St15-2EHA70-St15) was studied by AFM (Figure V.3) and confirmed by TEM (Figure V.4). The top surface of the polymer film (Figure V.3a) studied by AFM shows the existence of two different

populations of particles having lower and higher amount of styrene, visible as white dots.

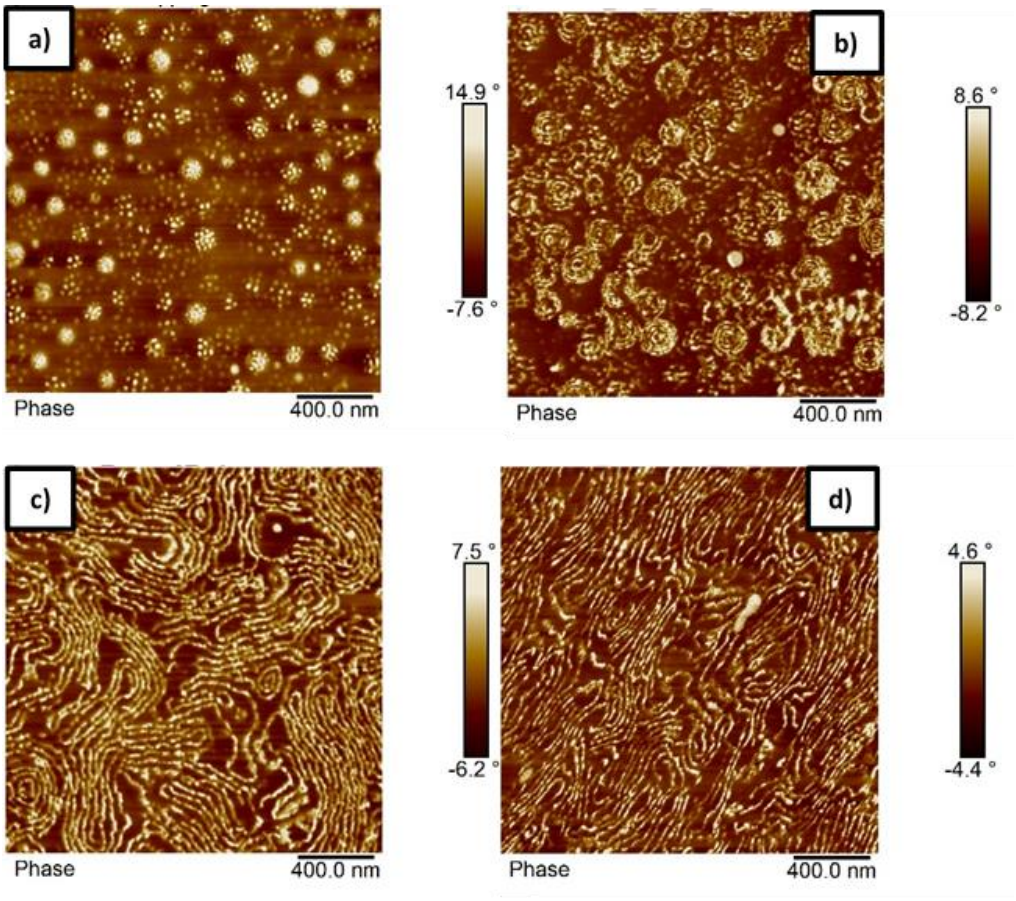

Figure V.3. AFM phase images of the sample p(St15-2EHA70-St15) a) top surface of the film dried at room temperature b) cross-section of the film dried at room temperature, c) cross-section of the film dried at 100°C and d) cross section of a film cast from THF-solution.

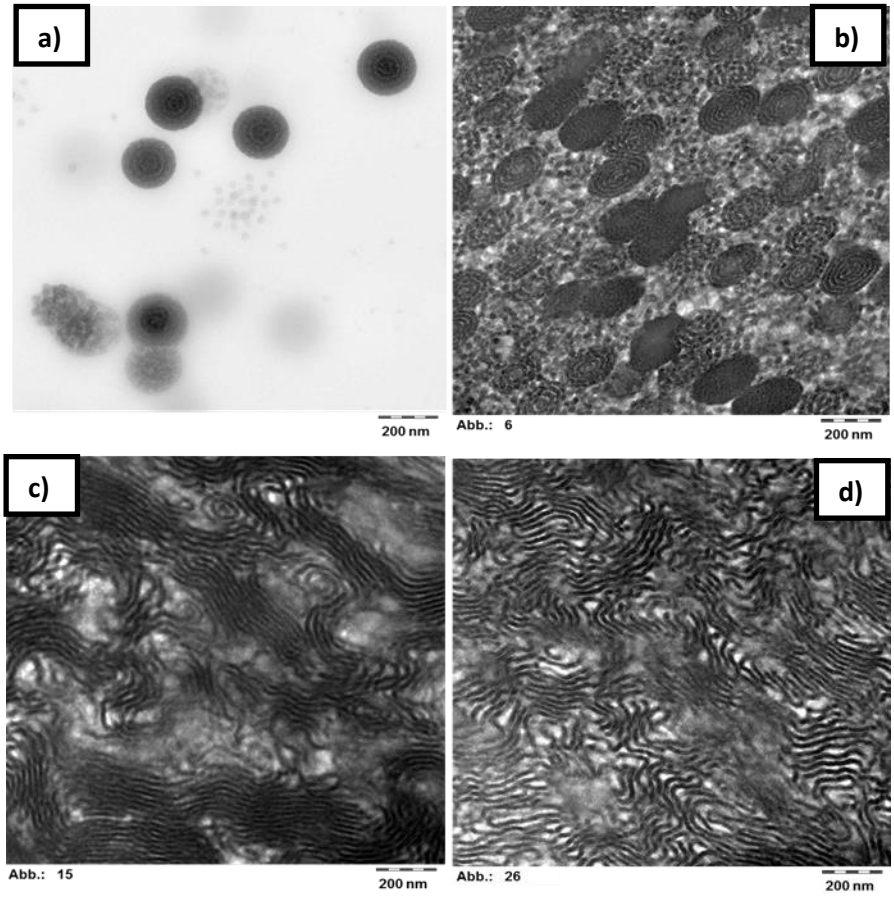

Figure V.4. TEM images of the sample p(St15-2EHA70-St15) a) particles dispersion b) film dried at room temperature c) film annealed at 100 °C and d) film cast from THF-solution. The bar of all the images is 200 nm.

The AFM imaging performed on a fresh surface cut through the thickness of a latex film allowed to dry at room temperature reveals the presence of spherical particles inside of which “onion-ring” lamellar morphology can be distinguished (Figure V.3b). These findings were also confirmed by TEM (Figure V.4b) where it is clearly visible that almost all the particles show the same structure. Moreover, from the TEM images it is seen that the rings are perforated which could be the reason of observing the white dots on the particles in AFM (Figure V.3a). Although measurements derived from AFM are only an approximation, the size of the spherical objects shown in Figure V.3b is in good agreement with the average particle size measured by DLS (189 nm). The thermal treatment of the polymer film caused complete particle coalescence and transformed the “onion-ring” structure into more classical lamellar morphology. To completely erase the impact of the emulsion polymerization process and thermal history, the latex film was dissolved in THF (Figure V.3d). This yielded a morphology as close as possible to equilibrium morphology and the obtained structure resembled the one obtained at 100 °C, even if in the film annealed at 100ºC, the presence of onion-ring structures was not completely erased, as it has been after the treatment in THF. Based on the general diagram, block copolymers with a volume fraction of hard domain in the range of 20% should phase separate as either spheres or cylinders. On contrary the microscopic data clearly demonstrate that block copolymer phase separates into lamellar structure. However, as Matsen and Thompson[22] stated in their article ABA block

copolymers phase separate slightly different than AB block copolymers. They predicted that the lamellar region for ABA block copolymers was reached for lower f_A compared to AB block copolymers, which is exactly what it has been observed for p(St15-2EHA70-St15). The sample p(St15-2EHA100-St15) with longest soft block was very sticky, thus it was not possible to analyze.

The sample with highest pSt content p(St25-2EHA50-St25) shows hard spherical particles with no particular outer morphology as evident form the AFM image of the top surface of the polymer film (Figure V.5a). AFM images of the cross section of the film dried at room temperature on the other hand show single or bilayer particle morphology (Figure V.5b). At this stage, the differences observed for the top and cross-sections of the films dried at room temperature have to be pointed out. In all three latexes analyzed so far, the differences have been significant, but they are very clear here. The top view only shows the surface of the particles, whereas the cross-section shows their interior. If only the top view would have been considered, no phase separation would have been envisaged from Figure V.5a. Annealing of the film led to complete coalescence of the hard particles and homogeneous distribution of the p2EHA domains through the hard pSt matrix (Figure V.5c). Presence of small voids was also visible in annealed films which could not be seen in the film obtained from THF solution (Figure V.5d). According to the general diagram based on the volume fraction either lamellar or gyroid structure should be expected for this sample.

The images obtained, especially from the film cast from THF-solution V.5.d suggest that we have a gyroid structure.

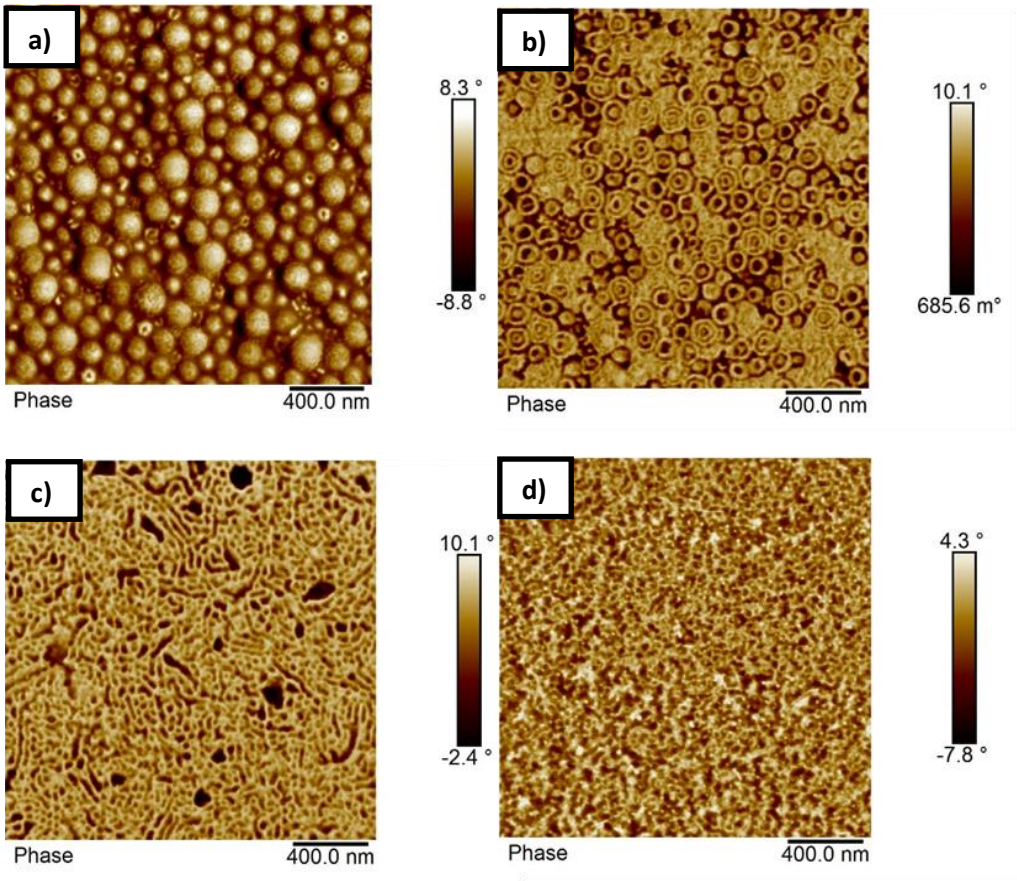

Figure V.5. AFM phase images of the sample p(St25-2EHA50-St25) a) top surface of the film dried at room temperature b) cross-section of the film dried at room temperature, c) cross-section of the film dried at 100 °C and d) cross section of a filmcast fromTHF solution.

V.3.2. Viscoelastic properties of the ABA hard-soft-hard block copolymers

The viscoelastic properties of the hard-soft-hard block copolymers were investigated by DMTA measurements and the results are presented in Figure V.6.

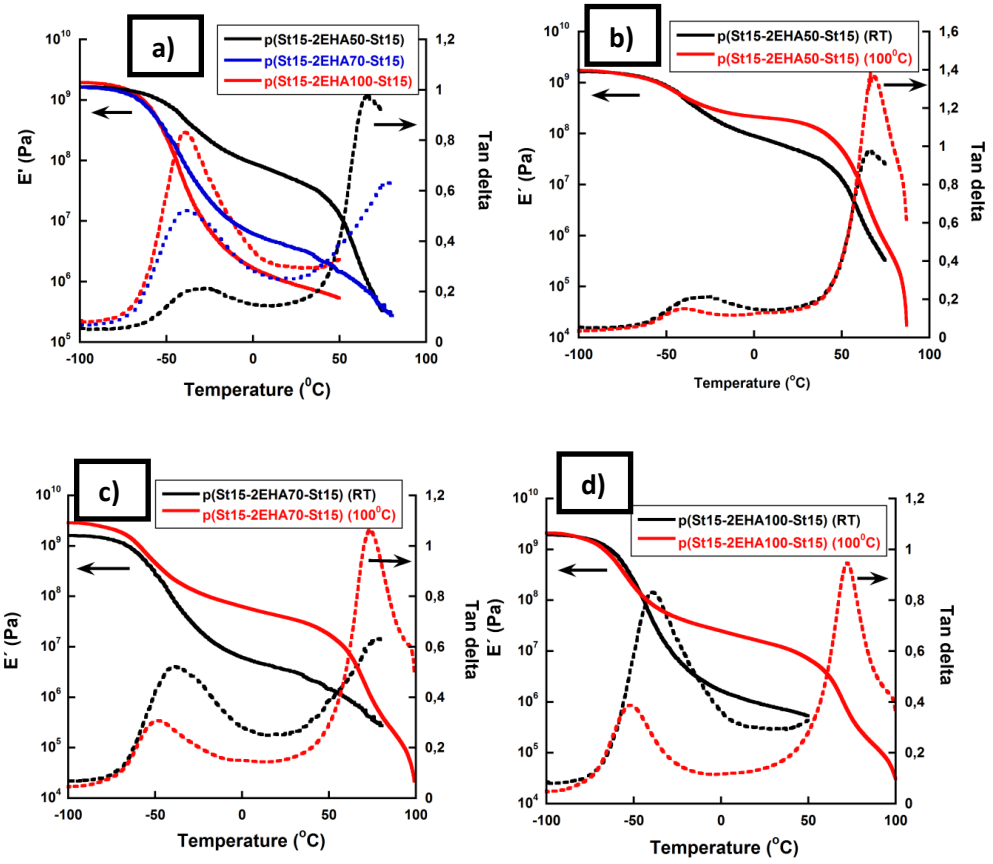

Figure V.6. Viscoelastic properties of the block copolymers, solid lines - dependence of elastic modulus on temperature and dashed lines-dependence of tan δ on temperature

The solid line presents the influence of temperature on storage modulus and dashed line the effect of temperature on tan δ. Viscoelastic properties of the films cast at room temperature presented in Figure V.6a, indicate that the elastic modulus decreases as the length (Mn) of the middle soft p2EHA block increases. The elastic modulus decreases significantly in the rubbery plateau especially in the temperature range between 0°C and 50°C. Moreover, liquid like behavior induced by further temperature increase is evident from the significant drop of the modulus and abrupt increase in tan δ at temperatures close to the Tg of the hard domains. The viscoelastic properties of p(St25-2EHA50-St25) were not possible to be measured, because the sample was too brittle thus handling was very difficult. Additionally, in Figure V.6b,c,d the viscoelastic properties of the block copolymers latex films cast at room temperature were compared with the ones of the latex films cast at room temperature and annealed at 100°C. Shifting of the Tg (of soft domains) to lower temperatures and elastic modulus increase in the plateau region was clearly visible in all the samples upon annealing, irrespective of the composition of the block copolymers. When films were annealed, complete particle coalescence occurred as evidenced from the AFM images, thus pSt domains were able to move and uniformly distribute throughout the elastic matrix, which led to its reinforcement. As a result, hard thermoplastic rubber like materials were obtained with increased elastic modulus in the plateau region. Most likely when the films are dried at room temperature the contact between blocks is higher and thus their influence on each

other is higher. As a result, the lower and upper Tg's approach each other. On the other hand, when they are annealed less contact is achieved and the influence of the blocks on each other is lower. As a result, the two Tg's get apart of each other. In addition, the upper Tg of the hard domain gets more pronounced, most likely due to the fact that the domains get bigger by annealing and the interface region between the microdomains in which segments of both blocks mix gets narrower.

V.3.3. Morphology of the AB hard-soft block copolymers

AB block copolymers having hard-soft domains were synthesized using the asymmetric RAFT agent. Initially pSt latexes with targeted Mn of 30,000 g/mol and 50,000 g/mol were synthesized and extended with 2EHA to form AB block copolymers. Since the conversion of the first block was not complete, the same consideration for the purity of the second soft block should be taken into consideration, as discussed before. Four block copolymers were formed, named through the text as p(St30-2EHA50), p(St30-2EHA70), p(St30-2EHA100) and p(St50-2EHA50), equivalent to the four symmetric ABA-type block copolymers shown in the previous section. The synthesis details and the results attained are given in chapter III.

The composition of the block copolymers was determined by NMR and the results are shown in Table V.2.

Table V.2. Block copolymer composition results determined by ^{1}HNMR spectroscopy

Material Code	Mole Fraction		Weight Fraction		Theoretical morphology
	% St	%2EHA+SA	%St+SA	%2EHA	
p(St50-2EHA50)	63.5	36.4	48.8	51.2	L
p(St30-2EHA50)	48.9	51.0	34.7	65.2	C
p(St30-2EHA70)	40.4	59.5	27.6	72.4	C
p(St30-2EHA100)	32.4	67.5	21.1	78.9	C

Figure V.7. shows the morphology of p(St50-2EHA50) under different film formation conditions, observed by AFM. The top surface of the polymer film (Figure V.7a) shows folded layers of flatted cylinder surfaces arranged in different directions. The AFM imaging performed on the cross-section of a latex film dried at room temperature shows the presence of some spherical particles inside of which “onion-ring” lamellar morphology can be distinguished (Figure V**.7**b). In addition, short stripes all over the surface placed in all directions can be seen as well. The AFM images were supplemented with TEM images (Figure V.8.) to get better understanding of the morphology obtained. The TEM image of the polymer latex dispersion (Figures V.8a) clearly showed two populations of particles (i) spherical with onion-ring morphology and (ii) oblate ellipsoid with striped polystyrene lamellae.

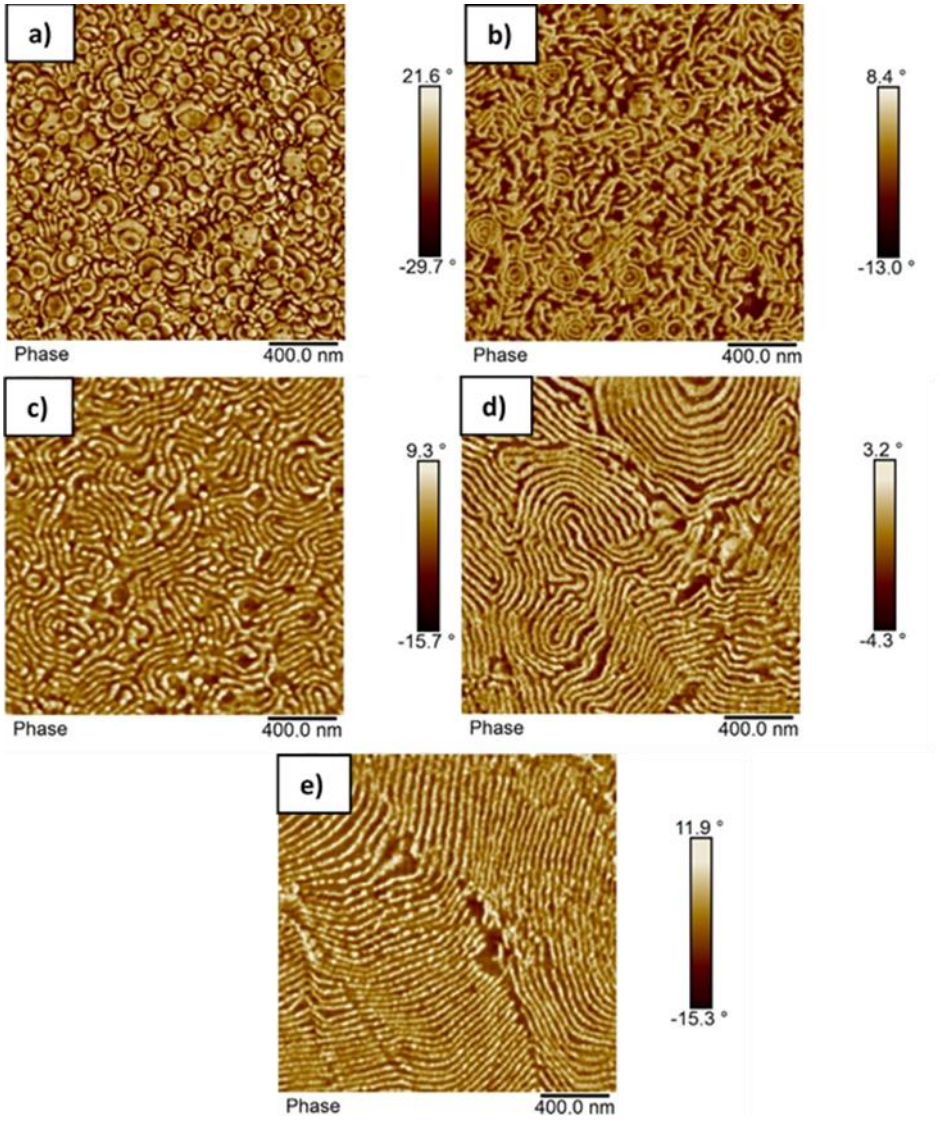

Figure V.7. AFM phase images of the sample p(St50-2EHA50) a) top surface of the film dried at room temperature b) cross-section of the film dried at room temperature, c) cross-section of the film dried at 100 °C for 30 min and d) cross-section of the film dried at 100 °C for 96 h e) cross section of a film cast from THF-solution.

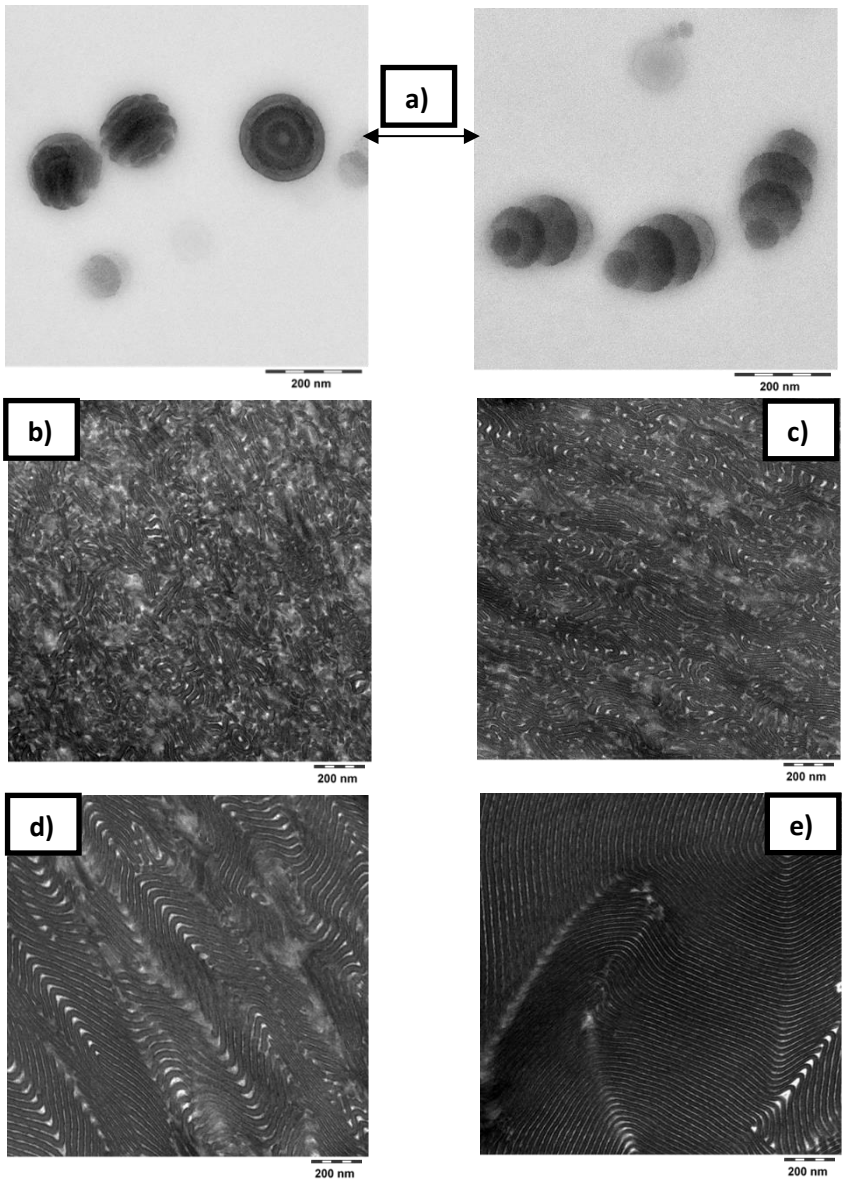

Figure V.8. TEM images of the sample p(St30-2EHA50) a) particles dispersion b) film dried at room temperature c) film annealed at 100 °C for 30 min, c) film annealed at 100 °C for 96h, e) film cast from THF-solution. The bar of all the images is 200nm.

Self-assembly of block copolymers confined in emulsion droplets, induced by evaporation of solvent from the interior phase of the emulsion, has already been described as a method for the preparation of ellipsoid-shaped and convex lens-shaped particles by tuning the interfacial interactions between the block copolymers particles and the surrounding aqueous solution[23–26]. A strategy to control these interfacial interactions is to use a mixture of surfactants that have selective interactions with each other block copolymer domain. When the surfactants at the interface exhibit nonselective or minimal preferential interaction with both blocks, geometry does not affect internal block copolymers nanostructure, but rather the internal structure affects the particle shape to minimize the free energy penalty associated with bending of the block copolymers. In this work, the ellipsoid particles were obtained directly from the synthesis route without use of any solvent.

To get insight into the kinetics of reordering and equilibration of the microphases, thermal annealing of the films at 100ºC was conducted for two different times. If the annealing was conducted for only 30 min at 100°C, complete particle coalescence occurred and the “onion-ring” structure disappeared and was transformed into classical lamellar morphology, but with short range ordering (Figure V.7c and V.8c). The pSt lamellae sizes did not exceed 400 nm, which means that the pSt present only in neighboring particles coalesced. However, the effect was more pronounced during prolonged annealing for 96 h (Figure V.7d and V.8d), where the pSt lamellae

exceeded 1000 nm range and therefore assumed the aggregation of pSt domains from particles more than 5 particles away. Dissolving the polymer film in THF and casting films from THF-solution yielded extended lamellar morphology visible both by AFM (Figure V.7e) and TEM (Figure V.8e). Based on the NMR results, these block copolymers have around 50% of hard domains, which perfectly matched the predicted lamellar morphology according to the diagram for asymmetric AB type block copolymers. The morphology of the block copolymer samples with composition p(St30-2EHA50), p(St30-2EHA70) and p(St30-2EHA100) are shown in Figure V.9., V.10., and V.11. The volume fraction of the hard-polystyrene based on the NMR results are 21.1, 27.6 and 34.7 % which according to the AB block copolymers diagram places their bulk morphology in the cylinder zone. The AFM imaging of the top surface of the films dried at room temperature (Figure V.9a., V10a., and V11a.) shows the presence of spherical microphase separated particles whose surface is composed of both polymer phases. The pSt hard domains three-dimensionally twist around the soft p2-EHA phases in a helical axis. The more pSt content is present in the sample the more the helix is pronounced. The cross-section of the polymer films dried at room temperature (Figure V.9b., V10b., and V11b.) shows that the dominant inner morphology are particles with one or bilayers and only few particles show onion ring morphology. Moreover, polystyrene domains spread all over the matrix as white spots are visible.

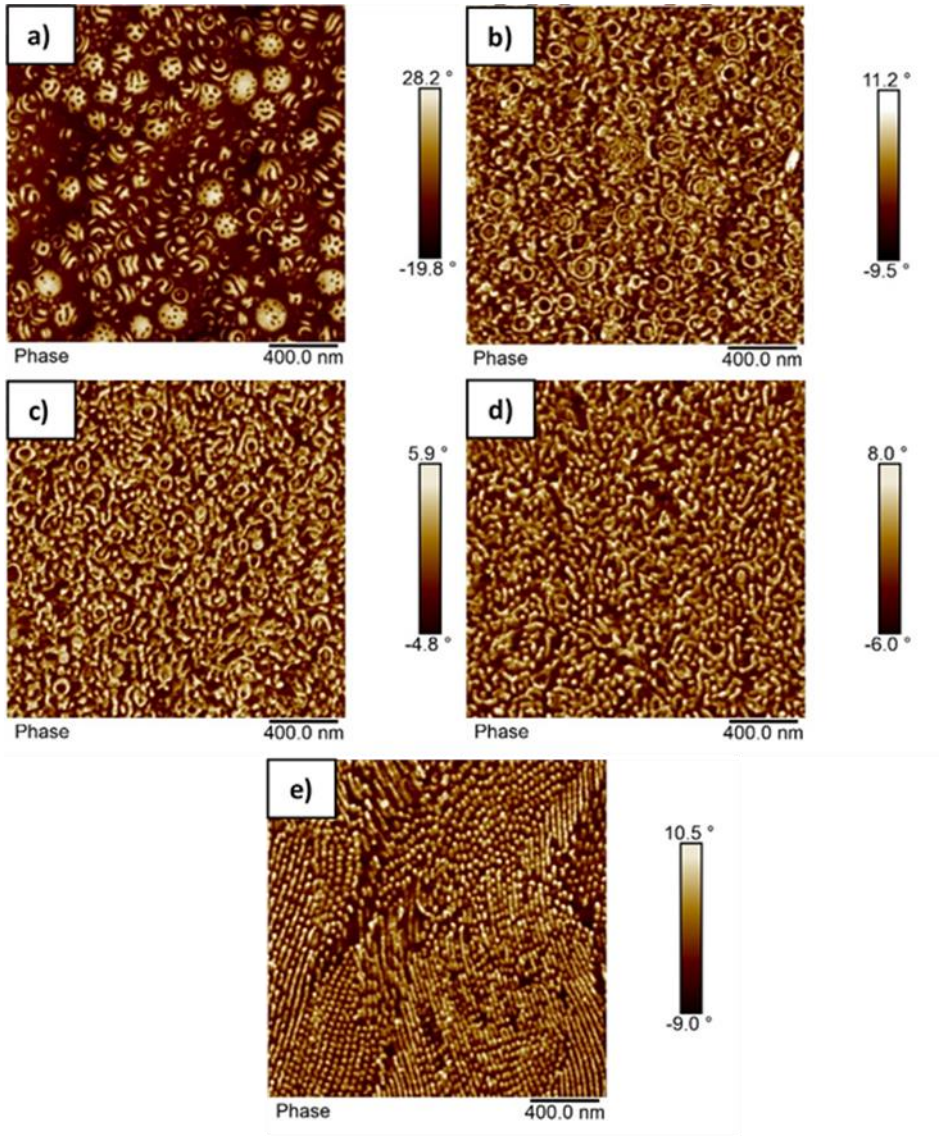

Figure V.9. AFM phase images of the sample p(St30-2EHA50) a) top surface of the film dried at room temperature b) cross-section of the film dried at room temperature, c) cross-section of the film dried at 100 °C for 30 min and d) cross-section of the film dried at 100 °C for 96 h e) cross section of a film cast from THF-solution.

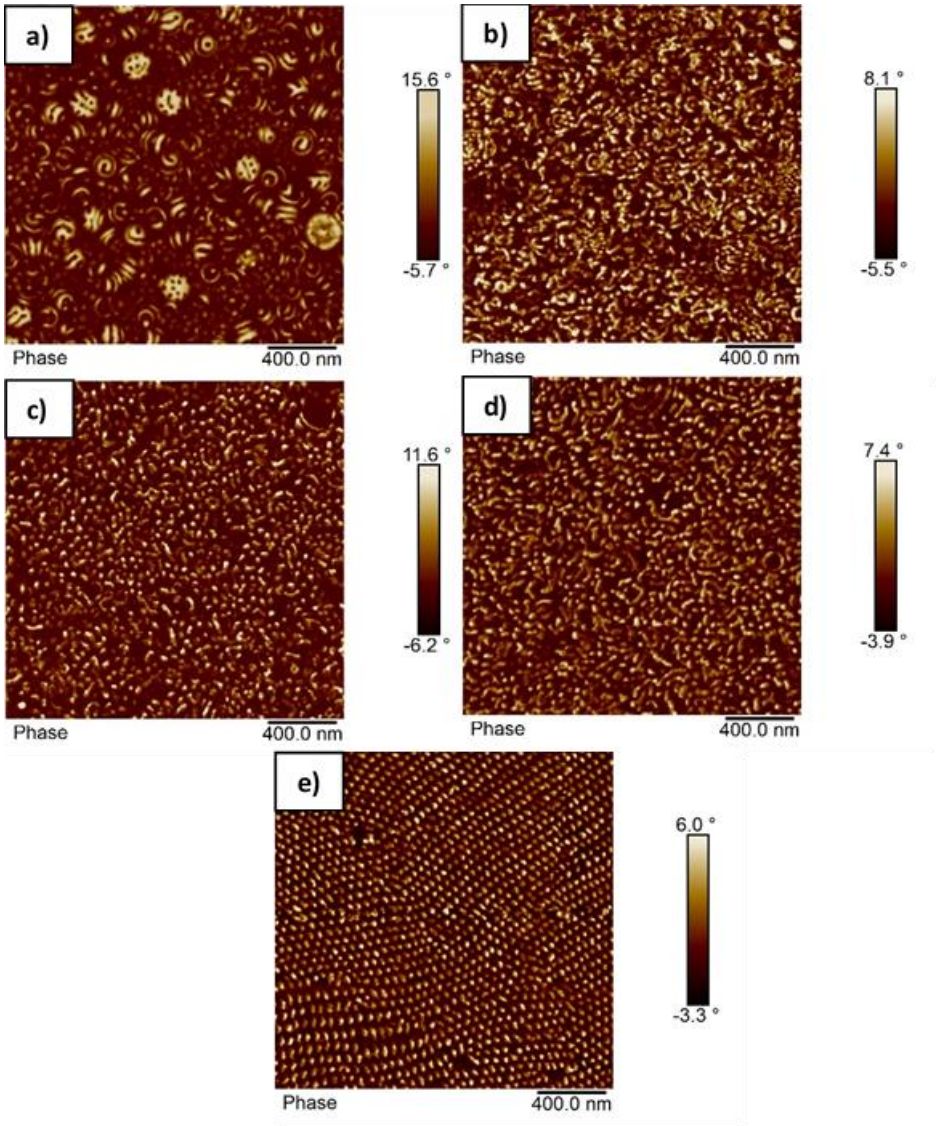

Figure V.10. AFM phase images of the sample p(St30-2EHA70) a) top surface of the film dried at room temperature b) cross-section of the film dried at room temperature, c) cross-section of the film dried at 100 °C for 30 min and d) cross-section of the film dried at 100 °C for 96 h e) cross section of a film cast from THF-solution.

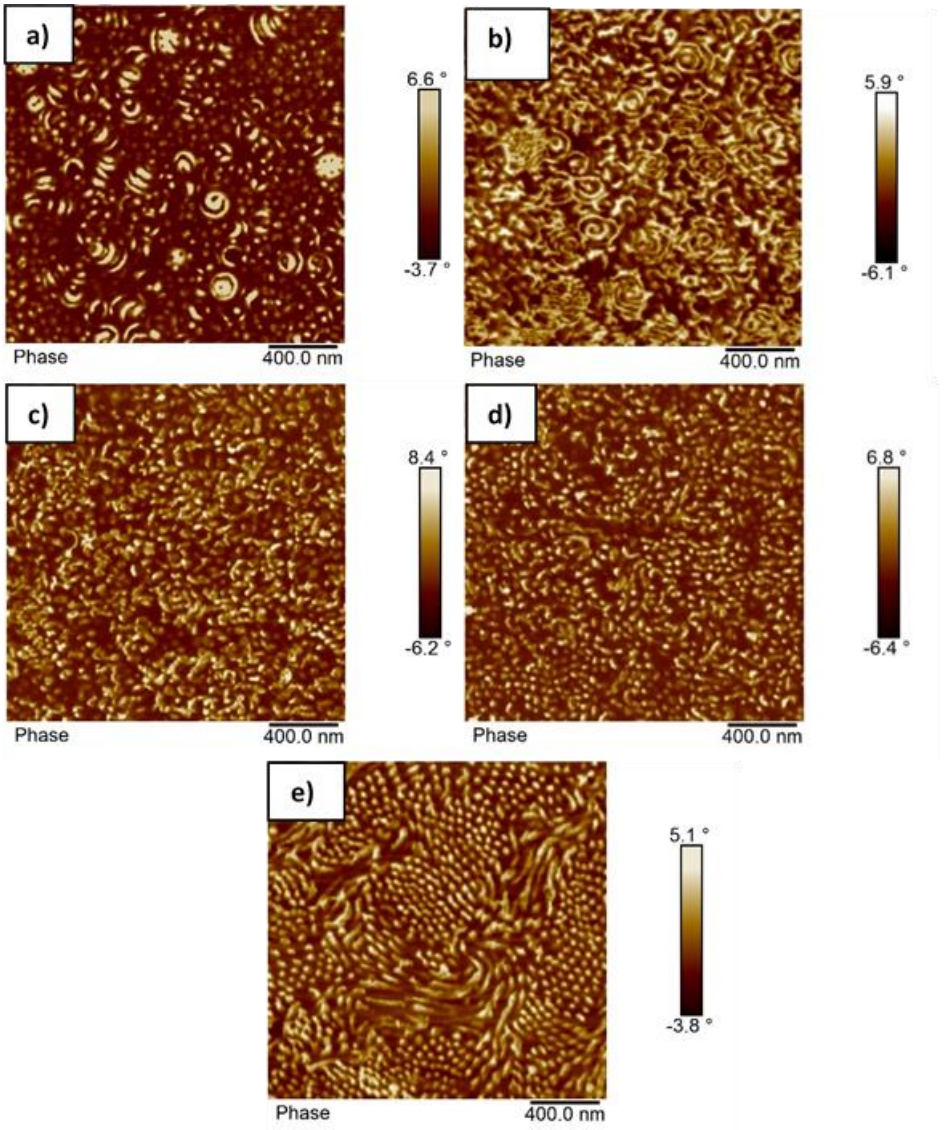

Figure V.11. AFM phase images of the sample p(St30-2EHA100) a) top surface of the film dried at room temperature b) cross-section of the film dried at room temperature, c) cross-section of the film dried at 100 °C for 30 min and d) cross-section of the film dried at 100 °C for 96 h e) cross section of a film cast from THF-solution.

Thermal annealing of the polymer films led to rearrangement of the hard domains. The effect is especially pronounced for longer annealing times and for the block copolymers with higher proportion of soft domains (V10d. and V11d.). Dissolving the polymer film in THF erased completely the thermal history of the sample and in the films cast from THF-solution a clear phase separation was observed where cylinders are placed in either horizontal or perpendicular direction parallel to each other (Figure V.9e., V.10e, and V.11e.).

V.3.4. Viscoelastic properties of AB hard-soft block copolymers

Mechanical properties of the AB hard-soft block copolymers were investigated by means of DMTA measurements and the results are presented in Figure V.12. Two different transition temperatures, one at lower temperature corresponding to the Tg of the soft rubbery block and one at higher temperature corresponding to the Tg of the hard domains could be distinguished, with a rubbery plateau in between them. It must be reminded that the glass transition temperature corresponding to the maximum of tan δ of the pSt could not be measured for films prepared from symmetric ABA block copolymers dried at room temperature (see Figure V.6). The chosen film measurement geometry of the DMTA instrument does not allow to measure to higher temperatures when the film sample starts to flow.

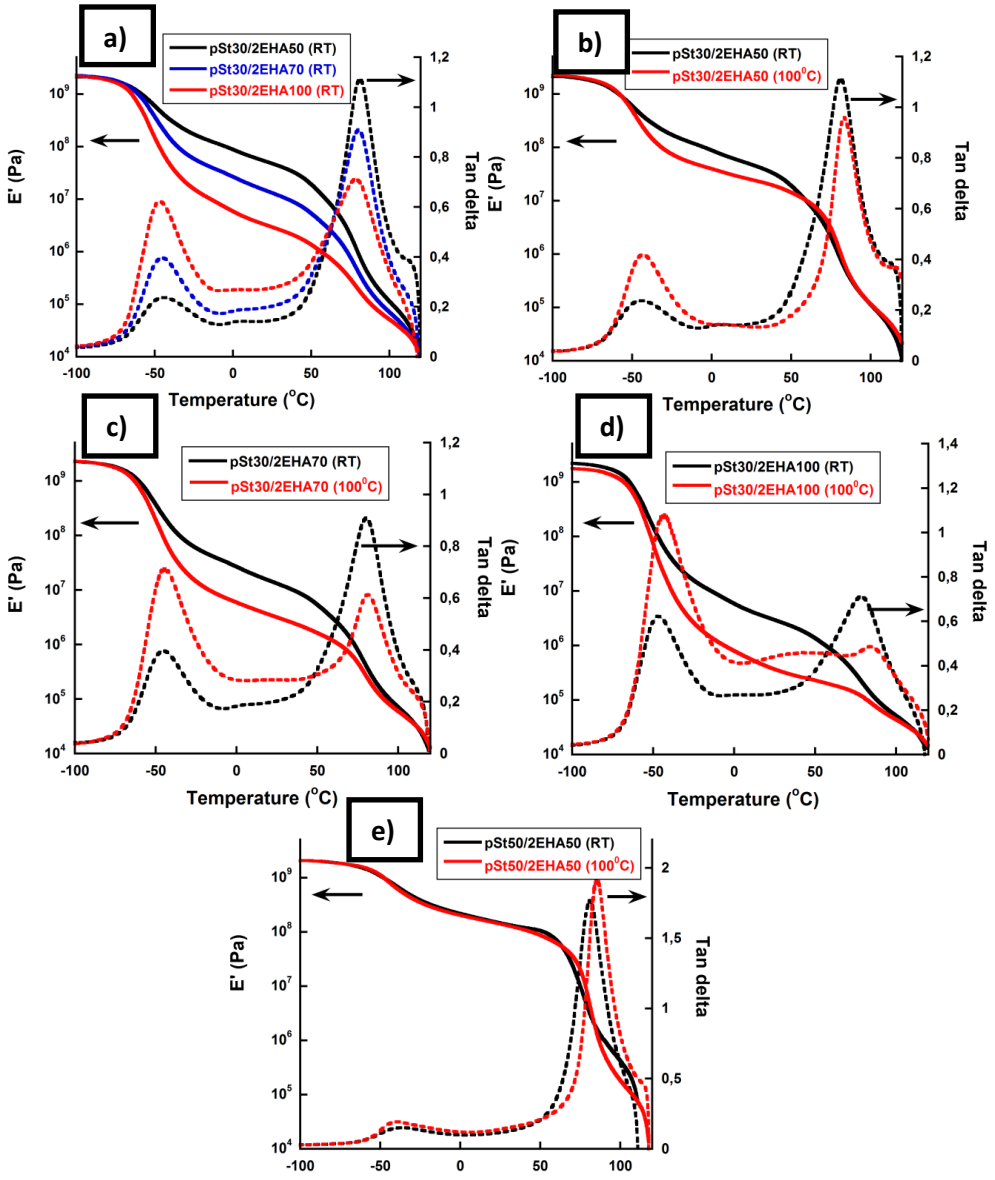

Figure V.12. Viscoelastic properties of the block copolymers, solid lines - dependence of elastic modulus on temperature and dashed lines-dependence of tan δ on temperature

The most probable reason for this difference is the larger pSt block size for the asymmetric block copolymers compared to the symmetric ABA type block copolymers with the same overall composition, indicating that for the AB-type block copolymers with larger polystyrene blocks the flow of the film specimen starts at somewhat higher temperature.

The viscoelastic properties of the films cast at room temperature presented in Figure V.12a, indicate that the elastic modulus decreases as the length (Mn) of the soft p2EHA block increases. This finding was also observed for the ABA hard-soft-hard block copolymers. Moreover, elastic modulus decreases significantly in the rubbery plateau in the temperature range between -30°C and 30°C.

In Figure V.12. b,c,d,e it can be observed that the elastic module decreases in the plateau for the block copolymers annealed at 100ºC, contrary to what happened for the symmetric block copolymers (Figure V.6). Below the Tg of polystyrene the ABA block copolymers behave similar to a vulcanized rubber and form a physical crosslinking. On the contrary in the case of AB block copolymers the soft block is linked to only one hard domain so when heated the polymer flows since there is no network to withstand the flow. The difference in the decrease of elastic modulus upon annealing in the rubber plateau is larger, the higher the amount of soft domains and this effect is negligible for the sample with lowest amount of p2EHA or highest amount of styrene domains (Figure V.12e).

V.3.5. Morphology of the ABA crystalline-soft-crystalline block copolymers

Block copolymers of ABA type where A is a crystalline block formed from polystearyl acrylate (pSA) and B is a soft copolymer based mainly on 2EHA units, containing also small quantity of SA units (which were non reacted from the first step), were prepared by seeded semibatch emulsion polymerization. The homopolymer pSA latexes with around 80% conversion served as seed for the second block polymerization. The synthesis characteristics and results obtained were symmetrized in chapter IV.

The morphology of the films cast at different conditions (i) room temperature, (ii) cast at room temperature and annealed at 60°C for 96 h, (iii) cast at room temperature and annealed at 100°C for 20 h and (iv) film obtained from THF dissolution and annealed at 100 for 20h, were analyzed by TEM and AFM. The samples for TEM analysis were stained with RuO_4. This staining agent reacts with any oxidizable moiety and stains not only aromatic molecules but in principle most of the polymer, however to a different degree depending on the diffusion rate. In crystalline polymers due to the faster diffusion in the amorphous regions, RuO_4 staining leads to a darker contrast in the amorphous regions as compared to crystalline regions where no or less staining happens. Crystalline lamellae are therefore clearly visible with a bright contrast[27–29].

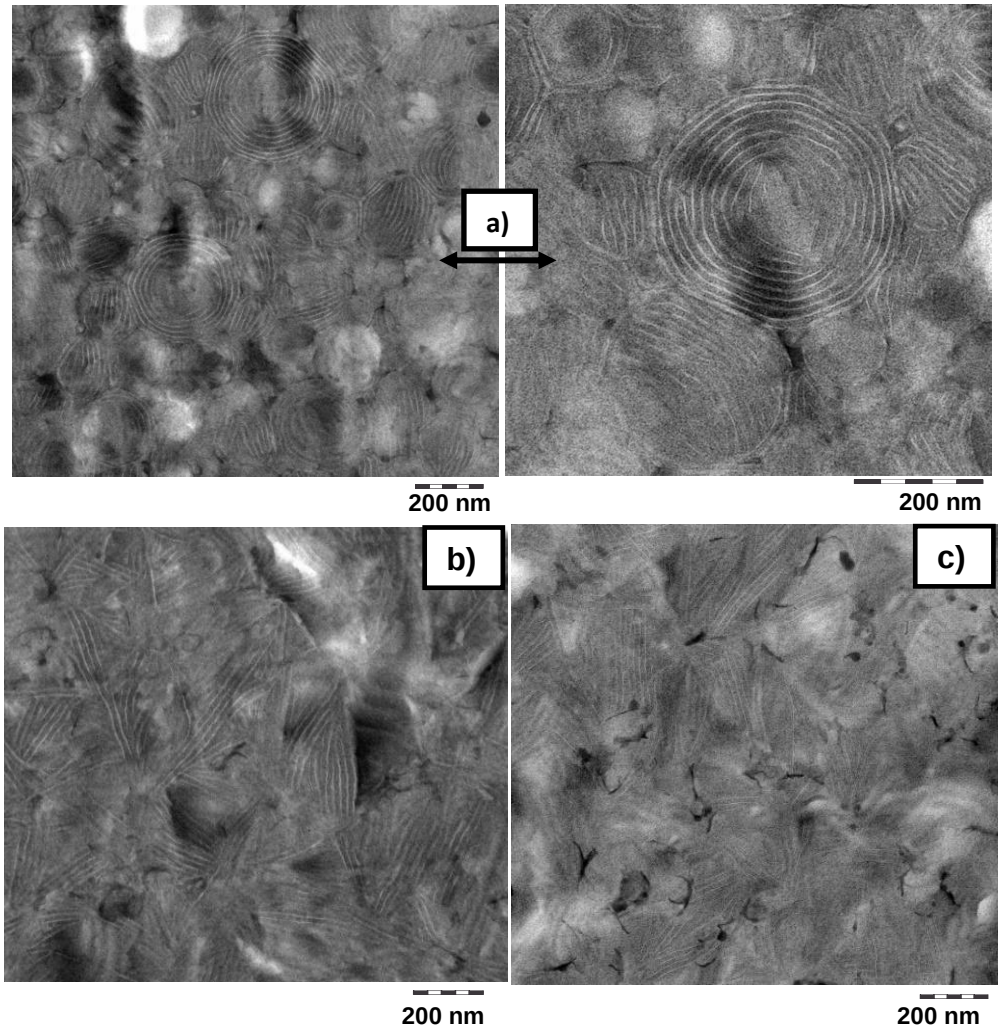

Figure V.13. TEM images of p(SA15-2EHS50-SA15) films a) cast at 23°C, b) cast at 60°C and c) after solvent casting from THF and annealing at 100°C for 20h

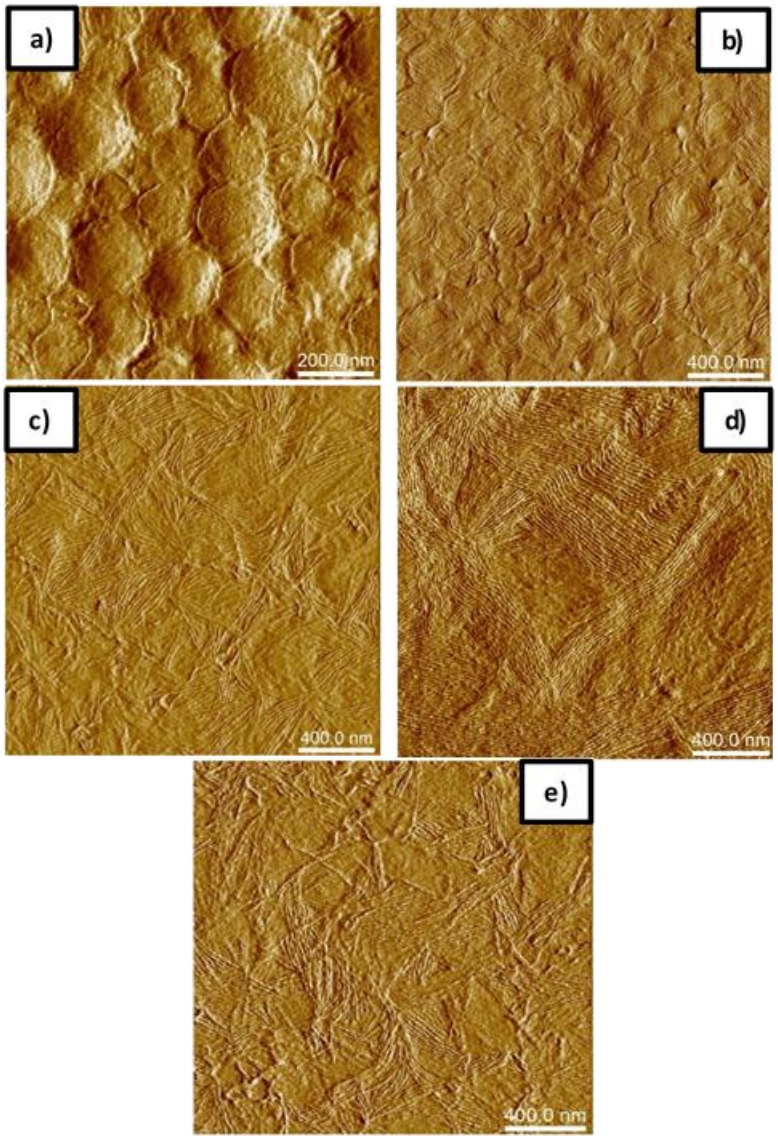

Figure V.14. AFM images (peak force error) of the p(SA15-2EHA50-SA15) films dried at 23°C a) top surface and b) cross-section, and cross sections of the films dried at c) 60 °C and d) 100°C, e) cast from THF-solution and annealed at 100°C for 20h.

TEM image of the film p(SA15-2EHA50-SA15), cast at 23°C (Figure V.13a) illustrate lamellar structure confined in each particle. Since the casting temperature is lower than the melting temperature of the crystalline hard domains (47-50ºC), block copolymer chains were probably not able to interdiffuse between neighboring particles in the film. As a result, we can observe an incomplete particle coalescence and a phase separation induced by crystallization which is confined in each particle. The lamellae are confined in different ways inside the polymer particles (concentric onion like lamellae, parallel lamellae …). On the other hand, when the films were annealed at a temperature of 60 °C, which is above the melting temperature of the pSA crystalline phase[30–33], complete coalescence of the particles occurred enabling the interdiffusion of polymer chains and re-arrangement of the crystalline domains on a larger scale (Figure V.13b). The formed lamellar structures extend in length beyond the original colloidal particles size. The TEM image obtained from the film cast from THF-solution is comparable to the one obtained after annealing at 60 °C. Therefore, it can be concluded that thermal annealing at 60 °C, already resulted in a crystalline morphology close to thermodynamic equilibrium, by the more stable morphology which is a lamellar structure. Further information on the self-assembly of the block copolymers were obtained with AFM measurements done on the films cast and annealed at different temperatures.

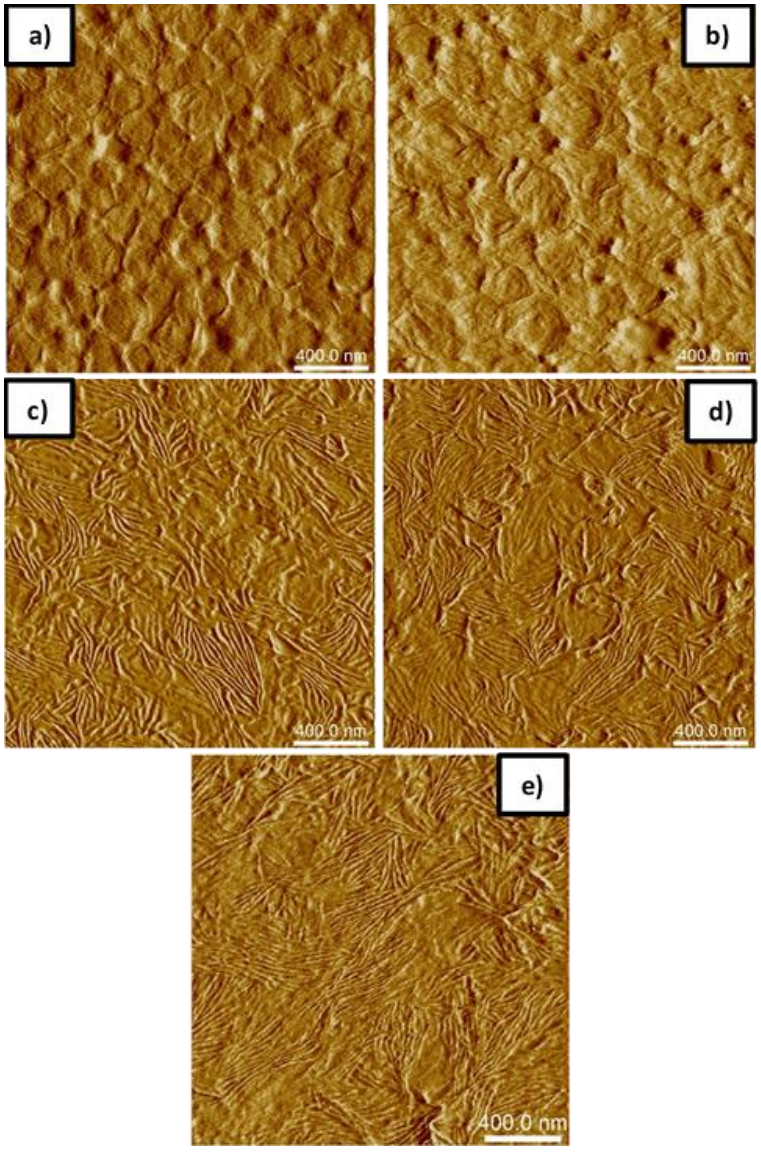

Figure V.15. AFM images (peak force error) of the p(SA15-2EHA100-SA15) films dried at 23°C a) top surface and b) cross-section, and cross sections of the films dried at c) 60 °C and d) 100°C, e) cast from THF-solution and annealed at 100°C for 20h.

AFM analysis of the top surface of the polymer films prepared by drop casting the block copolymer latexes (Figure V.14a and Figure V.15b) on a glass substrate at room temperature, reveal that the particle coalescence is not complete, and the boundaries of the particles are still visible. The visibility of the colloidal particle boundaries is more pronounced with the block copolymers with higher proportion of pSA domains (Figure V.14a). These findings are in correlation with the TEM images obtained from the films cast at room temperature.

To study the morphology within the particles, AFM study was done on a cross-section of the films cast at room temperature. Lamellar structures oriented parallel to each other and confined in each particle could be observed (Figure V.14b and V.15b). The lamellar spacing was found generally in the range of 20–25 nm. Considering the dimension of the particles, one could derive that there are about 8–10 lamellae present in each particle. When the films were annealed at higher temperatures (Figure V.14c and d and Figure 15c and d), extended lamellar structure was observed, which extends in size well beyond the original particles dimensions. No significant difference in morphology was seen between the films annealed at higher temperature (100°C) and the ones cast from THF solution (Figure V.14e and Figure 15e), indicating that close to equilibrium morphology was already reached by thermal treatment of the films. The AFM images of block copolymers films annealed at 100 °C having different composition were compared in Figure V.16. It was observed that all the block copolymers show more or less ordered lamellar structures

despite the variation in block length and variation in relative proportion of the individual blocks. In this context, as stated in the review article published by Nojima[34] and Chen's group[35], crystalline–amorphous block copolymers are able to form microdomain structure at temperatures above the melting point of crystalline blocks (Tm).

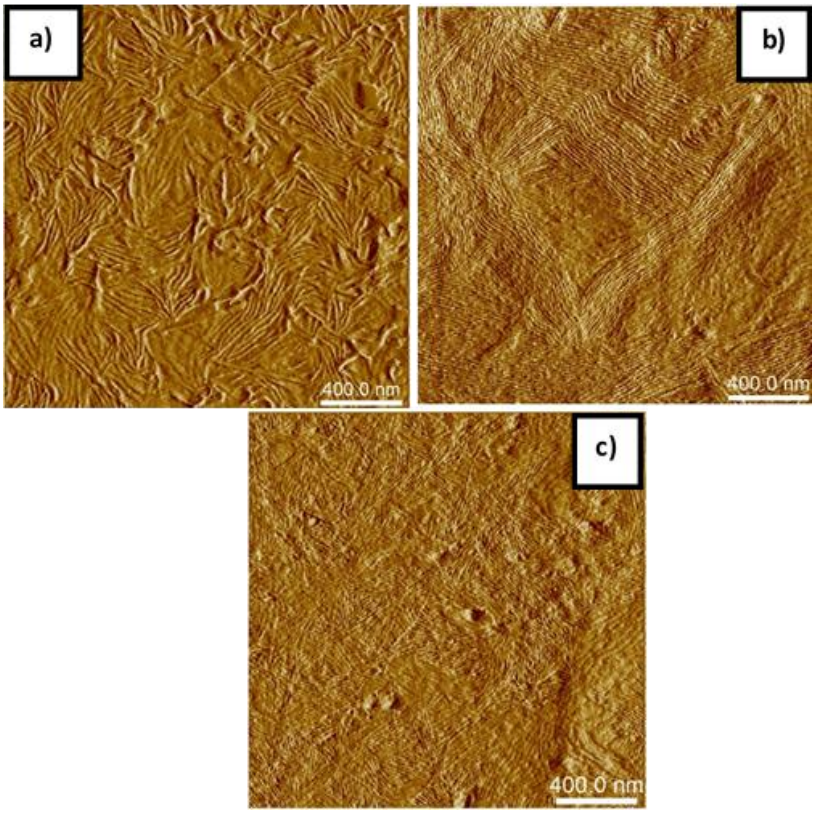

Figure V.16. AFM images (peak force error) of the cross sections of the films dried at 100°C, a) p(SA15-2EHA100-SA15), b) p(SA15-2EHA50-SA15), c) p(SA25-2EHA50-SA25).

When these microphase-separated block copolymers are quenched to lower temperatures, the crystalline block starts to crystallize to produce a certain morphology in the system, the details of which depend intimately on the molecular characteristics of block copolymers. If the initial microdomain structure is not sufficiently stable against the crystallization, which is the case when the segregation strength between different blocks is not large enough, the structure is completely replaced with a crystalline lamellar morphology. This is an alternating structure consisting of lamellar crystals and amorphous layers, after the crystallization of constituent blocks or break-out crystallization. Often this is also the case when the crystallization occurs in soft nanodomains and which can deform moderately according to the crystallization and increase the total crystallinity of the confined block. Since the Tg of the soft domains in the synthesized block copolymers is very low (−60 °C) and the segregation strength between the blocks is not large enough (T_{ODT}) > Tc > Tg, as discussed in chapter IV), the annealed samples will always end up with break out lamellar morphology irrespective of the chain length of the individual blocks.

V.3.6. Viscoelastic properties of ABA crystalline-soft-crystalline block copolymers

To analyze if the morphological changes with temperature affected the mechanical properties of the films, DMTA measurements were done and the results

are shown in Figure V.17. The graphs show dynamic mechanical behavior like triblock thermoplastic elastomers with two different transition temperatures: one at lower temperature corresponding to the Tg of the soft rubbery block and one at higher temperature corresponding to the melting temperature of the crystalline domains, a rubbery plateau in between them and a terminal region above the Tm of the crystalline block, in which the polymer goes to flow. The solid lines present the temperature dependence of the storage modulus. Looking at the DMTA results of the block copolymers cast at room temperature (Figure V.17a), as expected, it can be observed that as the length of the middle soft block increases, the elastic modulus in the rubbery plateau in the temperature range between -20°C and 35°C decreases, because the overall volume fraction of soft block in the block copolymer increases. In addition, higher damping properties are obtained. Approaching the melting point of the crystalline blocks, liquid like behavior is induced with significant drop of the storage modulus which makes further DMTA measurements of the film specimen at these regions impossible. Figures V.17b) c) and d) present the viscoelastic properties of different ABA-block copolymers films cast at room temperature and annealed at 60°C for 96 hours. As a general trend, we can see that in the annealed films there is a somewhat bigger drop in modulus in going from the low temperature glassy state to the rubbery plateau. This trend could suggest that during annealing, the effective volume fraction of hard crystalline phase has decreased. In addition, bigger crystals

formed after annealing which brings lower interaction with the soft part, leading to a decrease in the elastic modulus and increase of the damping properties.

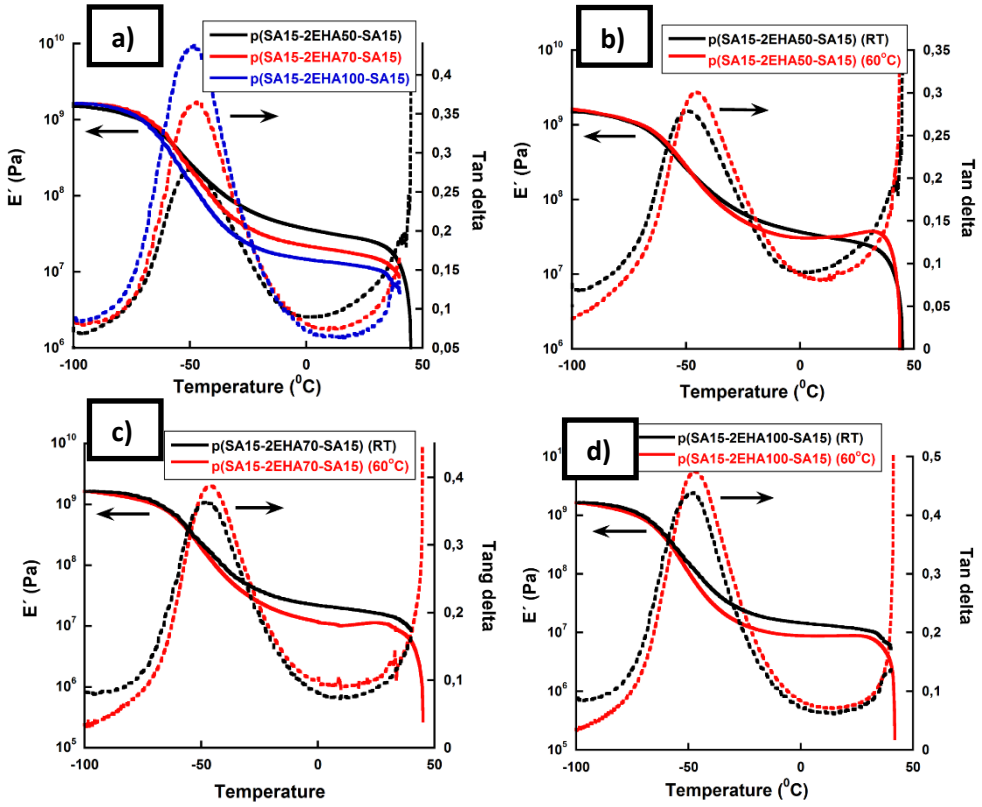

Figure V.17. Viscoelastic properties of a) films cast at room temperature (RT) and b-d) films cast at both room temperature and 60°C, solid lines - dependence of elastic modulus on temperature and dashed lines-dependence of tan δ on temperature.

V.4. Conclusions

In this chapter the effect of particle morphology on the film morphology at different thermal treatments for various types of block copolymers were investigated by means of microscopic techniques. Three different types of block copolymers dispersions were used, namely ABA or AB block type where A was formed from pSt hard domains or pSA crystalline domains and B was formed from soft p2EHA domains. Films cast from these dispersions were treated at different temperatures and their mechanical properties were compared. It was shown that when the films were casted at room temperature, the particle deformation and coalescence was not complete, and the crystalline phase separation occurred within the particles. Once thermal treatment was applied, particle coalescence and ordering on a bigger length scale was achieved which was close to the equilibrium morphology. Furthermore, it was shown that the composition of the block copolymers as well as the thermal treatments of the polymer films greatly influenced the viscoelastic properties of the block copolymers.

Regarding the morphological analysis, it was found to be very important to analyze films cross-sections and not just the films surfaces by AFM. The observed morphology on the film surface can be different compared to the inside of the films, especially concerning the study of the particle inner morphology.

The equilibrium morphology obtained for ABA was not the same as the one obtained for AB copolymers of the same composition.

The kinetics of the microphase rearrangement could be followed by annealing the hard-soft block copolymers at 100ºC for different times. It was seen that 30 minutes of annealing already erased the particle morphology, but the ordering only ranged 2 or 3 particles away.

One of the most interesting conclusions of this chapter has been the different viscoelastic behavior of the block copolymers. On one hand, ABA hard-soft-hard block copolymers showed an increased elastic modulus when annealing the films, while the AB hard-soft block copolymers showed a decrease of the modulus after annealing. This shows the importance of the architecture of the block copolymers. ABA block copolymers behave like a vulcanized rubber which after annealing increased the rubber plateau modulus. Regarding ABA crystalline-soft-crystalline block copolymers, which showed break-out morphology, independently from the monomer composition, the annealing produced a decrease in the elastic modulus of the rubber plateau, contrary to what happened with the hard-soft-hard block copolymers. The formation of bigger crystals after annealing most likely reduced the possibility of the crystalline domains to interact to the soft phase, leading to reduction of the elastic modulus and increase in damping properties.

V.5. References

1 L. L. Ruzette, A. Valérie, *Nat. Mater*, 2005, **4**, 19–31.

2 R. K. O'Reilly, C. J. Hawker and K. L. Wooley, *Chem. Soc. Rev.*, 2006, **35**, 1068–1083.

3 N. Saito, R. Takekoh, R. Nakatsuru and M. Okubo, *Langmuir*, 2007, **23**, 5978–5983.

4 C. Park, J. Yoon and E. L. Thomas, *Polymer*, 2003, **44**, 6725–6760.

5 J. Bang, S. H. Kim, E. Drockenmuller, M. J. Misner, T. P. Russell and C. J. Hawker, *J. Am. Chem. Soc.*, 2006, **128**, 7622–7629.

6 M. Okubo, R. Takekoh and N. Saito, *Colloid Polym. Sci.*, 2003, **281**, 945–950.

7 M. Okubo, N. Saito, R. Takekoh and H. Kobayashi, *Polymer*, 2005, **46**, 1151–1156.

8 J. Nicolas, A. V. Ruzette, C. Farcet, P. Gérard, S. Magnet and B. Charleux, *Polymer*, 2007, **48**, 7029–7040.

9 A. Bowes, J. B. Mcleary and R. D. Sanderson, *J. Polym. Sci. Part A Polym. Chem.*, 2007, **45**, 588–604.

10 A. Butte, G. Storti and M. Morbidelli, *Macromolecules*, 2001, **34**, 5885–5896.

11 Y. Luo and X. Liu, *J. Polym. Sci. Part A Polym. Chem.*, 2004, **42**, 6248–6258.

12 R. Wei, Y. Luo and Z. Li, *Polymer.*, 2010, **51**, 3879–3886.

13 Z. Wang, Q. Zhang, X. Zhan, F. Chen, G. Rao and J. Xiong, *J. Polym. Res.*, 2013, **20**, 1–13.

14 R. Wei, Y. Luo, W. Zeng, F. Wang and S. Xu, *Ind. Eng. Chem. Res.*, 2012, **51**, 15530–15535.

15 P. Froimowicz, B. Van Heukelum, C. Scholten, K. Greiner, O. Araujo and K. Landfester, *J. Polym. Sci. Part A Polym. Chem.*, 2014, **52**, 883–889.

16 L. Yang, Q. Han, Q. Song, H. Li, Q. Zhao, Y. Shen and Y. Luo, *Colloid Polym. Sci.*, 2017, **295**, 891–902.

17 F. S. Bates and G. H. Fredrickson, *Annu. Rev. Phys. Chem.*, 1990, **41**, 525–557.

18 T. Higuchi, K. Motoyoshi, H. Sugimori, H. Jinnai, H. Yabu and M. Shimomura, *Soft Matter*, 2012, **8**, 3791.

19 T. Higuchi, A. Tajima, K. Motoyoshi, H. Yabu and M. Shimomura, *Angew. Chemie - Int. Ed.*, 2008, **47**, 8044–8046.

20 H. Yabu, T. Higuchi and H. Jinnai, *Soft Matter*, 2014, **10**, 2919–31.

21 Y. Mai and A. Eisenberg, *Chem. Soc. Rev.*, 2012, **41**, 5969–5985.

22 M. W. Matsen and R. B. Thompson, *J. Chem. Phys.*, 1999, **111**, 7139–7146.

23 K. H. Ku, H. Yang, J. M. Shin and B. J. Kim, *J. Polym. Sci. Part A Polym. Chem.*, 2015, **53**, 188–192.

24 K. H. Ku, J. M. Shin, M. P. Kim, C. H. Lee, M. K. Seo, G. R. Yi, S. G. Jang and B. J. Kim, *J. Am. Chem. Soc.*, 2014, **136**, 9982–9989.

25 S. J. Jeon, G. R. Yi and S. M. Yang, *Adv. Mater.*, 2008, **20**, 4103–4108.

26 S. G. Jang, D. J. Audus, D. Klinger, D. V. Krogstad, B. J. Kim, A. Cameron, S. W. Kim, K. T. Delaney, S. M. Hur, K. L. Killops, G. H. Fredrickson, E. J. Kramer and C. J. Hawker, *J. Am. Chem. Soc.*, 2013, **135**, 6649–6657.

27 S. Tencé-Girault, V. Woehling, E. K. Oikonomou, S. Karpati and S. Norvez, *Macromol. Chem. Phys.*, 2018, **219**, 1–11.

28 D. Montezinos, B. G. Wells and J. L. Burns, *J. Polym. Sci. Polym. Lett. Ed.*, 1985, **23**, 421–425.

29 J. Trent, J. I. Scheinbeim and P. R. Couchman, *Macromolecules*, 1983, **16**, 589–598.

30 E. Mehravar, J. R. Leiza and J. M. Asua, *Polymer.*, 2016, **84**, 167–177.

31 A. Agirre, C. D. Las Heras-Alarcón, T. Wang, J. L. Keddie and J. M. Asua, *ACS Appl. Mater. Interfaces*, 2010, **2**, 443–451.

32 X. Zhu, Y. Gu, G. Chen, Z. Cheng and J. Lu, *J. Appl. Polym. Sci.*, 2004, **93**, 1539–1545.

33 F. Dutertre, P. Y. Pennarun, O. Colombani and E. Nicol, *Eur. Polym. J.*, 2011, **47**, 343–351.

34 S. Nakagawa, H. Marubayashi and S. Nojima, *Eur. Polym. J.*, 2015, **70**, 262–275.

35 B. Nandan, J. Y. Hsu and H. L. Chen, *Polym. Rev.*, 2006, **46**, 143–172.

Chapter VI. Application of the block copolymers as heat seal lacquers

VI.1. Introduction

In this chapter, the study of the adhesive properties of the block copolymers as heat seal lacquers is investigated. This work was carried out in BASF, Heerenveen, Netherlands with the support and guidance of Christof van Sluijs and Hilly Maandag.

Heat seal lacquers stand for an expedient and effective method to seal paper, foil, and other films to a diversity of packaging materials. Increasing urbanization and changing lifestyles has led to an increase in consumer preference for processed foods and convenience-oriented products, such as ready-made meals, single serve cups for a variety of wet and dry food[1] where sealants for lidding are seen more and more on the items. In heat seal lacquers a flexible substrate is coated on one side, stored and transported or otherwise processed. The substrate is later sealed to another surface with heat and pressure. Heat seal lacquers are generally stored in a wound roll or they are stacked in sheets, thus the coatings should be carefully designed to have a proper Tg to avoid sticking of the coating to the layer above and at the same time maintaining the desired low sealing initiation temperature. Water-based dispersions can be tailor-made to many specific uses due to the ability to create multi-phase particles, amongst which heat seal lacquers can also be found. In principle, and due to the different behaviors needed at different heat seal steps (first non-adhesive and adhesive upon heating), low and high Tg polymers are

desirable in heat-sealants. Alteration of the Tg of the hard polymer can generally impact block resistance and adhesion of the coating to the substrate under pre-seal conditions, although other factors can also influence the final heat seal properties. Many patents have been reported by companies[2–8] where they design dispersions with core-shell morphology with a higher Tg shell and a lower Tg core. When exposed to heat and pressure, the Tg of the hard phase can be overcome, mixing of the phases can occur, forming a continuous softer phase. The surface of the substrates will be wetted as chains will be mobile and formation of good bond strength upon cooling will be formed. The final bond strength is determined by the interaction of several different materials and processing factors. It is related to the adhesion of the sealant to each surface as well as the cohesive strength of the sealant layer itself.

In this chapter a different approach is tried, namely waterborne block copolymers dispersions of ABA symmetric or AB asymmetric type are synthesized where A is either the hard or the crystalline domain and B is the soft domain. The synthesis of such dispersions gives us the freedom to design the Tg of the hard phase or the Tm of the crystalline domains in a such way to bring a low seal initiation temperature and at the same time to enable good blocking resistance at room temperature.

VI.2. Experimental part

VI.2.1. Materials and methods

The block copolymer dispersions were drawn to Incada Silk White Back Folding Box Board (GC1). Prior to casting, 5 wt% isopropyl alcohol (based on total dispersion) was added dropwise to the dispersion while mixing, to improve wetting and to form continuous and homogenous films (Figure VI.1). Figure VI.1 shows the drawdowns made on aluminum foil for a better contrast.

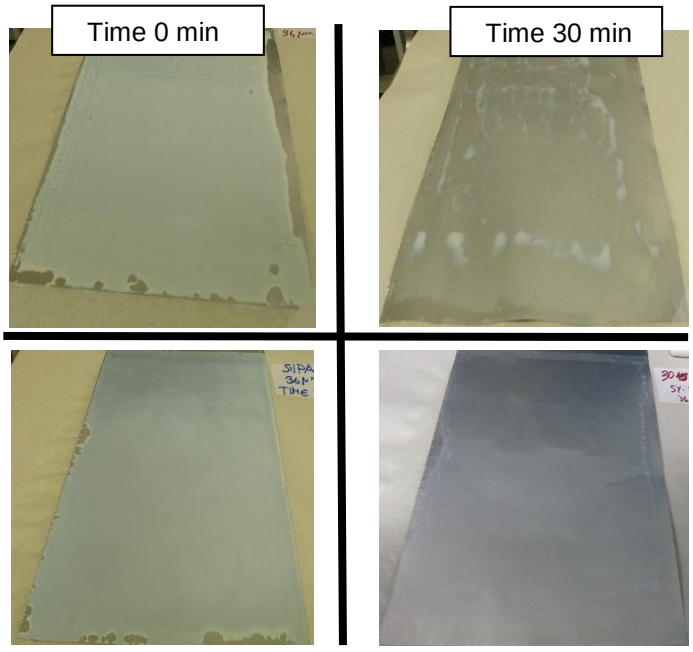

Figure VI. 1. Emulsion polymers casted onto aluminum foils with bar coater (defined film with a wet layer thickness of 36 µm): ABA block copolymers dispersion (upper images) and ABA block copolymers dispersion + 5 wt% isopropyl alcohol (lower images)

The mixture of block copolymer dispersion with 5% isopropyl alcohol was stored overnight to ensure good mixing between components. The paper boards were coated and dried at three different conditions: (i) at room temperature overnight, (ii) at 60°C overnight (for the crystalline-soft-crystalline block copolymers) and (iii) at 100 °C overnight (for the ABA hard-soft-hard and AB hard-soft block copolymers). The dry coat weight was approximately 5-6 g/cm^2. After drying overnight, the coated paper boards were heat sealed using a pressure of 100N/cm for 2s and 10s, with various jaw temperature setpoints starting from room temperature, 60°C, 100°C, 150°C and 200°C. The coated paper boards were sealed face-to-face to another coated paper board dried at the same conditions (= “lacquer to lacquer sealing”). Moreover, the coated paperboard was sealed to different uncoated substrates: PVC, PS and PET. A heat seal sealing machine Brugger HSG-C where the 20 mm metal top bar was heated, and the 20 mm lower silicone bar was non-heated, was used for sealing the substrates. After the surfaces were sealed together and allowed to cool, bond strengths were measured by 180° peel tests performed with a Lloyd LR5K tensile tester, at a peel speed of 150 mm/min. Bond strengths were measured in N/15mm.

The obtained results were then compared to a trade latex J HSL 9011; a dispersion based on p(BA/2EHA/MMA), Mw > 200,000 Da, (75% of the total product) having a Tg of -30°C and containing an alkali soluble resin styrene/alpha-

methylstyrene/butylacrylate/acrylic protective colloid, Mw= 7,500 (25% of the total product) having a Tg of 75 °C.

VI.3. Results and discussion

VI.3.1. Heat sealing properties of ABA hard-soft-hard block copolymers

The heat sealing properties of four different ABA block copolymers dispersions p(St15-2EHA50-St15), p(St15-2EHA70-St15), p(St15-2EHA100-St15) and p(St25-2EHA50-St25)), having different Mn were investigated. The synthesis of these block copolymers was described in Chapter II. Initially the block copolymers dispersions were applied to paper substrate and sealed face-to-face (= “lacquer to lacquer sealing”) to another paper substrate. The results of the bond strengths are shown in Figure VI.2. The blue bars represent the peel force or bond strength obtained from the drawdowns dried at room temperature and the green bars represent the peel force obtained from the drawdowns annealed at 100°C overnight. On the other hand, the solid filled bars are the data obtained from the substrates pressed for 2s and the patterned bars represent the data obtained from the films pressed for 10s. The preferred mode of opening failure in paper to paper heat seal lacquers is paper tear, so the plateau bond strength should be greater than the cohesive strength of the paper. This limit is around 5.5 N, meaning above this value the paper substrate is not able to withstand the cohesive strengths of the polymer

coating and paper tears occurs. These values sometimes can be a bit higher and depend on the mechanical properties of the polymeric coating, the penetration of the coating into the paper fibers, the adhesion of the coating to the paper, and so on. This means that at a certain peel force sometimes paper tear will occur and with another coating cohesive failure. From the graphs shown in Figure VI.2, the samples p(St15-2EHA50-St15) and p(St25-2EHA50-St-25) having highest portion of hard domains, 35.7 wt% and 40.6 wt% respectively, as detected by NMR (shown in Chapter V), did not show any tackiness at room temperature. Tackiness at room temperature was not observed neither for the samples pressed for 2s nor for the ones pressed for 10s. Moreover, the sample with the highest portion of hard domains (p(St25-2EHA50-St-25)) did not show tackiness even at temperatures as high as 60°C. This was not the case for the block copolymers in which soft domains dominate (p(St15-2EHA70-St15) and p(St15-2EHA100-St15)). These samples showed tackiness already at room temperature. Room temperature tackiness or blocking is highly undesirable property, because this will lead to difficulties in unwinding of the drawdowns and surface defects during the converting process as described in Chapter I.

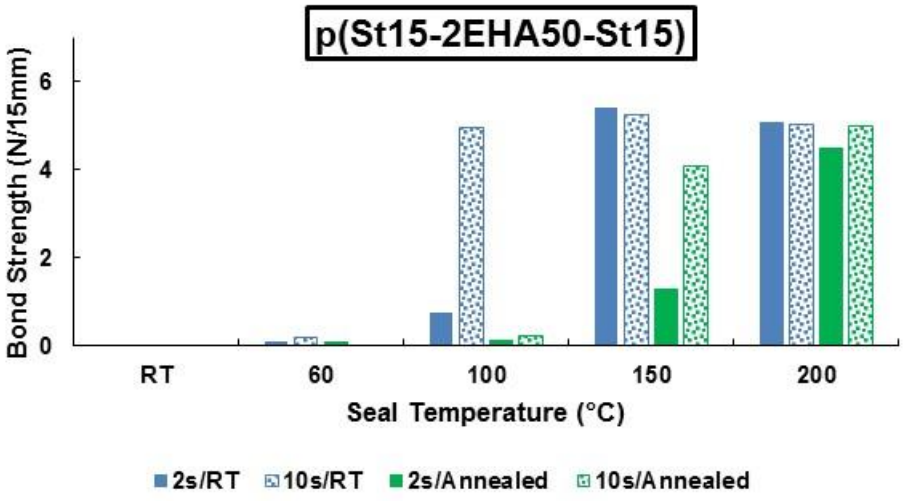
p(St15-2EHA50-St15)
Bond Strength (N/15mm)
0
2
4
6
RT
60
100
150
200
Seal Temperature (°C)
2s/RT
10s/RT
2s/Annealed
10s/Annealed

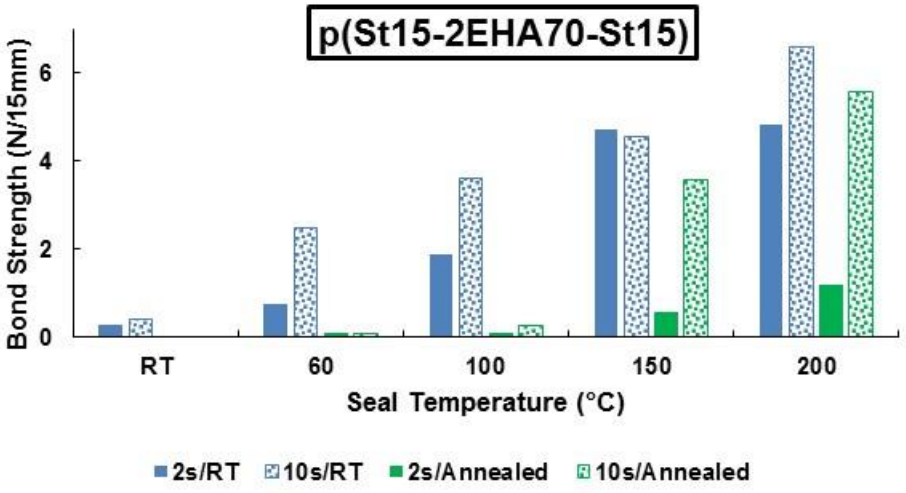
p(St15-2EHA70-St15)
Bond Strength (N/15mm)
0
2
4
6
RT
60
100
150
200
Seal Temperature (°C)
2s/RT
10s/RT
2s/Annealed
10s/Annealed

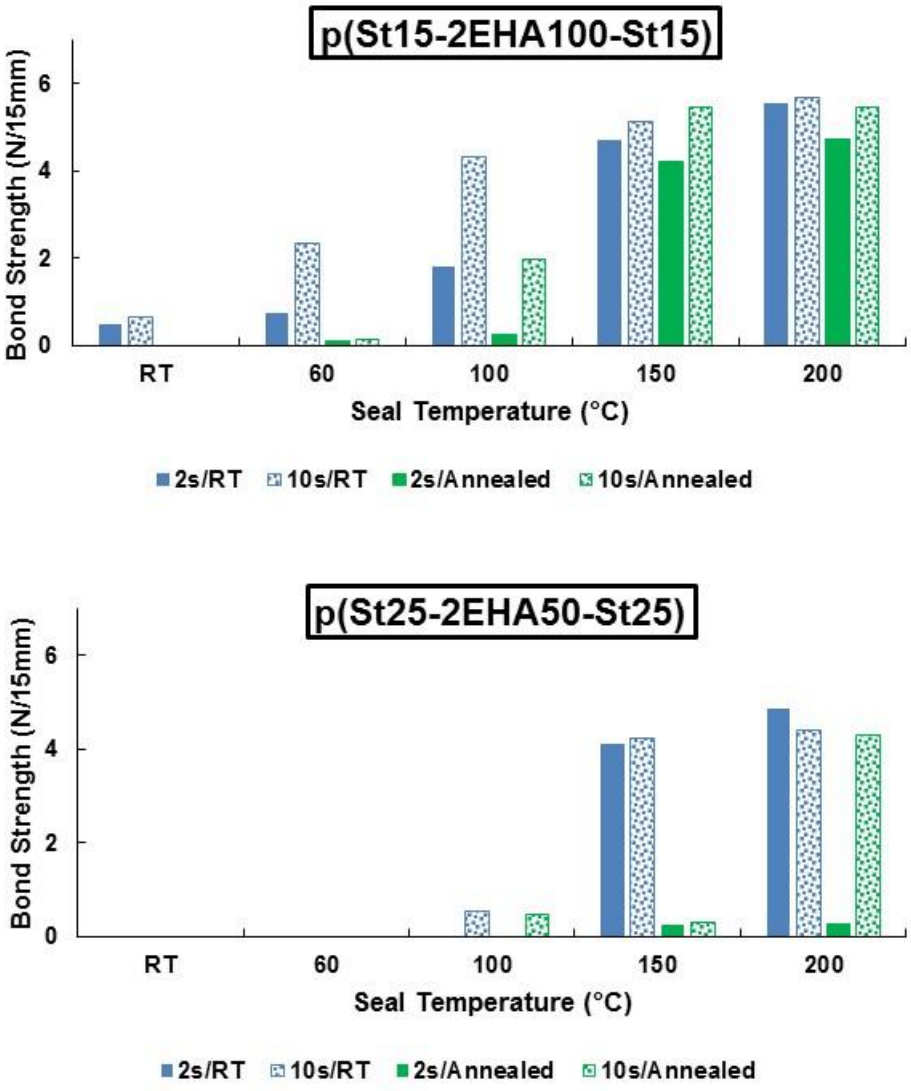

Figure VI.2. Bond strength of hard-soft-hard block copolymer dispersions on coated paper (paper to paper seal). Green bars: coated papers have been annealed at 100 °C over night

Furthermore, the highest seal strength obtained manifested as a paper tear was observed for the samples that have highest amount of pSt domains (p(St15-2EHA50-St15) and p(St25-2EHA50-St-25). Within the sample p(St15-2EHA50-St15) high bond strength (paper tear) was obtained already at 100°C seal temperature, but only for a dwell time of 10s compared to the sample p(St25-2EHA50-St-25) where high bond strength was obtained only at 150°C seal temperature, for both dwell times of 2s and 10s. The block copolymers showed two different glass transition temperatures, a lower one at around -60°C and a higher one at around 60°C (shown in Chapter II Figure II.15). Thus, one would expect them to already activate at 100°C which is well above the Tg of the hard domains, however this was not seen in the graphs. To further investigate the reasons for this behavior, additional analysis was made and the relation between the set temperature and actual temperature of the coated paper was better studied. The temperature in the seal area was measured during sealing and a temperature profile over time was done using a coated paper board with HSL 9011 dispersion sealed on PET substrate, using 2 different dwell times (2s and 10s), by which the coated paper sheet and the non-coated PET sheet are pressed together. The results are shown in Figure VI.3. It can be seen from the figure that the in-seal temperature differs from the target set temperature of the machine, and this difference is higher for lower dwell times. An increase from 20°C to 40ºC with dwell time increase from 2s to 10s was observed for different target temperatures. For example, even though the display temperature of the machine for

the sealing tool was 200°C and the substrates were pressed for 10s, the actual temperature that the substrate reached was only 160 °C (see upper blue dotted curve in Figure VI.3). This is because certain time is needed to transfer the heat from the hot plates of the machine to the cardboards and the lacquer layer. From the Figure VI.3 it gets clear that higher set temperature of the tool needs to be applied to achieve the desired temperature of the lacquer layer to activate the polymer.

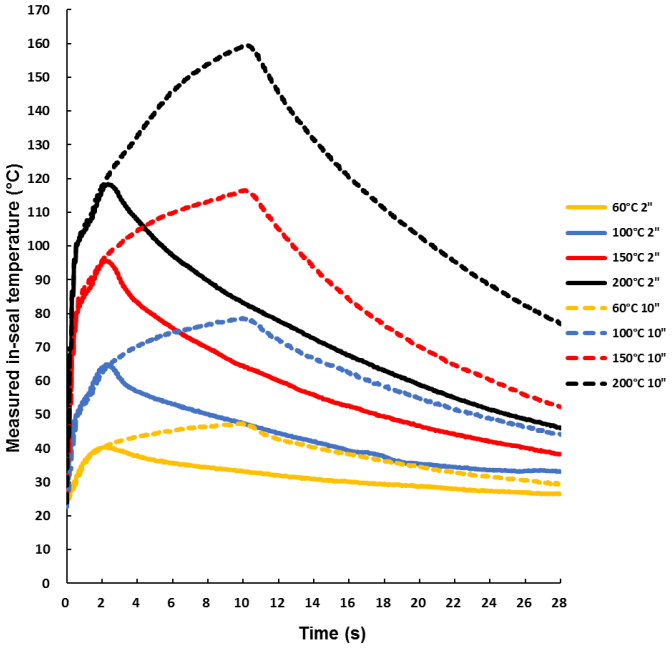

Figure VI.3. In-Seal temperature profile measured for a commercial standard reference polymer dispersion; variations of real seal temperatures versus time for different target set temperatures and two different dwell times (2'' and10'') by which the coated paper sheet was pressed against non-coated PET.

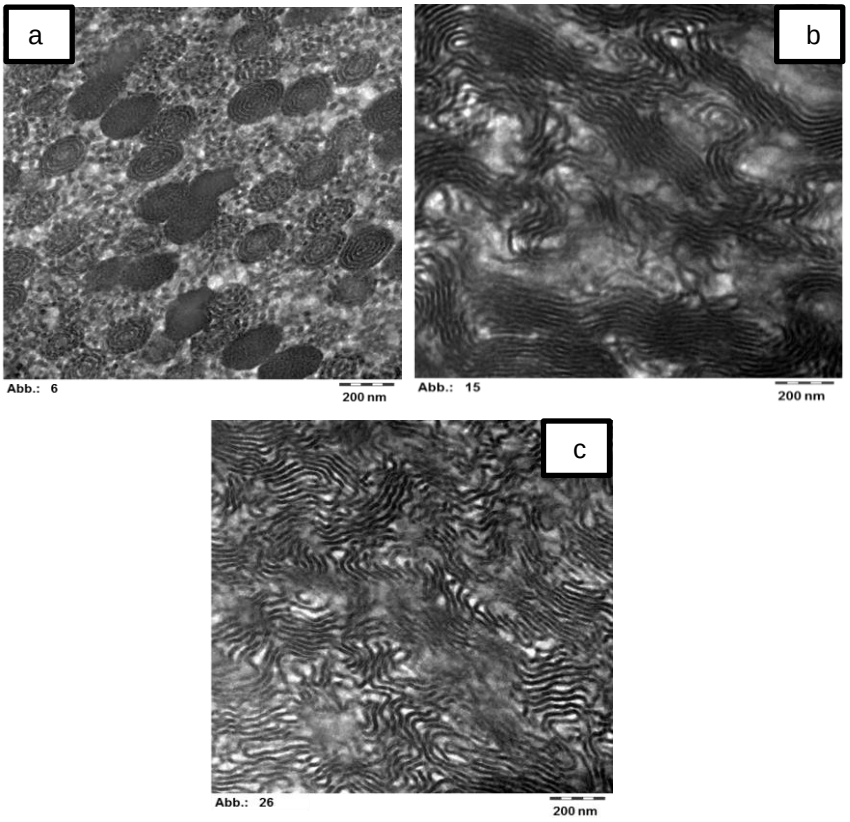

Figure VI.4. TEM images of the sample p(St15-2EHA70-St15) a) film dried at 23°C, b) film dried at 100 °C and c) film casted after a dissolution in THF. The bar of all the images is 200nm

As explained above the sample p(St25-2EHA50-St25) activates at higher temperatures (150 °C for a dwell time 2s and 10s) as seen in graph VI.2. This is most likely due to the higher amount of pSt present (40.6 wt%) in the system, thus higher temperature is needed to activate the hard pSt domains to achieve the desired cohesive forces and bond strength. Paper tear is obtained also for the sample

p(St15-2EHA70-St15), however at much higher temperatures (200°C). The sample which has highest amount of soft domains p(St15-2EHA100-St15) shows high values of peel force, however since not enough cohesive strengths are present in the polymer (low amounts of hard domains), peeling failure is obtained at all temperatures.

Another feature observed is that within the drawdowns annealed at 100°C overnight prior to sealing, high bond strength is obtained only at high temperatures and high dwell times. Namely above 100°C for the p(St15-2EHA50-St15) and above 150°C for p(St25-2EHA50-St25). This is most likely because of two ongoing effects during annealing: (i) migration of surfactant to the surface and/or (ii) substantial phase separation and re-rearranging of the domains, such that higher temperatures and/or more time is needed to achieve adhesiveness. From the TEM images shown in Figure VI.4 (as well as in Chapter V) we can see that room temperature dried films (Figure VI.4a) show no complete particle coalescence. On the other hand, the thermal treatment of the polymer film (at 100 °C) (Figure VI.4b) caused complete particle coalescence and led to morphology which resembled the one of the block copolymers films obtained from THF solution (Figure VI.4c). This is an indication that already by annealing at 100°C for 96 hours close to equilibrium morphology is approached. We can therefore expect that during annealing of the coated paper boards (100°C overnight), particle coalescence occurred, and the re-organization of

the block copolymer microphase separation morphology happened already at the paperboard. Thus, when the two surfaces were sealed, the mobility of the chains that were already at equilibrium was rather low, at least for lower temperatures. This led to low peeling forces unless very high temperature and dwell time was applied.

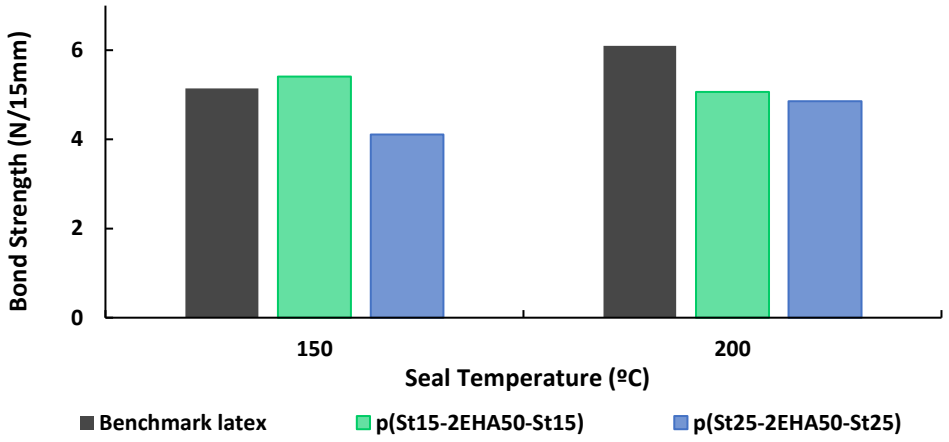

Figure VI.5. Bond strength of hard-soft-hard block copolymer and benchmark dispersions on coated paper (paper to paper seal, applied dwell time: 2s, films dried at room temperature).

The samples p(St15-2EHA50-St15) and p(St25-2EHA50-St-25) which showed the highest bond strength and paper tear failure were then compared to a benchmark latex J HSL 9011 and the results of the obtained peel strength using a dwell time of 2s are shown in Figure VI.5. Higher bond strength at lower temperatures (150°C) is obtained for the block copolymer dispersion p(St15-2EHA50-St15)

compared to the benchmark latex J HSL 9011, which on the other hand showed higher bond strength at higher temperatures (200 °C). This is most likely connected to two factors (i) activation temperature and (ii) the molecular weight of the polymers. The hard polymer in the benchmark latex shows a Tg of around 75 °C, thus a sealing temperature of 150 °C, with an actual temperature in the seal area of around 95 °C and a dwell time of 2s is most likely not yet optimum to effectively join the two polymer coated paper surfaces to form maximum bonding upon cooling. It is assumed that under these conditions the interdiffusion of polymer chains is not yet high enough to form a uniform and cohesive seal layer between the two paper sheets. On the other hand, the block copolymer p(St15-2EHA50-St15) can already be well activated at this temperature and provides good bonding of both paper sheets upon cooling. Another possible reason is the molecular weight of the polymer. The block copolymer has a lower molecular weight than the benchmark making the polymer diffuse more quickly. On the contrary at higher temperatures the benchmark polymer completely molten enabling even the bulky high molecular chains to diffuse across the interfaces forming good bond once the substrates are cooled down.

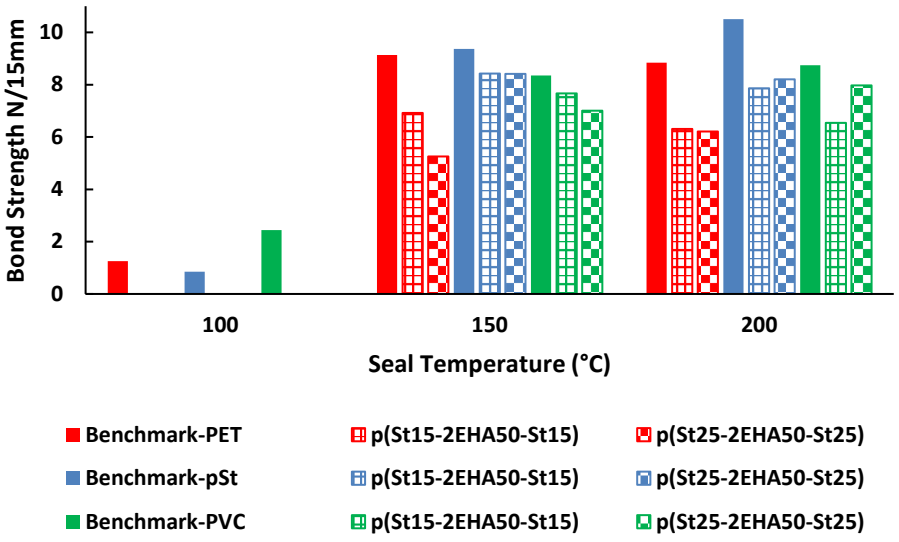

Figure VI.6. Bond Strength of hard-soft-hard block copolymer and benchmark dispersions tested on coated paper in sealing to non coated plastic films: PET (red), pSt (blue), PVC (green) substrates.

Coated paper boards with the samples p(St15-2EHA50-St15) and p(St25-2EHA50-St-25) were sealed for 2s onto three different substrates: PET, pSt and PVC and the results are shown in Figure VI.6. These substrates were chosen because they are relevant in the packaging industry. The block copolymers did not seal onto the substrates at 100°C and the benchmark latex showed only very low bond strengths manifested as pealing failure at this temperature. Moreover, as seen from the Figure VI.6, the block copolymer dispersions showed generally lower bond strength compared to the benchmark latex. Nevertheless, they all showed paper tear

failure and the highest bond strength obtained was achieved for pSt substrate. This is most likely because the block copolymers composed of hard polystyrene domains were more compatible to the pSt substrate and showed better mixing of the phases, which resulted in formation of better bond after cooling.

VI.3.2. Heat sealing adhesive properties of the AB hard-soft block copolymers

The heat sealing properties of p(St30-2EHA50), p(St30-2EHA70), p(St30-2EHA100) and p(St50-2EHA50), AB block copolymers having different Mn were investigated. The synthesis and characterization of these block copolymers was presented in Chapter III. The results of the bond strengths of the paper to paper heat sealable lacquers are shown in Figure VI.7.

The results presented in Figure VI.7 show the same trend as the ABA type block copolymers. The high pSt content samples, p(St30/2EHA50) and p(St50/2EHA50), with 48.8 wt% and 34.7wt% of pSt respectively (from NMR results shown in Chapter V), show no tackiness at room temperatures. On the other hand, the samples with higher content of soft domains; p(St30/2EHA70) and p(St30/2EHA100) showed certain tackiness and certain bond strengths already at room temperature manifested as peel failure. This behavior makes them unsuitable for the usage of heat sealable lacquers for the reasons discussed above.

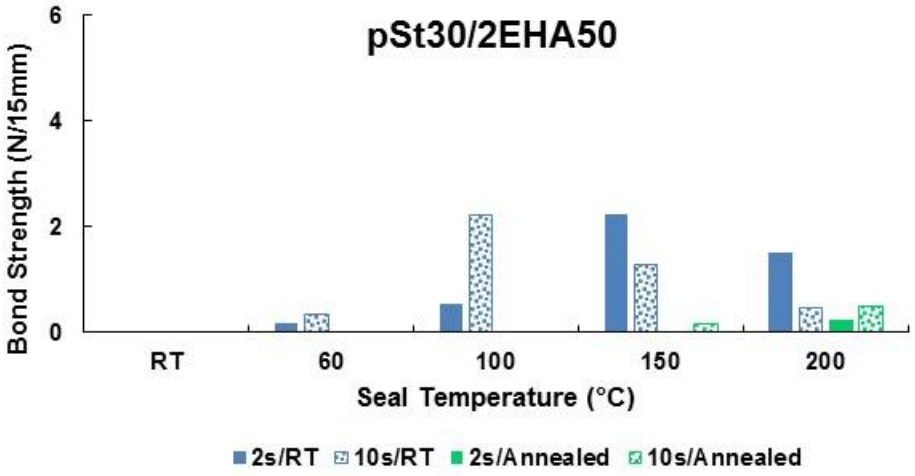
pSt30/2EHA50
Bond Strength (N/15mm)
6
4
2
0
RT
60
100
150
200
Seal Temperature (°C)
2s/RT
10s/RT
2s/Annealed
10s/Annealed

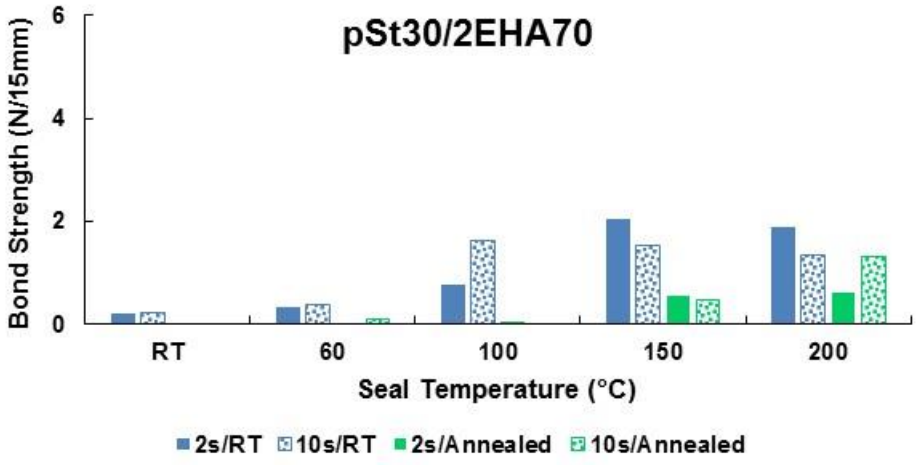
pSt30/2EHA70
Bond Strength (N/15mm)
6
4
2
0
RT
60
100
150
200
Seal Temperature (°C)
2s/RT
10s/RT
2s/Annealed
10s/Annealed

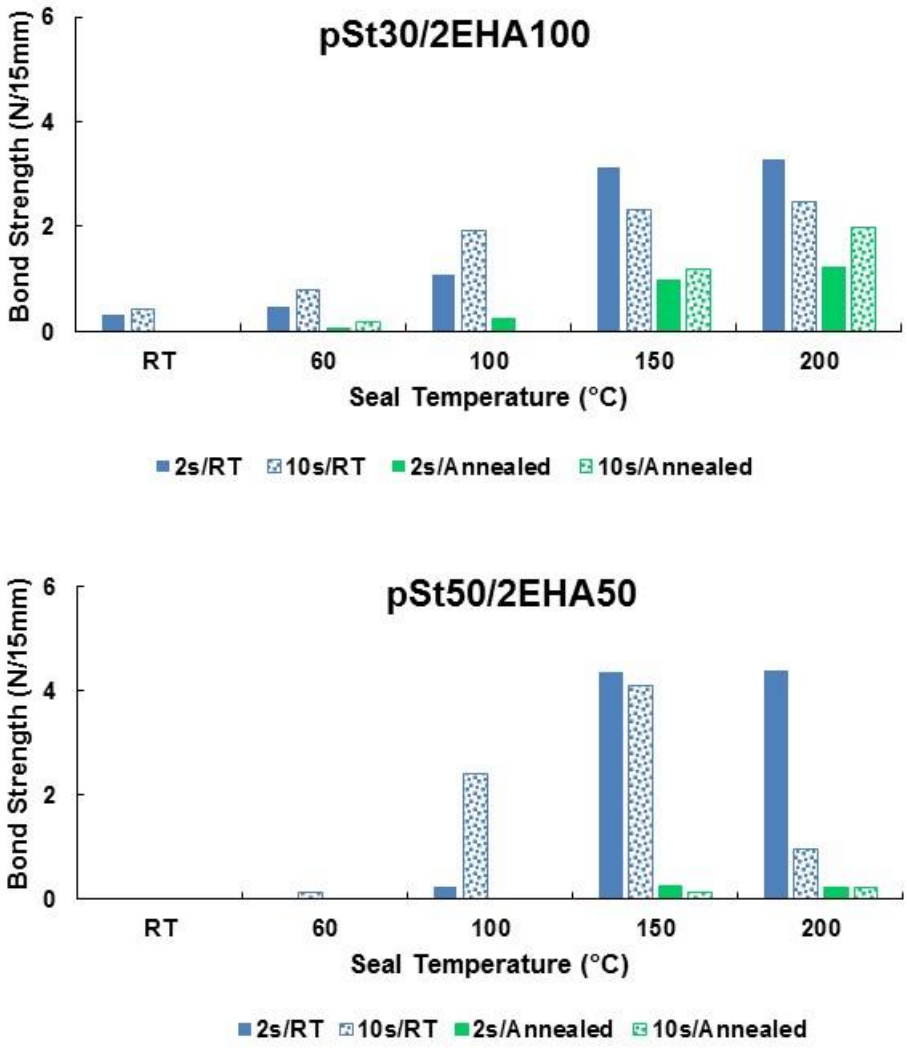

Figure VI.7. Bond strength of hard-soft AB block copolymer dispersions on coated paper (paper to paper seal); sealing experiments done at dwell times of 2s and 10s; coating preparations: "RT": coated papers where dried at room temperature; "Annealed": coated papers where in addition stored at 100°C over night

Furthermore, we can observe that at lower temperatures (100°C) higher bond strengths are obtained for higher dwelling times. This is not surprising if we take into an account that for a dwell time of 2s at a display temperature of 100°C only 65°C is reached in the seal layer. This temperature is not high enough to soften the hard domains and allow enough interdiffusion that both coating layers can effectively create a solid bonding after cooling. An interesting phenomenon observed at higher temperatures above 100°C is that the samples sealed at higher dwell times (10s) show lower bond strengths than the ones sealed at lower dwell times (2s). This finding was not observed in the ABA hard-soft-hard block copolymers. Most likely the AB block type copolymers show lower melt viscosity at higher temperatures compared to the ABA block copolymers and when pressed, the polymer film diffuses into the pores of the paper. Thus, there is lower effective thickness and less surface contact. In the annealed samples the same behavior is observed as within the ABA block copolymers, annealed samples show no/lower bond strengths for the reasons explained above.

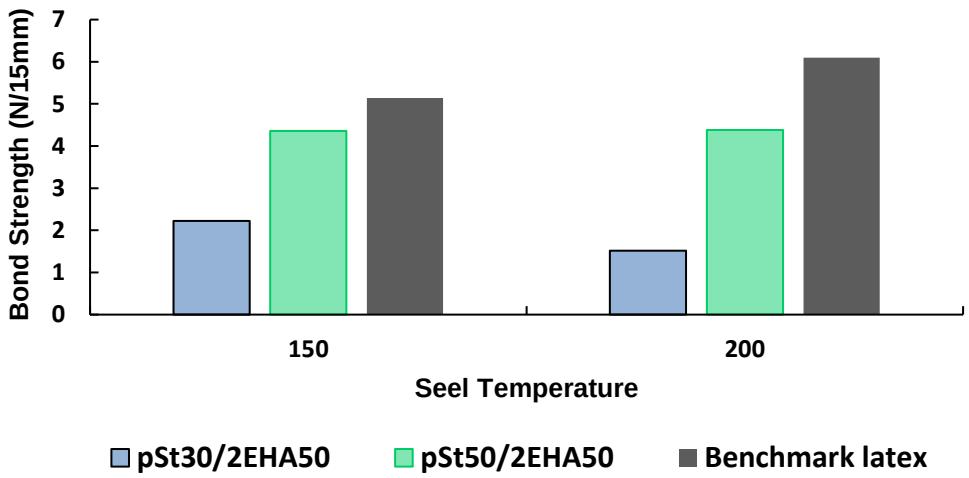

Figure VI.8. Bond strength of hard-soft-hard block copolymer and benchmark dispersions on coated paper (paper to paper seal), dwell time 2s

The samples pSt30/2EHA50 and pSt50/2EHA50 were compared to the benchmark latex J HSL 9011 and the results of the paper to paper heat seal lacquers using dwell time of 2s are shown on Figure VI.8. The sample pSt30/2EHA50 showed lower bond strength compared to the benchmark. Furthermore, at 150°C there was not a huge difference between the bond strength values of the sample pSt50/2EHA50 and the benchmark latex. On the other hand, as the temperature is increased to 200°C, the difference between the samples became more obvious.

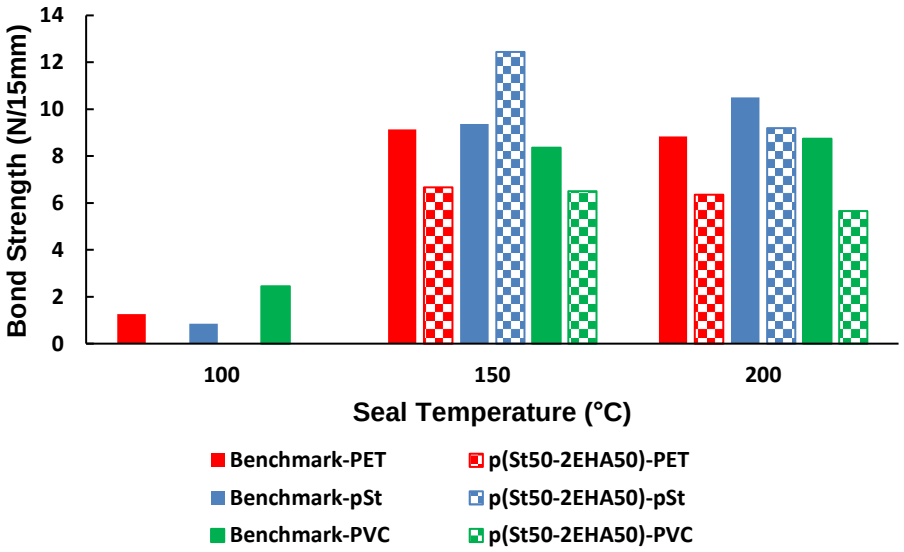

Figure VI.9. Bond Strength of a hard-soft AB block copolymer compared to the benchmark dispersion; testing of coated papers in sealing to non coated plastic films: PET (red), pSt (blue), PVC (green) substrates

The sample pSt50/2EHA50 was coated on a paperboard and sealed for 2s to three different substrates: PET, pSt and PVC and the results are shown in Figure VI.9. We can see that the block copolymers did not seal onto the substrates at 100°C and the benchmark latex showed only very low bond strength manifested as pealing failure at this temperature. Furthermore, the block copolymer dispersion showed lower bond strength compared to the benchmark latex for PET and PVC substrates

at 150ºC. On the other hand, higher bond strength values were obtained compared to the benchmark latex when paper cardboard was sealed to pSt substrates at 150ºC. This is most likely due to the higher compatibility of the block copolymer with pSt rather than with PET and PVC. At higher temperatures the benchmark latex showed higher bond strengths. Most likely the block copolymer coating viscosity got substantially reduced at 200°C and the coating got partially absorbed by the paper. As a result, the efficient thickness got lower, which led to formation of weaker bond strength.

VI.3.3. Heat sealing adhesive properties of the ABA crystalline-soft-crystalline block copolymers

Paper to paper heat sealable lacquers of p(SA15-2EHA50-SA15), p(SA15-2EHA70-SA15), p(SA15-2EHA100-SA15) and p(SA25-2EHA50-SA25) ABA block copolymers, having crystalline and soft domains and different Mn were also investigated. For details on the synthesis of these block copolymers, Chapter IV can be seen. The results of the bond strengths of paper to paper seals are shown in Figure VI.10. The block copolymers show a melting temperature from 45-47°C (Chapter IV, Figure IV.4), thus one would expect that they will activate at lower temperatures. However, as seen from the results shown in Figure VI.10 no satisfactory results were obtained for the paper to paper heat sealable lacquers.

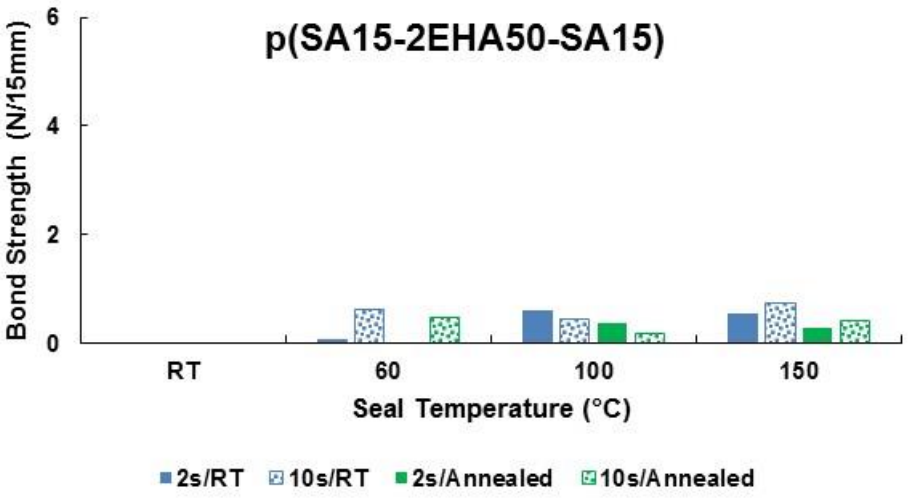
p(SA15-2EHA50-SA15)
Bond Strength (N/15mm)
6
4
2
0
RT
60
100
150
Seal Temperature (°C)
2s/RT
10s/RT
2s/Annealed
10s/Annealed

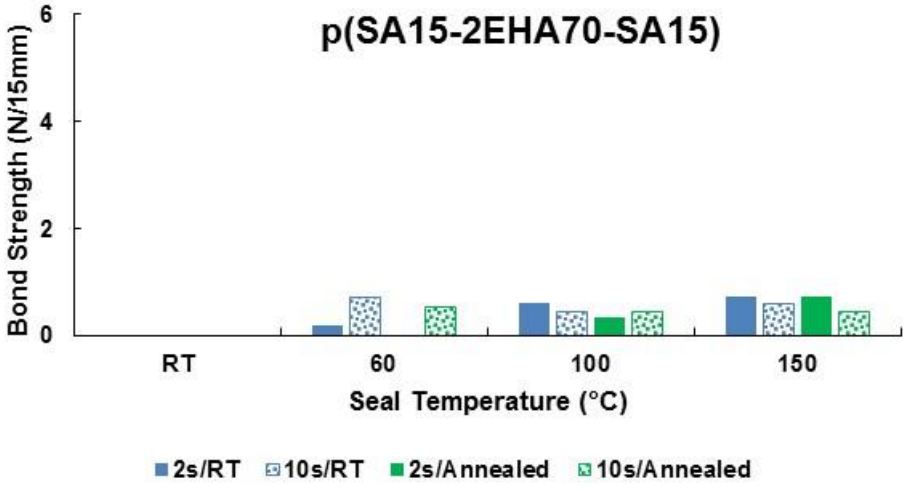
p(SA15-2EHA70-SA15)
Bond Strength (N/15mm)
6
4
2
0
RT
60
100
150
Seal Temperature (°C)
2s/RT
10s/RT
2s/Annealed
10s/Annealed

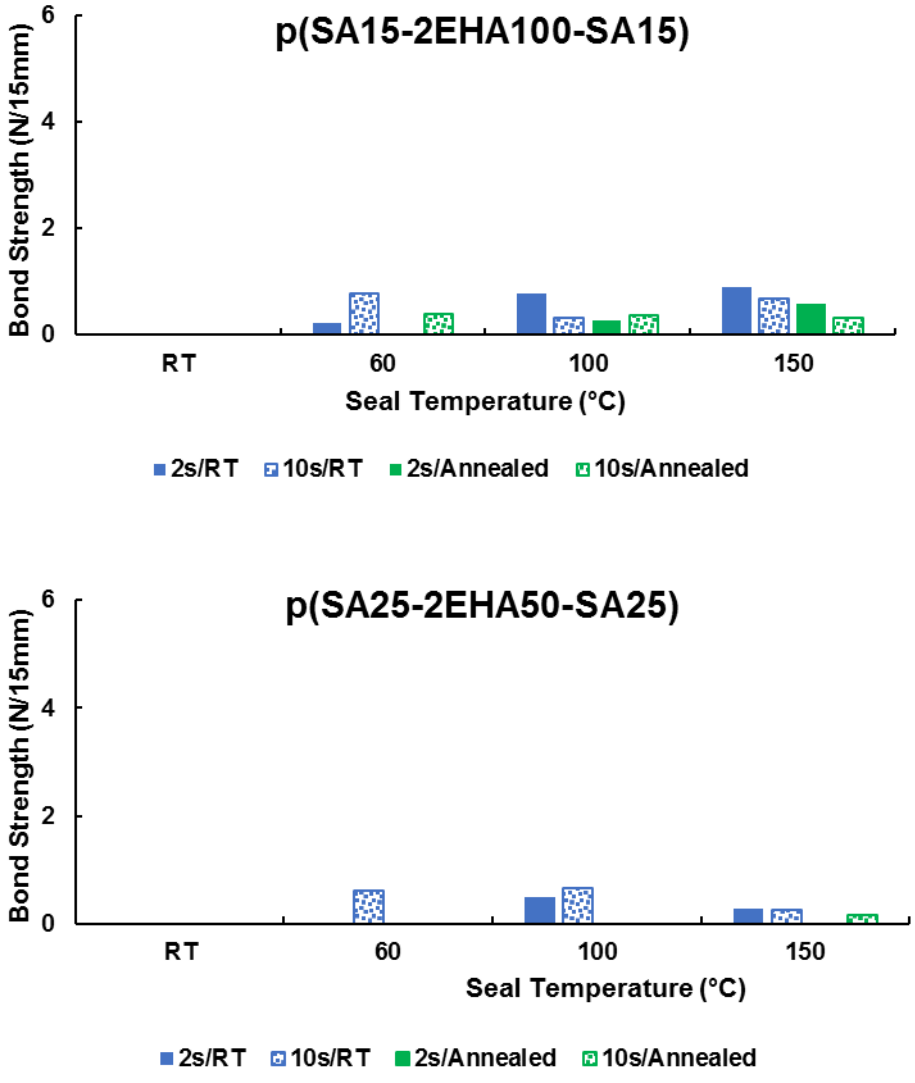

Figure VI.10. Bond strength of crystalline-soft-crystalline ABA block copolymer dispersions on coated paper (paper to paper seal).

Rather low bond strength values were obtained for all block copolymers manifested as peeling failure. Moreover, all the block copolymers despite the difference in their composition showed no tackiness at room temperature, which started to be more prominent at temperatures of 60°C and above. The bond strength was not improved even after increasing the seal temperature. This is a result most likely due to the fact that the coating at increased temperature and pressure got absorbed by the paper due to the low viscosity, leading to lower efficient thickness and thus not efficient material to wet the surfaces and provide good bonding after cooling. The block copolymer having highest amount of crystalline domains was expected to give highest bond strengths, finding observed also by Mehravar et al[9], who synthesized waterborne adhesives based on stearyl acrylate. Thus, a coated paper board with p(SA25-2EHA50-SA25) was sealed to three different substrates, namely pSt, PET and PVC and the results are shown in Figure VI.11, where the results of the benchmark latex are also presented.

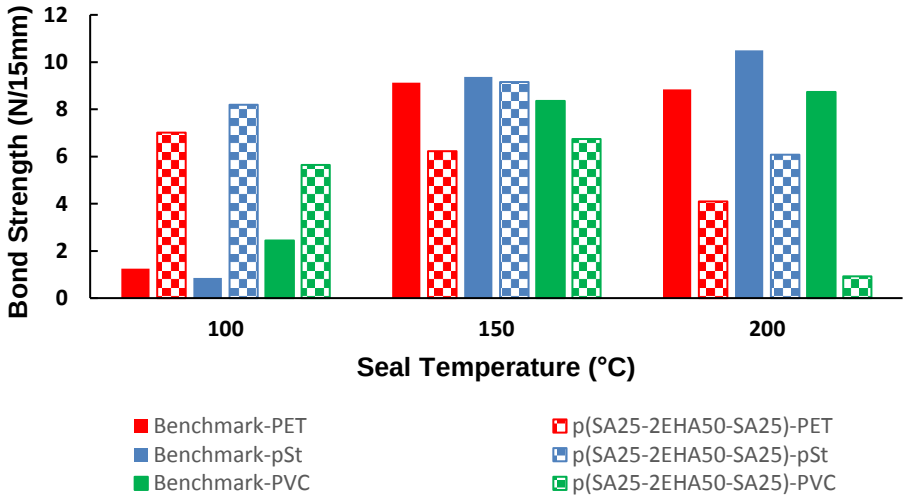

Figure VI.11. Bond Strength of a crystalline-soft-crystalline block copolymer compared to benchmark dispersions on coated paper to: PET (red), pSt (blue), PVC (green) substrates for a dwell time of 2s, dried at room temperature.

The results shown in Figure VI.11 indicate that the sample p(SA25-2EHA50-SA25) provides higher bond strength compared to the benchmark dispersion at a sealing temperature of 100 °C. This is most likely due to the lower transition temperature (Tm) of the block copolymer compared to the Tg of the benchmark latex making it possible to be activated already at 100°C.

VI.4. Conclusions

Adhesive properties in the form of heat seal lacquers were evaluated for ABA (hard-soft-hard), AB (hard-soft) and ABA (crystalline-soft-crystalline) block copolymers waterborne dispersions. The dispersions were applied to paper card board and dried at three different conditions; (i) room temperature, (ii) 60°C for the ABA (crystalline-soft-crystalline) and 100 °C for the ABA (hard-soft-hard) and AB (hard-soft). Then the coated paper card boards were sealed to another coated paper card board face to face at different temperatures and dwell times using constant pressure. Moreover, the paper board coated with dispersions was directly sealed to three different non-coated plastic substrates: pSt, PVC and PET.

For the ABA (hard-soft-hard) block copolymers it was shown that among all the samples p(St15-2EHA50-St15) and p(St25-2EHA50-St25) having highest pSt content showed no blocking at room temperature and highest bond strength values manifested as paper tear both for dwell times of 2s and 10s, when sealed paper to paper. Moreover, it was shown that coated papers annealed at 100°C demonstrated high bond strength only at higher temperatures and/or higher dwell times, probably because of migration of the surfactant to the surface and/or particle coalescence and reorganization of the block copolymer at the paperboard during annealing. Moreover,

compared to the benchmark, the sample p(St15-2EHA50-St15) showed higher bond strength at lower temperatures, due to the lower sealing temperature.

The ABA hard-soft-hard block copolymers were also successfully sealed to different substrates (pSt, PET, PVC). However, compared to the benchmark latex, lower bond strengths were obtained for the block copolymers. The difference in bond strength became more pronounced at higher temperatures.

Regarding the AB hard-soft block copolymers, the highest bond strength for paper to paper heat seal lacquers was obtained for the pSt50/2EHA50 block copolymer. It was noticed that at higher temperatures and higher dwell time lower bond strengths were obtained, probably as a result of the lower melt viscosity of the diblock copolymers, causing increased penetration of the block copolymer into the pores of the paper. Moreover, the bond strength values obtained were lower than the one of the benchmark latex. When sealed to pSt, PVC and PET, highest bond strength value is obtained when the paper was sealed to pSt substrate and the values exceeded the one of the benchmark latex.

For the ABA (crystalline-soft-crystalline) block copolymers no satisfactory results were obtained for the paper to paper heat sealable lacquers, most likely due to porosity of the paper, which somehow absorbed the polymer leading to lower effective thickness of the polymer sealing layer and therefore reduced bond strength.

Nevertheless, when the block copolymer with highest amount of crystallinity was sealed to pSt, PVC and PET substrates, high bond strength (paper tear) values were obtained for all three substrates from which the paper-pSt seal lacquers led to highest value. Moreover, it was shown that the block copolymer activates already at 100°C compared to the benchmark latex, which needs 150°C to activate and form solid bonds.

VI.5. References

1 C. Diamond, *Ink World*, 2016, **May-June**, 20–23.

2 US 5385 967A, 1995.

3 US 2017/0009111A1, 2017.

4 US 2015/0191619, 2015.

5 WO 2011/017388 A2, 2011.

6 US 6368 707 B1, 2002.

7 US 8025758 B2, 2011.

8 US 5837089A, 1998.

9. E. Mehravar, M. A. Grosse, A. Agirre, B. Reck, J. R. Leiza and J. M. Asua, *Eur. Polym. J*., 2018, **98**, 63-71.

Chapter VII. Conclusions

This PhD thesis has aimed at investigating the synthesis and characterization of temperature responsive waterborne nano-phase separated polymer dispersions composed of block copolymers produced by means of reversible addition-fragmentation (RAFT) chain transfer polymerization. A fundamental study of polymer microstructure on particle morphology and on film formation at different conditions was carried out with the aim of understanding the structure-property relations of the films. Finally, the application properties of the waterborne block copolymers were investigated as heat seal lacquers using different substrates.

Two-step RAFT polymerization was used for the synthesis of ABA block copolymers composed of hard (polystyrene-pSt) A block and soft (2-ethylhexyl acrylate B-2EHA) block using S,S-dibenzyl trithiocarbonate (DBTTC) bifunctional RAFT agent. Initially, the first A block was synthesized using miniemulsion polymerization and the reaction was stopped at 80% conversion. The second monomer 2EHA was fed to the system as a pre-emulsion to continue controlled polymerization to form the B block. The soft domains of the B block still contain a small fraction of styrene from the initial step. The effect of several reaction parameters such as (I) type of initiator, (II) molar ratio of RAFT-Agent to Initiator, (III) temperature and (IV) targeted Mn were initially investigated on the controlled miniemulsion polymerization of styrene. AIBN was shown

to be the most effective initiator among all the initiators used (water soluble, oil soluble and redox system), since it provided the lowest PDI and lowest deviation from the predicted theoretical Mn for a controlled polymerization. The most suitable reaction temperature and molar ratio of RAFT-Agent to Initiator was found to be 70°C and 5 :1 respectively. Furthermore, it was found out that targeting very high Mn of polystyrene (70,000 g/mol) led to substantial increase of PDI index, i.e. visible deviation from ideal living polymerization behavior. Thus, the synthesis of ABA block copolymers was focused onto a strategy of starting from seeds of A block with lower targeted Mn (50,000 and 30,000 g/mol). Several ABA block copolymers were successfully synthesized, as evidenced by MWD shift and linear increase in Mn, with different length of the middle soft block proven by GPC results. Nevertheless, a negative deviation of the obtained Mn compared to the theoretical Mn was observed in the polymerization of the second B block monomer. The reason for this behavior can be explained by the applied GPC evaluation method, in which the Mark-Houwink constant for polystyrene was used only, i.e. neglecting the other comomomers of the block copolymer with different Mark-Howink constant. DSC measurements of the pSt homopolymers showed a single Tg lower than 100°C (literature Tg of pSt synthesized by free radical polymerization) because of the comonomer stearyl acrylate used as costabilizer in the minimemulsion and the low Mn obtained. As expected, the block copolymers showed the presence of two Tg's, a lower one originating from the soft middle block and a higher one originating from the hard-polystyrene domain, indicating the presence of a two-phase system.

AB block copolymers of hard and soft domains were also synthesized via two-step reversible addition fragmentation chain transfer polymerization with an asymmetric RAFT agent. Two reaction parameters were investigated on the pSt homopolymerization, namely (i) type of RAFT agent and (II) molar ratio of RAFT-agent to Initiator. Three RAFT agents, two trithiocarbonates and one dithiocarbamate-pyrazole based RAFT-agent were inverstigated for the synthesis of polystyrene in miniemulsion and it was found out that the 2-(((dodecylthio)carbonothioyl) thio)propanoic acid mediated the polymerization of styrene in the most controlled way. AB block copolymers with different Mn were successfully formed, proven by the MWD shift and a linear increase of Mn versus conversion. The negative deviation of the Mn obtained compared to the theoretical Mn was obvious in these block copolymers as well, the reasons for this observation being the same explained above. The AB block copolymer revealed also the presence of two Tgs corresponding to the soft and hard domains. However, a significant difference was observed with respect to the ABA block copolymers. In this case, the Tg of the pSt domain was in the region of 78ºC, while for ABA block copolymers it was in the region of 60ºC. The higher Tg obtained for the AB asymmetric block copolymers can be explained by the higher molecular weight pSt chains produced in these AB block copolymers, compared with the corresponding symmetric block copolymers with the same target Mn, in which the molecular weight of each of the two pSt blocks is approximately half the value of the corresponding AB-block copolymer.

The research was also extended to the synthesis of ABA block copolymers made of crystalline A block obtained from stearyl acrylate (SA) and soft B block from 2EHA using the symmetric DBTTC RAFT agent. Two low PDI seeds of pSA were initially synthesized up to 80% conversion and succesfully extended with 2EHA to form ABA block copolymers with different Mn without removing the monomer from the first step. DSC measurements of the initial A block revealed the presence of an endothermic peak at 49°C originating from the melting of the pSA crystalline domains and a smaller one at 30°C attributed to the crystals of the unreacted SA monomer present in the first block polymer. Formation of the ABA block copolymer resulted in reduced crystalinity compared to the crystallinity of polySA block. Also the the melting peak corresponding to the non reacted SA disappeared, indicating its full conversion. For all block copolymers thermogravimetric analysis showed a single step decomposition (above 300ºC), i.e. below this temperature there is no degradation forming volatile decomposition products.

Once the block copolymers were synthesized, microscopic techniques were employed to study the effect of polymer microstructure on particle morphology and on the film morphology at different thermal treatments. When films were cast at room temperature, which is below the Tg of the hard domain or the Tm of the crystalline domain, no complete particle coalescence was observed and the phase separation within particles, leading to different morphologies could be studied. Thermal treatment was done well above the Tg (hard) or the Tm (crystalline) and complete particle

coalescence and ordering on a bigger length scale was achieved, which was close to the equilibrium morphology. Films were also casted from THF solution, in order to completely erase the history of emulsion polymerization and approach the closest possible equilibrium morphology. It was found out that annealing of the films at prolonged periods, led to approaching equilibrium morphology.

Furthermore, it was shown that the composition of the block copolymers as well as the thermal treatments of the polymer films greatly influenced the viscoelastic properties of the polymer films. As a general trend it was seen that increasing the length of the middle soft block led to a decrease in elastic modulus in the plateau region. In addition, an increase of the elastic modulus in the plateau region was only obtained from the ABA hard-soft-hard block copolymers as a result of the annealing, which transferred the ABA block copolymers into a “harder” rubber (like in a “vulcanization process”). On the other hand, the AB hard-soft and ABA crystalline-soft-crystalline block copolymers showed a decrease in the elastic modulus in the plateau region upon annealing. The possible reasons for this behavior was prescribed to the fact that the soft domains in AB block copolymers are attached only to the one hard domain and this not able to form a physical crosslink. In addition, the ABA crystalline-soft-crystalline block copolymers during annealing form bigger crystals which decreases the interaction with the soft domains leading to a decrease in elastic modulus in the plateau region.

Application properties in the form of heat seal lacquers using different substrates were tested for all the three types of block copolymers: ABA (hard-soft-hard), AB (hard-soft) and ABA (crystalline-soft-crystalline). The dispersions were applied to paper card board and dried at: (i) room temperature, (ii) 60°C for the ABA (crystalline-soft-crystalline) and 100 °C for the ABA (hard-soft-hard) and AB (hard-soft). Then the coated paper card boards were sealed to another coated paper card or to pSt, PVC and PET.

No blocking at room temperature and highest bond strength was obtained for the paper to paper sealant when ABA (hard-soft-hard) block copolymers having highest portion of pSt domains were used. The annealed coated paper boards showed high bond strength only at higher temperatures and/or higher dwell times, probably due to the migration of the surfactant to the surface and/or substantial phase separation already happening at the surface of the substrate. The results were comparable if not better than a commercial benchmark latex. Sealing of the ABA hard-soft-hard block copolymers to different substrates (pSt, PET, PVC) was also achieved with lower bond strength comparable to the benchmark.

Only one sample of the AB hard-soft block copolymers with highest pSt content resulted in highest bond strength for paper to paper heat seal lacquers. Interestingly at higher dwell time and temperatures, lower bond strengths were obtained, most likely

due to the lower melt viscosity of the diblock copolymers in comparison to the ABA hard-soft-hard block copolymers. This led to increased penetration of the block copolymer into the pores of the paper and thus less effective thickness of the polymer for sealing. In addition, highest bond strength was achieved when the paper was sealed to pSt substrate and the values exceeded the one of the benchmark latex.

When the ABA crystalline-soft-crystalline block copolymers were sealed paper to paper, no satisfactory results were obtained. Again, this is explained due to the low melt viscosity of these block copolymers, leading to strong penetration into the pores of both papers. On the contrary, sealing to pSt, PVC and PET substrates resulted in high bond strength values, especially for the paper to pSt seal lacquers, which also were already activated at lower temperature compared to the benchmark.

The research carried out in this PhD has shown the potential of waterborne RAFT polymerization to introduce unique morphology and film properties. The application studied in this work has been heat seals, but the range of applications can be widen to many other sectors in the future.

Resumen y Conclusiones

El objetivo de esta tesis doctoral ha sido investigar la síntesis y caracterización de dispersiones acuosas de polímeros con separación de nano-fases con capacidad de respuesta a cambios de temperatura, compuestas de copolímeros de bloque producidos mediantes polimerización RAFT (polimerización por transferencia de cadena con adición-fragmentación reversible). Se ha llevado a cabo un estudio del efecto de la microestructura de las cadenas poliméricas en la morfología de la partícula y en la formación de film en diferentes condiciones, con el objetivo de entender las relaciones estructura-propiedades de las películas de polímero formadas. Finalmente se han investigado como aplicación de los copolímeros de bloque dispersos en agua, su uso en lacas para sellado térmico.

Para la síntesis de copolímeros de bloque ABA, compuestos de bloques de polímero duro A y bloques de polímero blando B, se utilizó el agente RAFT difuncional S,S-dibenzil tritiocarbonato (DBTTC), en una polimerización controlada en dos etapas. Primero se sintetizó el bloque A de poliestireno (pSt) mediante polimerización controlada en miniemulsion y la reacción se paró al 80% de conversión. Posteriormente se alimentó una preemulsión del monómero 2-etilhexil acrilato (2EHA) a la siembra obtenida por miniemulsion, de manera que se formaran los dominios blandos (B), que contenían una pequeña fracción del estireno que no

había reaccionado en el primer paso. La síntesis de este copolímero de bloque se optimizó estudiando la influencia de diferentes factores como (I) tipo de iniciador, (II) relación molar RAFT:Iniciador, (III) temperatura y (IV) peso molecular objectivo (Mn) de la homopolimerización de estireno. Se comprobó que el AIBN era el iniciador más efectivo entre todos los utilizados (solubles en agua, solubles en el monómero e iniciadores rédox), dado que produjo el menor índice polidispersidad (PDI) del homopolímero y la menor desviación del Mn teórico. Por otro lado, la temperatura de reacción elegida fue 70ºC y una relación molar RAFT:Iniciador de 5:1. Por otro lado, se vio que al intentar conseguir pSt de alto peso molecular (70.000 g/mol), el PDI aumentaba en exceso. Por lo tanto, la formación de copolímeros de bloque ABA sólo se llevó a cabo a partir de siembras de homopolímero A, con Mn objetivo menores (50.000 y 30.000 g/mol). De esta manera se sintetizaron con éxito copolímeros de bloque simétricos ABA con diferentes longitudes de polímero A y B, en los que se comprobó el aumento progresivo de la distribución de pesos moleculares (MWD) y un aumento lineal del Mn. En cualquier caso, se observó una ligera desviación del Mn experimental comparad con el Mn teórico cuando se alimentó el segundo monómero (2EHA) al sistema. La razón para este comportamiento se ha atribuido a la diferencia entre las constantes de Mark-Houwink de los dos monómeros, dado que las medidas de GPC se realizaron usando pSt como estándar de calibración, y por tanto con sus constantes de Mark-Houwink.

Las medidas de DSC de los homopolímeros de PSt mostraron una única Tg, a temperaturas menores de 100ºC (Tg del pSt sintetizado por polimerización radicalaria libre). La razón para esta disminución de la Tg se ha atribuido a la utilización de estearil acrilato como coestabilizante durante la polimerización en miniemulsión del estireno y al bajo Mn obtenido. Por otro lado, los copolímeros de bloque mostraron la presencia de dos Tg, una a menores temperaturas procedente del bloque blando intermedio y otra a temperaturas mayores, procedente de los dominios de poliestireno duro: indicando así la presencia de un sistema con dos fases.

También se sintetizaron copolímeros de bloque asimétricos AB con dominios duros (pSt) y blandos (p2EHA), por polimerización controlada RAFT en dos etapas. Para la optimización de esta síntesis se tuvieron en cuenta dos factores; (I) el tipo de agente RAFT asimétrico y (II) la relación molar RAFT:Iniciador. Se probaron tres agentes RAFT, dos basados en tritiocarbonatos y uno basado en ditiocarbamato-pirazol. Se comprobó que la polimerización en miniemulsión del estireno se llevaba a cabo de manera más controlada si se utilizaba el agente RAFT ácido propanoico de 2-(((dodeciltio)carbonotioyl)tio). Con este agente RAFT y un método similar al de síntesis de copolímeros de bloque simétricos, se sintetizaron diferentes copolímeros de bloque asimétricos AB de manera exitosa; con un desplazamiento de la MWD a lo largo de la reacción y un incremento lineal de Mn en base a la conversión. Como ya

se ha explicado para los copolímeros simétricos, en este caso se observó una desviación del Mn experimental obtenido frente al teórico con la adición del 2EHA.

Para estos copolímeros de bloque también se encontraron dos Tgs correspondientes a los dominios blandos y duros. Sin embargo se observó una diferencia significativa con respecto a los copolímeros simétricos ABA. En el caso de los copolímeros asimétricos AB, la Tg correspondiente a los dominios de pSt se encontró alrededor de 78ºC, mientras que para el caso de los copolímeros ABA, estaba alrededor de 60ºC. Esta diferencia se ha relacionado con la mayor longitud de cada cadena de pSt obtenida en el caso de los copolímeros asimétricos, comparada con el obtenido en los copolímeros simétricos con el mismo Mn objetivo.

La investigación también se extendió a la síntesis de copolímeros simétricos ABA conteniendo bloques A cristalinos (compuestos de estearil acrilato, SA) y bloques B blandos (compuestos de nuevo de 2EHA). En este caso se utilizó de nuevo el agente RAFT simétrico DBTTC. La síntesis se llevó a cabo de nuevo en dos etapas. Se obtuvieron dos siembras con dominios cristalinos (pSA) con diferentes Mn objectivos, llevadas al 80% de conversión, que se extendieron posteriormente sin eliminar el monómero SA no reaccionado con 2EHA para formar copolímeros de bloque ABA con diferentes pesos moleculares.

Las medidas de DSC de los homopolímeros de pSA revelaron la presencia de un pico endotérmico a 49ºC, originado por el fundido de los dominios cristalinos, y otro más pequeño a 30ºC, atribuido a la presencia de cristalies de monómero SA no reaccionado en el bloque. La formación del bopolímero de bloque ABA llevó a una disminución de la cristalinidad comparada con la del bloque de pSA y a la desaparición del pico correspondiente a los cristales de SA no reaccionado, lo cual era indicio de la incorporación total del SA al copolímero. Se observó que todos los copolímeros de bloque ABA sintetizados con los dominios cristalinos poseían buenas propiedades térmicas, independientemente de su composión, con una descomposición térmica que se daba en una sóla etapa y por encima de los 300ºC.

Una vez sintetizados los diferentes copolímeros de bloque, se utilizaron técnicas de microscopía para estudiar el efecto de la microestructura del polímero en la morfología de las partículas dispersas en agua, además de estudiar el efecto de la formación de film de dichas partículas en diferentes condiciones sobre la morfología de las peículas de polímero formadas. Cuando las películas se formaron a temperatura ambiente, temperatura por debajo de la Tg del dominio duro o de la Tm del dominio cristalino, no se observó coalescencia completa entre las partículas en la película, de manera que se pudo observar la separación de fase que existía dentro de cada partícula. Si se trataba las películas por encima de la Tg del polímero duro o de la Tm del polímero cristalino, se obtenía una coalescencia completa de las partículas y morfologías muy similares a las de equilibrio. También se produjeron

películas de polímero disolviendo inicialmente los copolímeros de bloque en tetrahidrofurano (THF), para borrar completamente la historia asociada a la polimerización en emulsión, y obtener al mismo tiempo morfologías lo más cercanas posibles a las de equilibrio. Se encontró que las películas obtenidas mediante esta técnica y las obtenidas mediante el sinterizado a alta temperatura a partir de las dispersiones acuosas eran muy similares, y se aprosimaban a las de equilibrio.

Además se encontró que la composición de los copolímeros de bloque y el tratamiento térmico al que habían sido sometidas las películas de polímero tenían una gran influencia en sus propiedades viscoelásticas. Como norma general se observó que al aumentar la longitud del bloque duro central, el módulo elástico en la región de plató disminuía. Adicionalmente se encontró un aumento del módulo elástico en dicha región para los copolímeros de bloque ABA (duro-blando-duro) tras el tratamiento de sinterizado de las películas. Dicho efecto es el resultado del proceso denominado vulcanización, que transfiere copolímeros de bloque ABA a caucho duro. Por otro lado, los copolímeros de bloque AB (duro-blando) y ABA (cristalino-blando-cristalino) mostraron una reducción del módulo elástico en la región del plató tras el sinterizado. Dicho comportamiento se ha atribuido al hecho de que los dominios blandos de los copolímeros AB sólo están unidos a un dominio duro, lo cual no permite que se formen entrecruzamientos físicos. Por otro lado, los copolímeros ABA con dominios cristalinos, forman cristales de mayor tamaño

durante el sinterizado, lo que disminuiría la interacción entre los dominios cristalinos y los blandos, y un menor módulo elástico en la región del plató.

Las propiedades en la aplicación de lacas para el sellado térmico se analizaron sobre diferentes substratos utilizando los tres tipos de dispersiones de copolímeros de bloque: ABA (duro-blando-duro), AB (duro-blando) y ABA (cristalino-blando-cristalino). Las dispersiones se aplicaron sobre paneles de papel y se secaron a: (i) temperatura ambiente, (ii) 60 ºC para los ABA con dominios cristalinos y (iii) 100ºC para los ABA y AB con dominios duros. Posteriormente los paneles de papel depositados con el polímero se sellaron a otro panel de papel o a películas de PSt, PVC o PET.

Las mejores propiedades de sellado papel a papel, ausencia bloqueo a temperatura ambiente y mayor fuerza de unión, se obtuvieron con los copolímeros de bloque ABA (duro-blando-duro) que contenía la mayor proporción de dominios de pSt. Los paneles de papel recubiertos y sinterizados sólo presentaron fuerzas de unión altas cuando se sellaban a mayores temperaturas o con mayores tiempos de sellado, debido probablemente a la migración de surfactante a la superficie de las películas y/o a la separación de fases que ya había ocurrido previamente en la superficie del substrato. Los resultado encontraron fueron comparables, incluso mejores que los de un látex de referencia. También se obtuvo el sellado a diferentes

substratos (pSt, PET, PVC) con los copolímeros de bloque ABA duro-blando-duro, aunque con menores fuerzas de unión que las producidas por el látex de referencia.

Sólo uno de los copolímeros AB duro-blando, el de mayor contenido en pSt, produjo buen sellado papel a papel. Curiosamente a mayores tiempos y temperaturas de sellado se obtuvieron mejores fuerzas de unión, probablemente debido a la menor viscosidad en fundido de estos copolímeros asimétricos comparados con los simétricos, lo que pudo originar su absorción en el papel. Por otro lado, se obtuvo un buen sellado papel a pSt, con valores incluso superiores a los del látex de referencia.

Finalmente los copolímeros de bloque ABA cristalino-blando-cristalino, no produjeron buenos sellados papel a papel. Pero sí que se obtuvieron buenos sellados a pSt, PVC y PET, especialmente para el caso del pSt, en el que se obtuvieron sellados activados a menores temperaturas que el látex de referencia.

La investigación llevada a cabo en esta tesis doctoral ha demostrado el potencial de la polimerización RAFT en fase dispersa acuosa para producir morfologías y propiedades de partícula únicas. Si bien la aplicación estudiada en este trabajo ha sido el sellado térmico, las aplicaciones se pueden extender a otros sectores en el futuro.

Appendix

Materials

For the synthesis of the block copolymers technical grade monomers styrene (St, 99.7% purity, 10-20 ppm inhibitor 4-tert-butylcatechol (TBC) from Quimidroga at POLYMAT and 99-100% purity, inhibitor 4-tert-butylcatechol (TBC) at BASF), and 2-ethylhexyl acrylate (2EHA) Quimidroga POLYMAT 10-20 ppm (4-methoxyphenol) MEHQ were used. To initiate the polymerization several initiators with different water solubilities were used. Two water soluble thermal initiators, potassium persulfate (KPS, 99% purity, KB Bernd Kraft) and 2,2'-Azobis[2-methyl-N-(2-hydroxyethyl)propionamide] (WAKO-086, WAKO chemicals), one oil soluble thermal initiator, azobisisobutyronitrile (AIBN, purity 98%, Sigma Aldrich) and one redox pair initiator, *tert*-Butyl hydroperoxide 6% solution (TBH, solution Sigma Aldrich) and ascorbic acid (AsAc, Sigma Aldrich), were used. S,S-Dibenzyl trithiocarbonate (DBTTC, kindly supplied by Arkema) was used as a bifunctional symmetric RAFT agent. Three monofunctional RAFT agents were used as well, (i) 2-(((dodecylthio)carbonothioyl)thio)propanoic acid (BM1430), (ii) 4-cyano-4-(((dodecylthio)carbonothioyl)thio)pentanoic acid (BM1432), (iii) 2-cyanobutanyl-2-yl 3,5-dimethyl-1H-pyrazole-1-carbodithioate (BM1542) and they were purchased from

Boron Molecular. To stabilize the droplets alkyldiphenyloxide disulfonate -Dowfax 2A1 (0.45 active content, DOW Chemicals) was used as an anionic surfactant and Disponil A3065 (0.65% active content, BASF Company) as a non-ionic surfactant. Stearyl acrylate (SA, Sigma Aldrich) was added as a costabilizer to prevent Ostwald ripening and sodium bicarbonate ($NaHCO_3$, Aldrich) was added as a buffer to control the miniemulsion viscosity by reducing the electrostatic interactions among droplets. All the chemicals were used as received without any further purification. Deionized MilliQ water was used as polymerization media and 1 wt% hydroquinone (HQ, purity 99%, Pan-Fisher) water solution was used for quenching the reaction in the samples withdrawn from the reactor at certain time intervals. Tetrahydrofuran (THF, 99.9% GPC, Scharlab) and toluene (Sigma Aldrich) were used as solvents for the GPC analysis.

Characterization methods

Stability of the miniemulsion. The stability of the miniemulsions was determined by means of a Turbiscan LabExpert apparatus. In this equipment, the miniemulsion was placed in a vial (55 mm path length) heated at 60°C for 6h and the stability was determined by studying the evolution of the light backscattered by the miniemulsions.

The conversion of the volatile monomers was followed gravimetrically. The samples withdrawn from the reactor (1 mL latex) at each time interval were placed in an aluminium cup where a drop of 1 wt% of hydroquinone water solution was initially added and dried in an oven (60°C) overnight.

The conversion of SA was measured by NMR ^{1}H NMR spectra were recorded on a Bruker 400 AVANCE equipped with a z gradient BBO probe.

Monomer droplet and particle sizes were measured in POLYMAT using dynamic light scattering (Zetasizer Nano Z, Malvern Instruments). For the measurements, a drop of miniemulsion or latex was diluted in distilled water to avoid multiple scattering. Reported droplets and particle diameters are a mean of the Z-average of 3 measurements, each of them analysed in 11 runs of 30 s each.

Monomer droplet and particle sizes were determined in BASF by using a NANO-flex particle sizer from Microtrac using 780 nm laser light (3 mW) at a 180 ° scattering angle. Measurements were done with samples diluted to the required concentration with demineralized water at room temperature. Reported droplets and particle diameters are based on a volume fraction. Three measurements were done, each of them analysed in 3 runs of 30 s each.

Molecular Weight Distribution and the average molecular weight of the obtained latexes were determined in POLYMAT by size exclusion chromatography (SEC-GPC) at 35 ºC using solvent delivery unit LC-20AD (Shimadzu Corp.), with RI and UV detectors. The setting consisted of a pump, an autoinjector (Waters 717 plus) refractive index detector (Waters Corp. 2410), a UV detector (Waters 2487) and three columns in series (Styragel HR2, HR4 and HR6; with a pore size from 10^2 to 10^6Å). The analyses were performed with THF as solvent at a flow rate of 1 mL min^{-1}. The polymer was dissolved in THF and filtered (polyamide filter Φ = 0.45 μm). Toluene (100 µL) was added as internal standard prior injection in the SEC. The Mn values obtained were based on polystyrene standards.

Molecular Weight Distribution and the average molecular weight of the obtained latexes were determined in BASF by size exclusion chromatography (SEC-GPC) at 40 ºC with RI and UV detectors. The setting consisted of a pump, an autoinjector (Agilent LC-1260 ALS) refractive index detector (Agilent LC- 1260 RID), a UV detector (Agilent LC- 1260 VWD) and two identical columns in series (Agilent, Polypore 7.5 mm*300 mm); with MW range of 200 to 2,000,000 g/mol. The analyses were performed with THF as solvent at a flow rate of 1 mL min^{-1}. The polymer was dissolved in THF and filtered (polyamide filter Φ = 0.20 μm). The Mn values obtained were based on polystyrene standards.

Thermal characterization

Melting temperature and heat of fusion (ΔH_f) for the ABA crystalline-soft-crystalline block copolymers were measured using differential scanning calorimetry DSC (Q1000, TA Instruments). DSC measurements were done on the films cast at room temperature. The scanning cycle consisted of first cooling to – 80°C at 10°C min^{-1} (isothermal for 2 min), then heating to 80 °C (isothermal for 2 min), second cooling to – 80°C (isothermal for 2 min) at 10°C min^{-1} and then heating to 80 °C at 10°C min^{-1} and cooling again to 25°C. The crystallinity of the polymers, Xc, was calculated as the ratio of ΔHf (first cycle calorimetric heat of fusion of existing crystals) and ΔHf0 (heat of fusion for the 100% crystalline phase) reported to be 218 J/g.

The glass transition temperature of the room temperature cast films of ABA hard-soft-hard and AB hard-soft block copolymers were measured on a (DSC, Q1000, TA Instruments). The scanning cycle consisted of first cooling to – 80°C at 10°C min^{-1} (isothermal for 2 min), then heating to 150 °C (isothermal for 2 min), second cooling to – 80°C (isothermal for 2 min) at 10°C min^{-1} and then heating to 150 °C at 10°C min^{-1} and cooling again to 25°C. The second cycle was used for the determination of the Tg.

Thermal stability of the polymers was measured by Thermal Gravimetric Analysis (TGA) on a TGA Q 500 (TA) instrument at a heating rate of 10°C min^{-1} from 40°C to 800 °C in nitrogen atmosphere.

Wide-angle X-ray diffraction **(WAXS)** analyses of the films were performed on a D8 Advance (Bruker) (CuKa radiation with l = 0.154056 nm). The range of the diffraction angles was 2θ = 10–50° at a scanning rate of 0.05° x $(5\ s)^{-1}$.

DMTA measurements were performed in tensile geometry on 0.5-0.8 mm thick films using Q800 von TA-Instruments, heating rate of 4°C min^{-1}, frequency of 1 Hz and at constant strain.

Morphology. The morphology of the block copolymers films was investigated using Transmission Electron Microscopy (TEM) and Atomic Force Microscopy (AFM). For the TEM measurements, the block copolymers dispersions having hard domains were embeded in Natrosol HR 250 = hydroxyethylcellulose (HEC) and stained with RuO_4. Ultrathin cross sections (about 100 nm thick, perpendicular to the surface) of RuO_4 stained films dried at different conditions were prepared via cryo ultratmicrotomy (Leica UC 7). The sections were examined at a Zeiss Libra 120 microscope with an omega filter operating at an accelerating voltage of 120 kV in elastic mode. The preparation and measurements of the samples was done in BASF analytics lab for electron microscopy.

The **nanomechanical properties** of the ABA crystalline-soft-crystalline block copolymers at the nanoscale were investigated with a Dimension Icon™ AFM from Bruker AXS in PeakForce QNM™ mode. The PeakForce QNM™ AFM images were

measured with a RTESPA-150 silicon cantilever (k=5 N/m), a peak force on tip of 3nN, a modulation frequency of 2 kHz and under ambient conditions.

The **morphology** of the ABA hard-soft-hard and AB hard-soft block copolymers was analyzed using Bruker Dimension Icon AFM using Olympus OMCL-AC160TS cantilever for Tapping with a resonant frequency of 300kHz and spring Constant 42N/m (34-50). Samples were cryocut at −80 °C.

Both for TEM and AFM measurements were performed in several positions thus the images are representative.